DESIGN OF A PNEUMATIC ARTIFICIAL MUSCLE FOR POWERED LOWER LIMB PROSTHESES

Thesis submitted to the Department of Mechanical Engineering in partial fulfillment of the requirements for the degree of

Master of Applied Science

By

Jaime Murillo

January 2013

Ottawa-Carleton Institute for
Mechanical and Aerospace Engineering

University of Ottawa
Ottawa, Ontario, Canada K1N 6N5

ABSTRACT

Ideal prostheses are defined as artificial limbs that would permit physically impaired individuals freedom of movement and independence rather than a life of disability and dependence. Current lower limb prostheses range from a single mechanical revolute joint to advanced microprocessor controlled mechanisms. Despite the advancement in technology and medicine, current lower limb prostheses are still lacking an actuation element, which prohibits patients from regaining their original mobility and improving their quality of life.

This thesis aims to design and test a Pneumatic Artificial Muscle that would actuate lower limb prostheses. This would offer patients the ability to ascend and descend stairs as well as standing up from a sitting position. A comprehensive study of knee biomechanics is first accomplished to characterize the actuation requirement, and subsequently a Pneumatic Artificial Muscle design is proposed. A novel design of muscle end fixtures is presented which would allow the muscle to operate at a gage pressure surpassing 2.76 MPa (i.e. 400 psi) and yield a muscle force that is at least 3 times greater than that produced by any existing equivalent Pneumatic Artificial Muscle. Finally, the proposed Pneumatic Artificial Muscle is tested and validated to verify that it meets the size, weight, kinetic and kinematic requirements of human knee articulation.

ACKNOWLEDGEMENT

I would like to thank all people who have helped and inspired me during my Master's thesis. This research would not have been possible without the support of many people. In the first place, I wish to express my gratitude to my supervisor, Prof. Dr. Marc Doumit who was abundantly helpful and offered invaluable assistance, support and guidance. His constant energy and enthusiasm in research had motivated me during my exploration and study at the University of Ottawa. In addition, he was always accessible and willing to help me with my work which made my research life smooth and rewarding, without his knowledge and assistance this study would not have been achievable.

I also wish to express my gratitude to my co-supervisor Prof. Dr. Natalie Baddour for her valuable advice in science discussion, supervision of the mechanical design work, advice about the new product development process and furthermore, using her precious times to read this thesis and patiently correcting my writing. It was a great learning experience working under my supervisor's and co-supervisor's excellent guidance.

I love the mechanical engineering discipline and enjoyed working for the industry; however, I was always inspired to work with the human body. Thanks to God, this was possible through this project. My deepest gratitude is also due to Prof. Dr Atef Fahim who introduced me to the Biomedical Mechanical Engineering field by accepting me as one of his students to work for lower limb prostheses, someone who regrettably passed away in 2011, at the very early stage of my research work.

I wish to express my love and gratitude to my beloved family Camilo, Matheo and Ana for their understanding & endless love, through the duration of my studies. Words fail me to express my appreciation to my wife Ana whose dedication, love and persistent confidence in me has taken the load off my shoulders.

Finally, I would like to thank everybody who was always supporting me and encouraging me with their best wishes and I would also like to convey thanks to the University of Ottawa for providing the financial means and laboratory facilities.

TABLE OF CONTENTS

LIST OF FIGURES

LIST OF TABLES

Chapter 1

INTRODUCTION

The loss of mobility and independence is commonly described as one of the most horrific mental and physical traumas that an individual can endure. This is the case of an amputated person faced with the loss of one or more limbs, thus prohibiting freedom of movement. To cope with this challenge, amputees rely on prostheses, which are defined as artificial limbs that replace amputated biological limbs. In the United States, there are currently more than 1.7 million people living with a limb loss (excluding fingers and toes) [**1**]and it is estimated that more than 185,000 people undergo an amputation of an upper or lower limb each year[**2**]. According to the American Academy of Orthotists and Prosthetists, by the year 2020, the total number of prosthesis users is expected to reach 2.4 million in the United States[**3**].

Several factors may result in a limb amputation; these can be categorized as self-amputation, cancer, traumatic injury, circulatory disorders related. Amputations that are associated with vascular diseases (circulatory disorders) account for 82 percent of limb loss discharges in the United States. Moreover, lower limb amputations account for 97 percent of all vascular disease related limb loss discharges [**4**]. The statistics of limb amputations for different causes are shown in Figure 1-1.

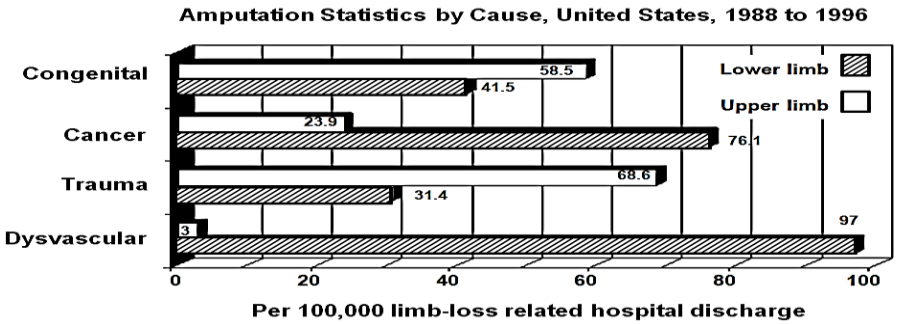

Figure 1-1: Statistics of lower limbs versus upper limb amputation, 1997**[**4**]**

Whereas any limb loss or impairment dramatically changes the life of an individual, lower limb amputation cases are far more common and harmful than upper limb cases. This is attributed to the substantial change in muscle activity that a patient must perform in order to compensate for movement disability. According to [**5**], above knee amputees show an increase in energy consumption of ambulation over normal individuals by 33% and 120% for unilateral and bilateral amputation cases, respectively.

Despite progression in technology and medicine, lower limb prostheses users still endure many challenges that prohibit them from regaining their original movement abilities. Current developed devices have been drastically improved in the last two decades; however, they still lack the actuation element which corresponds to the skeletal muscle in a biological limb. From a mechanical perspective, currently available prostheses assist patients by absorbing and dissipating energy. However, they are incapable of generating sufficient power for high energy movements [**6**]. This may be acceptable for level ground walking, since during this motion the knee joint primarily acts as a damper and a torsional spring to resist the body from collapsing during the stance phase and to assist the leg in swinging forward during the swing phase. However, as an individual attempts to ascend and descend stairs or to stand up from a sitting position, substantial muscle activity is required about the knee and hip joints [**6**]. Thus, lower limb amputees are hindered from achieving high energy movements such as sit to stand due to the dominant passive prostheses that are commercially available.

Developing powered lower limb prostheses has been an engineering challenge for the last few decades. The main obstacle to this achievement has been the lack of a high power, small and light actuator. Electrical motors, hydraulic and pneumatic cylinders are very effective for most industrial applications; however, they are not suitable for prostheses-type applications. In this thesis, the feasibility of a Pneumatic Artificial Muscle (PAM) for powered lower limb prostheses is investigated.

1.1 OBJECTIVES

Recognizing that actuation has been the main challenge for developing powered lower limb prostheses, this thesis aims to design, test and validate the PAM as an effective actuation solution. The designed PAM must satisfy the kinetic and kinematic requirements of knee joint articulation throughout normal gait, stair ascending and descending, as well as sit to stand movements. Moreover, the designed PAM must meet the weight and size constraints of a human leg.

1.2 METHODOLOGY

The PAM is not a new device; however, it was never designed nor tested for actuation behaviour for powered lower limb prostheses. To achieve the stated objectives, a three phase methodology is implemented to guide the research activities. First, the mechanical properties of currently available PAM are identified and analyzed, as well as the biomechanical requirements for a PAM. Second, based on the biomechanical requirements of a human knee during gait, a novel PAM design is proposed. This includes a design of PAM end fixtures and the selection of a combination of muscle braided sleeve and muscle bladder materials. The last phase consists of fabricating numerous PAM prototypes for testing and validation of feasibility for powered lower limb prostheses.

1.3 CONTRIBUTIONS OF THE THESIS

Whereas there have been many claims [**7**][**8**][**9**][**10**] that the PAM is an ideal actuator for biomedical applications, to the author's knowledge, there is currently no study that quantitatively confirms its feasibility for powering lower limb prostheses. This thesis first demonstrates the failure of current PAM designs to meet the mass and geometry constraints as well as the kinetic and kinematic requirements of lower limb prostheses. Then based on biomechanical analysis of human gait, an innovative PAM design which offers an actuation solution for powered lower limb prostheses is proposed. Distinctively, the PAM design presented in this thesis has sustained an operating pressure surpassing 2.5 MPa that resulted in a muscle force of 3887 N that is 300 % greater than any another equivalent PAM.

1.4 THESIS OUTLINE

This thesis is organized into 6 chapters. Chapter 1 introduces the motivations for developing PAM for powered lower limb prostheses, presents thesis objectives, methodology as well as the contributions of the thesis.

Chapter 2 presents the results of a literature survey. This includes a historical background review of PAM, PAM essential analytical models, as well as an analysis of currently available PAM designs. Moreover, this chapter includes a review of presently available lower limb prostheses and their limitations.

Chapter 3 reviews the biomechanical behaviour of a human knee. This consists of characterizing the musculoskeletal system, kinematic as well as kinetic requirements of the human knee. This chapter aims to identify actuation requirements of the knee such that the design criteria for the proposed PAM can be determined.

Chapter 4 proposes a novel PAM design that satisfies the actuation requirements for powered lower limb prostheses during high power gait, such as a sit-to-stand movement. The novel PAM design includes muscle end fixtures and a novel combination of braid and bladder material that permits the muscle to operate at a very high pressure while withstanding extreme muscle pulling forces.

Chapter 5 presents the experimental validation results for the proposed PAM design. These tests demonstrate that the newly developed PAM meets the kinetic and kinematical requirements for powered lower limb prostheses. Moreover, this chapter includes the development of the experimental setup for testing the muscle prototypes.

Chapter 6 presents conclusions of the thesis. This chapter also presents future research considerations that are recommended for PAM.

Chapter 2

LITERATURE REVIEW

2.1 PNEUMATIC ARTIFICIAL MUSCLES

For industrial applications, many forms of actuators have been developed such as electrical motors, hydraulic and pneumatic cylinders and piezoelectric actuators. However, none of these actuators have been shown to be feasible for medical assistive devices such as powered lower limb prostheses. To ensure the effectiveness of the prostheses, the implemented actuator must be very light but also very powerful.

PAM is a pneumatically-powered actuator whose structure and behavior differ significantly from other type of actuators. In its most common configuration, PAM consists of a tubular braided mesh that wraps around an elastic bladder and both are strapped to end fixtures as shown in Figure 2-1. PAM operation is simple, as the PAM is inflated through the end fixtures, radial expansion of the muscle diameter occurs and causes the braid angle to steepen which in turn forces the tubular braid to foreshorten and thus produces a muscle contraction distance (see Figure 2-1).

Figure 2-1: PAM prototype: (a) pressurized state (b) deflated state **[**11**]**

If the muscle contraction is resisted, PAM produces a substantial pulling force. This force is the result of internal forces acting on the bladder due to muscle gage pressure. Subsequently these internal forces are transferred by the braid structure as longitudinal forces along the muscle

contraction axis. PAM offers a combination of properties that makes it very appealing for powered lower limb prostheses compared to other forms of actuators. These properties have been characterized in [**10**]as follows:

PAM mass: PAM is distinctively light; its mass can be less than 50 grams. This is attributed to the thin braided mesh and an elastic bladder that constitute the muscle structure.

PAM force: In spite of its light mass, PAM produces a substantial force that is approximately six times greater than the force produced by a pneumatic cylinder of the same diameter.

PAM stiffness: PAM offers non-linear stiffness behaviour which is essential for legged locomotion and beneficial for passive-type actuation.

PAM compliancy: PAM offers a safe interaction with the user. This is attributed to the inherent pneumatic compliant behavior and to the flexibility of its outer shell.

PAM mechanical connection: Whereas typical actuators require a transmission mechanism and a precise alignment with the apparatus, PAM can be directly connected to deliver muscle contraction distance and muscle force.

PAM speed and bandwidth: Attributed to its unidirectional contraction and no transmission mechanism, the PAM is a relatively fast linear actuator.

BPM Contraction distance: A typical PAM achieves a contraction distance ratio with respect to the muscle unstressed length of 30%. This is comparable to biological skeletal muscles [**12**]**.**

2.1.1 PAM Historical Background

The Pneumatic Artificial Muscle was originally invented by Charles R. Johnson and Robert C. Pierce in 1941. It was patented as an "Expansible Cover" [**13**]and was proposed as an alternative to dynamite in the mining industry where its radial expansion would cause a coal rock to crack open. In 1949, De Haven patented a tensioning device for producing a linear pull for a crash safety belt apparatus for pilots [**14**]. The actuation of this device was triggered by a charge of gun powder that yields a sudden contraction distance and force. In 1955, the PAM was reinvented by Gaylord [**15**] and patented as a fluid-actuated motor system and stroking device which is similar to the PAM used today. Among the first users of this invention was the physicist Joseph L. McKibben who incorporated PAM to activate a Wrist-Driven Wrist-Hand Orthotic for his polio

stricken daughter. In 1963, Nickel et al [**16**] used a PAM to actuate a hinge splint for a severely paralyzed hand as shown in Figure 2-2.

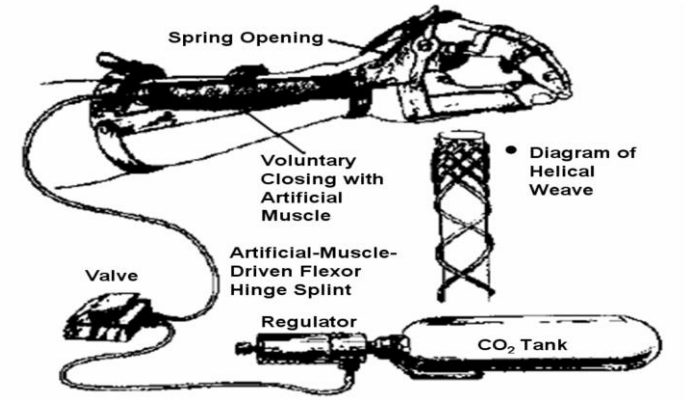

Figure 2-2: McKibben muscle application for an upper limb orthosis **[**16**]**.

During its early years, the PAM was perceived as an innovative actuator; however, it had limited success due to its compliant behaviour, control challenges, and provision of a power source. It was not until the 1980s that researchers rediscovered the PAM. The main attraction was the similarity of the behaviour between the PAM and a biological muscle. Figure 2-3 shows the biological muscle force behaviour as the muscle contracts and expands with respect to the muscle unstressed length $L_{m,o}$. Here, F_m and L_m denote the actual muscle force and length, respectively, where the additional subscript *o* denotes the unstressed state of the muscle.

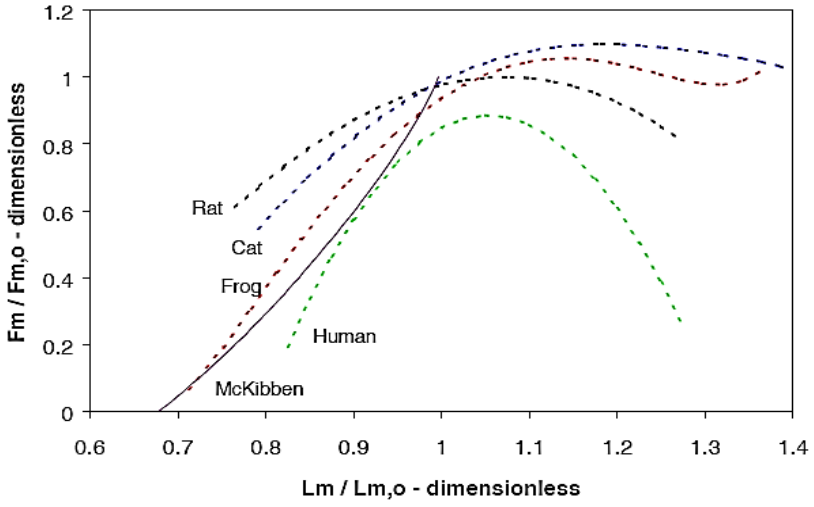

Figure 2-3: Dimensionless isometric contraction for various animals and the PAM pressurized to 500 kPa **[**12**]**.

In 1980, Bridgestone Rubber was first to commercialize PAM for robotic applications. However, an unsuccessful market release of their soft arm robots [**17**] led the company to discontinue their sale. Later in the 1990s, Shadow Robot introduced the Shadow Air Muscle to the market. In addition to individual muscles, Shadow Robot offered robotic systems such as the Dexterous Hand which was powered by PAM. In 2001, Daerden et al [**18**] introduced a new design of PAM called the pleated PAM. The new muscle design intended to eliminate any material deformation and friction by rearranging the muscle membrane so that unfurls when it is inflated (e.g. accordion bellows). This would ultimately yield a muscle operation with no hysteresis or energy loss. In 2002, Festo Corporation developed the Fluidic Muscle [**19**] where its external structure consisted of a single unit that was manufactured using aramid fibers that were embedded into chloroprene rubber. To avoid friction between fibers, the aramid fibers layers were placed at separate levels within the chloroprene rubber as shown in Figure 2-6.

Figure 2-4: Cross section view of the Fluidic Muscle by Festo Corporation **[**20**]**.

Historically, as its name would indicate, PAM has been powered by compressed air pressure that varies between 0.3 to 0.8 MPa. However, a hydraulically driven artificial muscle has also been considered by researchers, [**21**], to produce substantially larger muscle force. Using liquid fluid instead of gas drastically modifies the dynamic behaviour of the artificial muscle. This includes the loss of muscle compliance, passive behaviour as an air spring, and the loss of potential storage of compressed fluid. Among others, these factors eliminate the feasibility of using a hydraulic driven artificial muscle for prostheses-type of applications. As a consequence, hydraulically driven artificial muscle will not be further investigated in this thesis.

2.1.2 PAM Current Status

Throughout the last decades, various types of PAM have been developed; they can be mainly distinguished by the design of their external membrane and end fixtures. Currently, PAMs are manufactured only by two companies, namely Shadow Robot and Festo Corporation.

As shown in Figure 2-5, similar to the majority of PAM, the Shadow Air Muscle by Shadow Robot is made of an elastic bladder protected by a separate plastic braided sleeve. Both materials constitute the wall structure of the muscle. To transfer muscle force and retain muscle pressure, gear clamps and crimp rings are used to hold the bladder and the sleeve together with plastic end-fixtures. In this case, the muscle expansion is governed by the braided sleeve geometrical properties; the sleeve contracts axially when the tube inflates and expands radially. The use of gear clamp and crimp rings in these muscle designs limits the mechanical load that can be transferred by the muscle and also provides a weak gas seal at the muscle end-fixture. As a consequence, Shadow Robot[**22**] recommends that the Shadow Air Muscle should not be inflated to a gage pressure surpassing 206.8 KPa (30 psi) without load and should never surpass an operating pressure of 413.6 KPa (60 psi).

Figure 2-5: The Shadow Air Muscle by Shadow Robot **[**22**]**.

Shadow Robot does not offer detailed technical information about their PAM; however, primary muscle performance for the three available muscle sizes is presented on their websites shown in Table 2-1. According to the provided information, the maximum muscle force generated by the largest muscle size (30 mm in Diameter) is 686.5 N. As will be shown later in Chapter 3, the magnitude of this muscle force is insufficient to actuate a transfemoral prosthesis and the size of this muscle diameter cannot be accommodated by the apparatus of the prosthesis.

Table 2-1: Shadow Air Muscle Range **[**23**]**

Products	Braid Diameter	Length (Stretched)	Air fixtures size	Pull at 50 psi	Maximum Pull
	6mm	150 mm	4 mm	29.4 N	69 N
	20mm	210 mm	4 mm	117.7 N	196 N
	30mm	290 mm	6 mm	343.2 N	686.5 N

Whereas the muscle produced by Shadow robot consists of a bladder that is wrapped by a braided sleeve, Festo Corporation offers a muscle design that consists of an elastic bladder embedded with aramid fibers that creates a trapezoidal pattern with a three-dimensional braid structure. Both muscles operate similarly, as the muscle is inflated, the muscle expands in diameter causing the braid or fiber angle to steepen and forcing the muscle to shorten. Distinctively, as shown in Figure 2-6, the Fluidic Muscle DMSP/MAS [**19**] incorporates a press fit design for the end-fixture which permits the muscle to withstand a large gage pressure and mechanical loading. The service life of this PAM is estimated between 100,000 and 10 million switching cycles for typical applications. This performance is a function of the relative contraction, operating pressure, loading behaviour and operating temperature of the muscle [**19**].

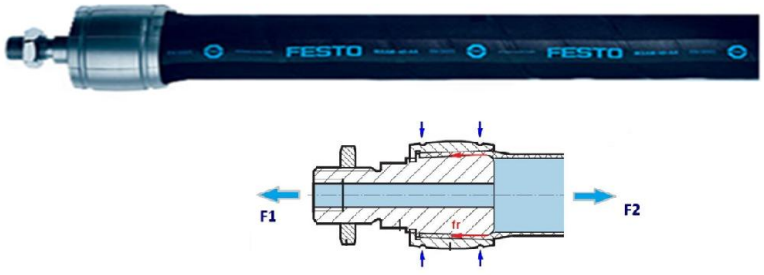

Figure 2-6: The Fluidic Muscle (DMSP) by Festo Corporation **[**24**]**

Similarly to a typical PAM, the Fluidic Muscle by Festo generates a maximum pulling force at full extension and decreases as the muscle contracts. Festo states that the effective operating

range of the Fluidic Muscle is up to 15% of contraction length [**24**]. The maximum pulling force by the Fluidic Muscle for the available diameter sizes is shown in Table 2-2. Whereas the largest muscle diameter (40 mm) produces a sufficient force to actuate a transfemoral prosthesis, the prosthesis cannot accommodate this muscle size. The press fit connection by FESTO holds the rubber tube by friction which depends on the transversal force as shown in Figure 2-6. This type of connection limits the muscle operating pressure to 120 psi which results in weak muscle forces for small diameter Fluidic Muscles.

Table 2-2: FESTO Fluidic Muscle Range

Products	DMSP Diameter	DMSP Length	Max. Pressure	Max. force
	10 mm	40 - 9000 mm	116 psi	630 N
	20 mm	60 – 9000 mm	90 psi	1500 N
	40 mm	120 - 9000 mm	90 psi	6000 N

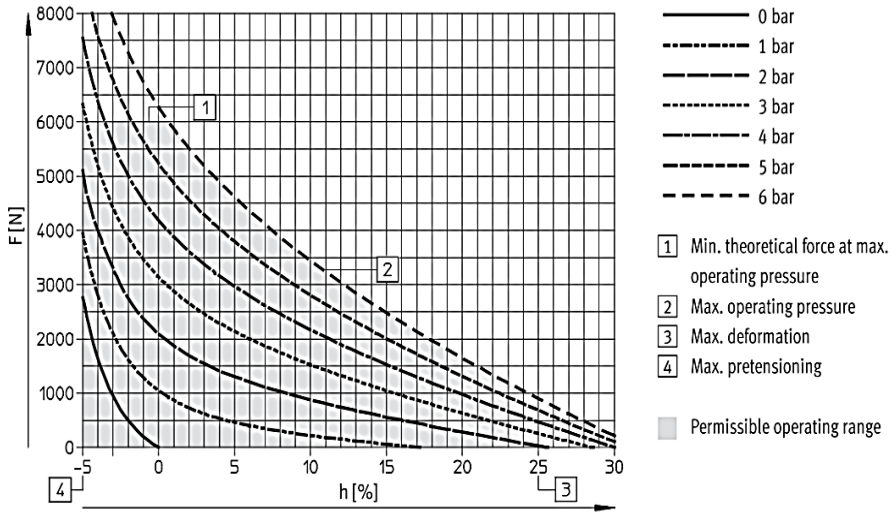

Figure 2-7: Testing results for Fluidic Muscle (DMSP- 40) by Festo Corporation. Plot presents muscle force as a function of muscle contraction distance (%) for a range of pressure of 0 to 0.6MPa (i.e. 6 bar) **[**24**]**

2.1.3 PAM Modeling

In this thesis, analytical models derived in [**10**]are used to predict muscle contraction distance and muscle force behavior before designing and fabricating PAM prototypes. The PAM consists of an elastic bladder that is enclosed by a braided mesh. Assuming that the muscle retains a cylindrical shape, its geometry is governed by the braid and its relationship is based on a helix form as shown in Figure 2-8.

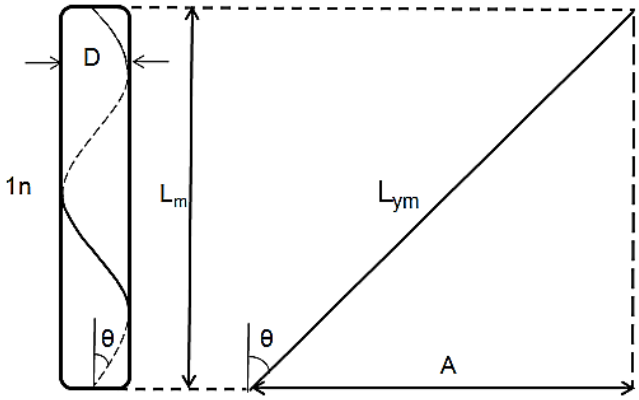

Figure 2-8: Geometrical properties for the braided mesh that reflects the muscle middle section **[**10**]**.

In Figure 2-8, θ is the braid angle, L_{ym} is the uncoiled fiber length and n is the number of fiber revolutions over the length L_m. The relationships between the muscle diameter D and the muscle length L_m are given by:

$$D = \frac{L_{ym} sin\theta}{\pi n} \tag{2-1}$$

$$L_m = L_{ym} \cos\theta \tag{2-2}$$

The PAM static model is obtained by balancing the longitudinal forces developed due to the muscle gage pressure P. Assuming that the muscle retains a cylindrical shape and that the wall thickness, muscle friction, and muscle bladder mechanical properties are ignored, the muscle static force F is given by [**10**]:

$$F = -P\left[\frac{L_{ym}^2 - 3L^2}{4\pi n^2}\right] \tag{2-3}$$

2.2 LOWER LIMB PROSTHESES

As previously stated, commercially available lower limb prostheses range from simple mechanical devices to advanced microprocessor controlled systems. These medical assistive devices can be classified into two main categories, passive or powered. For passive lower limb prostheses, the weight of the patient is simply transferred to the rigid body of the prosthesis and into the ground. Whereas passive devices do not add energy to a system, newly designed passive prostheses can store and release energy. Figure 2-9 shows the XT9 Energy-Storing Prosthetic Knee (ESPK), which implements a combination of an energy-storing spring with an air damper to absorb and convert energy[**25**].

Figure 2-9: (a) The "XT9" Energy-storing Prosthetic Knee (ESPK) by Symbiotechs USA **[**25**]**

More advanced passive knee joints also incorporate hydraulic or pneumatic cylinders that adjusts the flexion and extension rate of the artificial limb for comfortable gait at different walking speeds[**26**][**27**]. The adjustment of this rate can be accomplished manually for purely mechanical prostheses (e.g. Otto Bock-3R106) or automatically for advanced microprocessor controlled prostheses (e.g. C-Leg by Otto Bock) [**28**]. Among the most successful microprocessor controlled prostheses are the C-Leg by Otto Bock, and the RHEO knee by Ossur and the Mauch SNS by Ossur as shown in Figure 2-10.

Figure 2-10: (a) Mauch SNS by Ossur, (b) C-Leg by Otto Bock, (c) Rheoknee by Ossur **[**29**][**30**]**

According to [**31**], the three presented prostheses in Figure 2-10 use different technologies to deliver similar functionalities. Using gait sensors, patient gait phases are constantly identified and transferred to a microprocessor in order to control the impedance of hydraulic-based (C-Leg Otto Bock) or magnetorheologic-fluid–based (Rheo Knee by Ossur) damper [**28**]. The continuous and adaptive control of impedance within these systems yields improved ambulation performance as the patient varies walking speed. The control system maintains a free swing of the prosthetic during the swing phase and resists knee buckling during the stance phase.

Gait analysis in[**32**][**33**] has demonstrated that transfemoral amputees' ambulation performance (e.g. walking symmetry, walking speed, and comfort) improves significantly when using controlled impedance prostheses compared to pure mechanical prostheses. However, these advanced controlled prostheses do not provide significant improvement in terms of energy consumption over pure mechanical prostheses [**31**]. Thus, without powered prostheses, transfemoral amputees consume more energy than a normal individual during ambulation. Moreover, lack of power for the knee prosthesis prohibits transfemoral amputees from having a healthy normal gait.

Powered assistive devices may add substantial energy to the system such that patients avoid performing additional muscle activity to compensate for their disability and thus save energy and improve their gait. As an example, above knee amputees use their hip muscles excessively during ambulation so as to lift the prosthesis and clear the ground while swinging the device

forward. If a powered lower limb prosthesis is used such that the knee joint biomechanics are restored, this excessive hip muscle activity would be unnecessary and overall energy expenditure would be reduced. Analysis of the gait of transfemoral amputees in the frontal and transverse plane was presented in [**34**] and demonstrated gait asymmetry between the prosthetic and intact leg. Figure 2-11 shows the kinematics of the intact leg versus the prosthetic leg for the hip joint, which demonstrates the excessive kinematic activity that an amputee must perform for ambulation. Gait analysis results show positive obliquity of the hip, indicating hip-hiking by the amputee to avoid any contact between the prosthesis and the ground during the swing phase (see Figure 2-11).

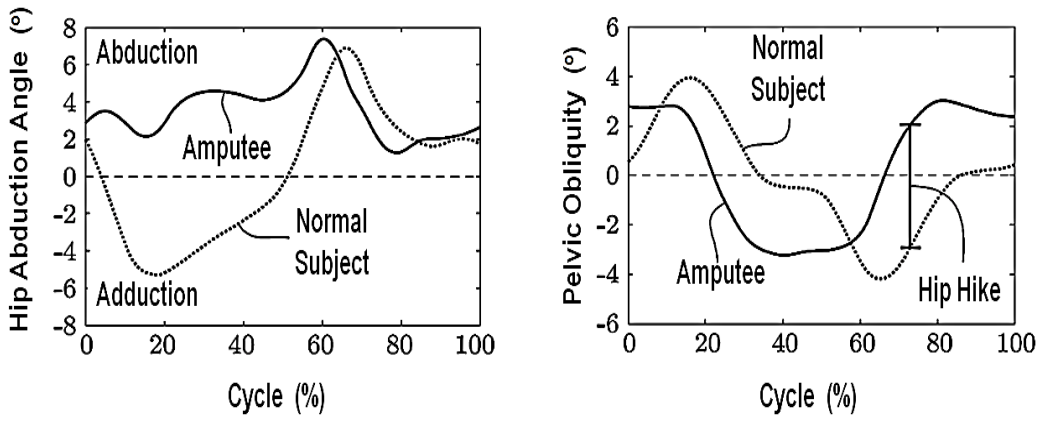

Figure 2-11: kinematics of the intact leg versus the pros**t**hetic leg of a subject for the hip joint. Graphs are plotted as percentage of gait cycle, where 0% is heel strike and 100% is subsequent heel strike **[**34**]**.

Whereas there has been a great effort towards integrating powered prostheses into assistive devices, transfemoral prostheses are still dominantly passive. This is attributed to the higher power and energy requirements of ambulation and the restriction of weight and space that a patient can accommodate [**6**].

Currently, there is only one powered knee prosthesis that offers more than just an impedance adjustment throughout walking. Relying on sensors, a ball screw mechanism, microprocessor and electrical power, the Power Knee by Ossur provides amputees with the ability to walk naturally without excessive physical and mental effort [**35**]. This is attributed to the ability of the Power Knee to bend and straighten the knee. Thus, patients are not required to perform additional muscle activities to compensate for their disability. However, the success of the Power

Knee prosthesis is hindered by many factors but mainly by its mass, cost, as well as energy consumption [**36**]:

- The mass of a Power Knee is 4.7 kg which is approximately 3 times the mass of comparable devices such as the C-Leg by Otto Bock [**36**].
- The cost of a Power Knee is $90,000 which is approximately 5 times the cost of comparable devices such as the C-Leg by Otto Bock [**37**]
- The Power Knee provides up to 6 hours of continuous operation to patient depending on level of activity [**37**]
- The Power Knee is unfeasible for bilateral amputees since the control system relies on feedback from the user's sound leg (i.e. echo control) [**36**]
- The actuation mechanism (i.e. ball screw) is noisy and draws attention[**38**]
- Given its size, only men in the top 50th percentile in height can use it [**38**]
- Given its size, there is limited compatibility with existing ankle and feet prostheses [**38**]
- Powered or active ankle joints are not an option

Figure 2-12: The Power Knee by Ossur **[**39**]**

In the author's opinion, the main factors that hinder the success of the Power Knee prosthesis are related to its electrical actuation. Unlike skeletal muscle or PAM, electrical motors are heavy and do not possess passive behaviour. Thus, continuous electrical energy must be consumed by the motor throughout the gait cycle. While skeletal or artificial pneumatic muscles can rely on their passive behaviour to resist knee flexion during the stance phase, the Power Knee prosthesis must consume energy to counterbalance the knee joint torque during the stance phase.

Though the Power Knee prosthesis by Ossur is the sole commercially available powered knee prosthesis, it is worth noting that powered knee prostheses have been in development in research laboratories since the 1970's [**40**][**41**]. In 1998, Klute et al. [**42**] presented a poster that offers the PAM as a solution to powered lower limb prostheses. In this document, a hydraulic cylinder placed in parallel with a pneumatic artificial muscle was proposed to mimic Hill's muscle model. Later, in [**43**], Klute et al. presented the design of a bio-robotic actuator intended for use in powered below-knee prostheses. To generate an appropriate large force, the design consisted of two pneumatic artificial muscles placed in parallel with a damper (hydraulic cylinder). Each muscle had a nominal diameter of 31.75 mm, operated at a maximum pressure of 0.5 MPa (72 psi) and together produced a peak force of approximately 2000 N.

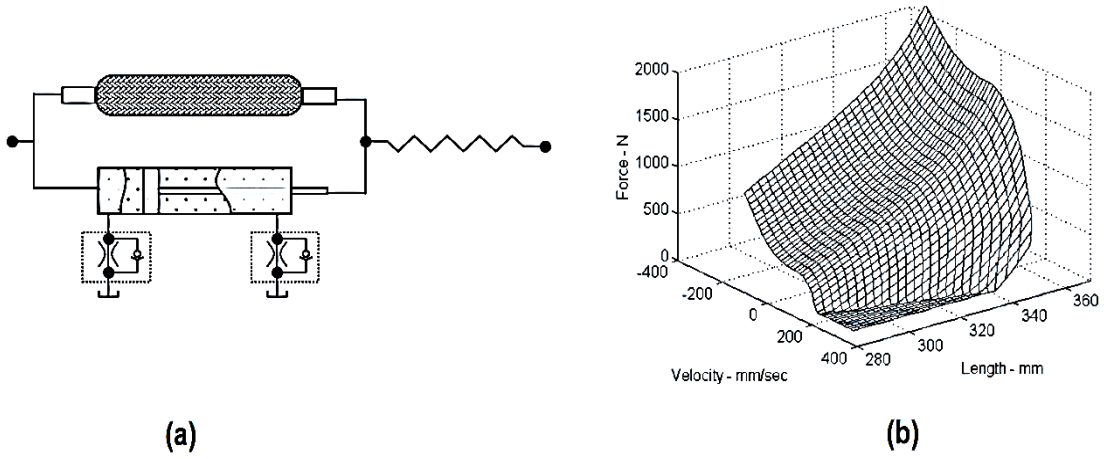

Figure 2-13: (a) Pneumatic artificial muscle placed in parallel with a hydraulic damper and together in series with an energy storing tendon(b) Predicted output force of PAM as a function velocity and contraction length based on the setup in (a) **[**43**]**

More recent research development, in 2008, Sup et al. [**6**]designed a pneumatically powered transfemoral prosthesis to serve as a laboratory test bed for a subsequent self-powered version. The knee and ankle joints of the prosthesis were powered by two double-acting pneumatic cylinders which were placed in a slider-crank configuration Figure 2-14 (b). Operating at a pressure of 2 MPa (300 psi), each actuator (Bimba model 17-2.75-DP) consisting of a 3.8 cm bore, is capable of producing an outward and return force of 2,270 N and 2,070 N, respectively. Test results in Figure 2-14(a) show the ability of the proposed prosthesis to deliver required knee joint torque during slow cadence, stair climbing and fast cadence; however, it fails to satisfy the ankle joint torque requirements for a user mass of 75 kg.

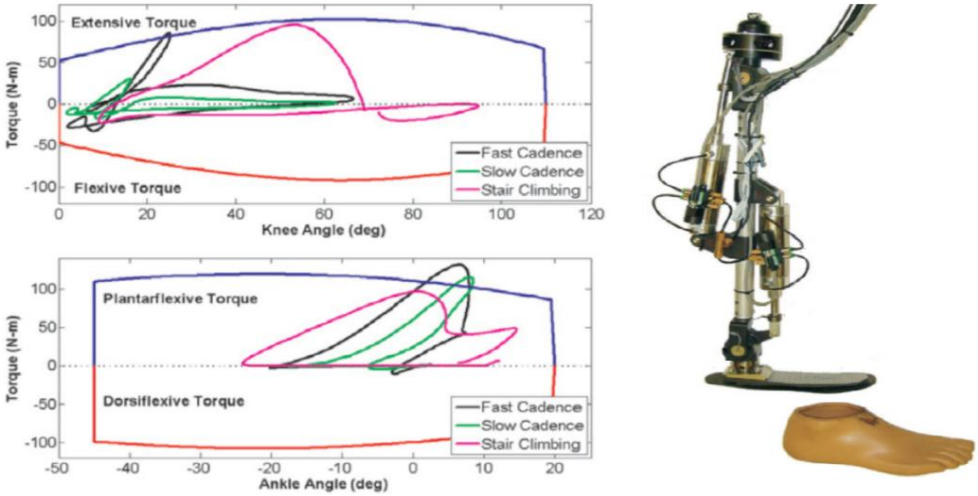

Figure 2-14: (a) Torque envelope of actuator configurations along with the data for a 75 kg normal human for slow and fast cadence and stair climbing. **[**6**][**44**][**45**]**. **(b)** Power-tethered prototype by Sup el al.**[**6**]**

Later in 2009, Sup et al.[**46**] proposed a similar slider-crank mechanism design and control for a fully self-contained prosthesis. Unlike the previous design, this device is electrically powered by motor-ball screw actuators and incorporates a spring at the ankle joint to contribute additional propulsive force at toe-off of the foot. Though the authors do not mention the maximum torque that can be produced by the prostheses, they state that the device provides knee torques over 40 Nm (during stance flexion) and ankle torques over 120 Nm during toe-off. Electrical power requirements suggest a battery life of approximately 1.8 hours of walking or 12 hours of standing.

Figure 2-15: Self-contained powered knee and ankle transfemoral prosthesis by Sup et al.**[**46**]**

In 2006 and 2008, Versluys et al. presented a prototype of pneumatically powered below-knee (BK) prosthesis [**47**][**48**]. Using Pleated PAM, the proposed prosthesis provides an active push-off that mimics the plantar flexion of a biological limb. Moreover, adaptable compliance of the prosthesis is achieved by regulating pressure. An ankle torque of 110.5 Nm is achieved by the back muscles during normal gait at a pressure of 0.15 MPa (21 psi). Whereas this pressure is significantly low, the authors do not mention the size of the PAM and the moment arm. From Figure 2-16, it can be seen that the prosthesis substantially surpasses the volume of a biological limb and thus would accommodate only a small percentile of population.

Figure 2-16: Prosthesis prototype by Versluys et al.**[**48**]**

In 2010, Yeh et al. [**49**] used PAM to power a lower-limb orthosis. Though the authors have not indicated the magnitude of the torque or force produced by the apparatus, Figure 2-17 shows that the orthosis incorporates the Air Muscle that is manufactured by Shadow Robot. The operating condition and capabilities of the Air Muscle have been previously presented and thus no further discussion will be reported.

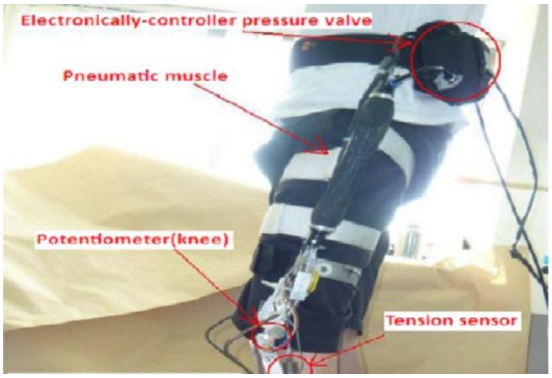

Figure 2-17: PAM powered Orthosis by **[**49**]**

In 2010, inspired by the unexplored application of PAM to transfemoral prostheses, Waycaster et al. [**50**] proposed the development of a transfemoral prosthesis powered by PAM. The prosthesis design incorporates two PAMs (DMSP-40-180N by FESTO) in an antagonist setup and a timing belt-pulley drive that is connected to the prosthesis structure as shown in Figure 2-18. The proposed design is intended to produce a knee joint torque up to 140 N-m so as to satisfy the gait requirements for a 75 kg user during level walking at normal and slow cadence.

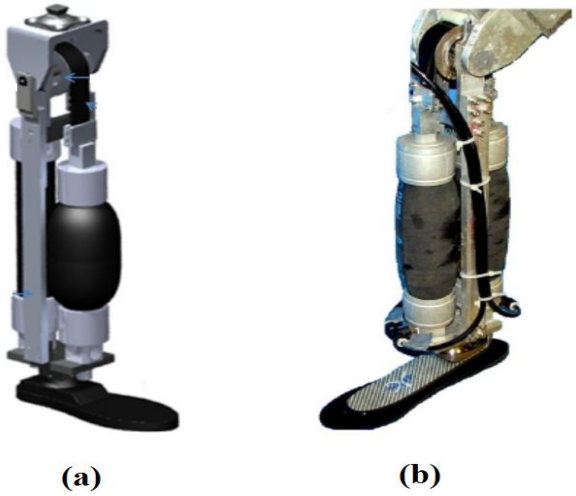

Figure 2-18: (a) Prosthesis design (b) Fabricated prototype **[**50**]**

To maximize the diameter of the PAM (to maximize muscle force) and minimize the volume of the prosthesis, Waycaster et al. designed an open-frame structure (no central beam) allowing the expansion and deflation of adjacent PAMs without interference with each other, Figure 2-18. Such a design permits the prosthesis to achieve a bi-directional actuation or simple knee joint extension and flexion. Operating at a pressure of 653 KPa (94.7 psi), the prosthesis was tested to generate a knee torque that satisfies gait requirements for a 75 kg user during level walking at a normal and slow cadence (Figure 2-19). Though the kinetics requirement was satisfied, significant PAM diameter expansion was observed.

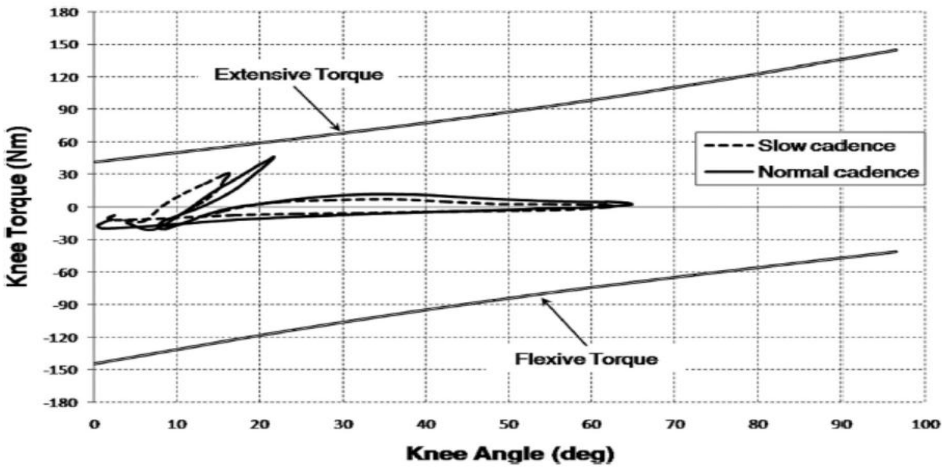

Figure 2-19: Torque trajectories for level walking at slow and normal cadence **[**44**]** compared joint actuation torque by prosthesis **[**50**]**

Although, it is not indicated by Waycaster et al., the DMSP-40-180 by FESTO has an unstressed diameter of 40 mm and upon inflation the muscle expands radially by more than 200 %. Such PAM expansion results in an unpractical prosthesis volume which may only be accommodated by a very small percentile of the population. Smaller diameters PAMs by FESTO are available; however, operating at a maximum pressure of 120 psi, they are incapable of providing sufficient force to produce the required knee joint during normal and slow cadence.

One of the objectives of Waycaster et al. for this research was to demonstrate the capability of PAM to generate sufficient knee torque to meet the locomotive requirements for a 75 kg user during slow and normal cadence. In the author's opinion, Waycaster et al. have demonstrated that existing PAMs do not have the capability to satisfy these requirements while offering a practical size for the assistive device.

Chapter 3

BIOMECHANICS OF A KNEE JOINT

The objective of this thesis is to design a PAM that satisfies the kinetic and kinematic requirements of a human knee throughout walking, stair ascending/descending and sit to stand movements. Moreover, the proposed PAM design should meet the weight and size constraints of a human lower limb. To achieve these objectives, chapter 3 presents the biomechanics of a human knee, in order that the design requirements of the PAM can be identified.

3.1 HUMAN KNEE JOINT

The knee is the largest and most complex joint of the human body. It has an indispensable role in our daily activities; it supports the body weight as an individual travels horizontally and vertically such as walking and ascending stairs. While transferring a substantial load from the upper body, the knee joint allow an impressive relative motion in three anatomical planes, namely sagittal, coronal and transverse plane, estimated as 6 degrees of freedom (Figure 3-1).

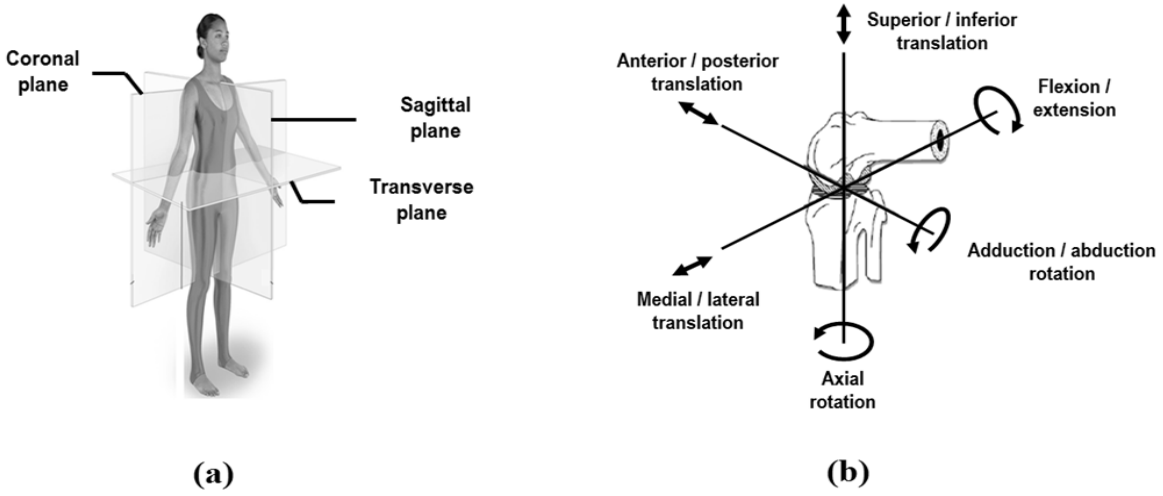

Figure 3-1: (a) Anatomical planes **[**51**] (b)** Degrees of motion of the knee joint **[**52**]**

As shown in Figure 3-2, the knee consists of three joints that are enclosed by one cavity. The articulating bones within these joints are the femur, tibia and patella. The femur is the largest and strongest bone in the body, it articulates proximally with the hip and distally with the tibia and patella. The patella is a sesamoid bone that protects the knee joint and assists in transmitting the pulling force of the quadriceps muscle to the tibia. Furthermore, the patella acts as a lever arm of the knee extension mechanism. The patella increases the mechanical advantage of extensor muscles (i.e. quadriceps femoris muscle) by transmitting forces across the knee at a greater distance from the axis of rotation. The tibia is the medial leg bone and articulates proximally with the femur and distally with the talus and tibia. The tibia transfers the weight of the body at the knee joint to the foot through the ankle joint. Two fibrous C-shaped cartilage pads, namely the medial and lateral menisci act as shock absorbers and conform to the shape of the articulating surfaces to distribute load as the femoral and tibial condyles articulate with respect to each other [**51**].

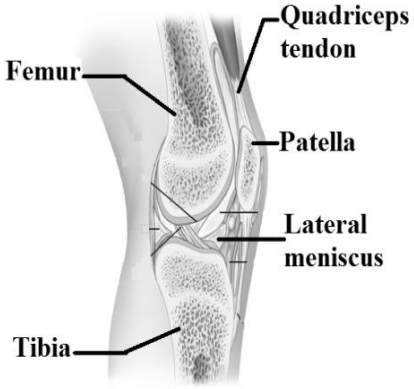

Figure 3-2: Knee joint anatomy **[**51**]**

Relative motion about the knee joint is achieved by a group of muscles and restrained by a set of extra-capsular and intra-capsular ligaments. There are three major muscle groups associated with the knee joint, the quadriceps group, hamstring group, and gastrocnemius and popliteus muscles. The quadriceps group corresponds to the anterior muscles which are identified as the flexors. They are connected to the highest border of the patella, which via the patellar ligament is connected to the tibia. This group of muscles is responsible of extending the leg about the knee joint. The hamstring group corresponds to the posterior muscles which are identified as the extensors. They are connected to the medial surface of the tibia and are responsible for flexing

the leg about the knee joint. The sartorius muscle is obliquely located and inserted anteriorly to the tibia. This muscle contributes to the tibia rotation when the knee joint is flexed and not bearing any weight. Finally, the popliteus is a posterior muscle about the knee joint which assists in inward rotation of the tibia and unlocks the knee before flexion [**53**].

3.2 HUMAN GAIT

Identifying PAM requirements for powered prosthesis applications requires a full understanding of human gait. Motions of the lower limbs have been extensively studied by performing clinical gait analysis which involves motion capture systems and force plates that record the kinematic and kinetic data of the subject, respectively. The simplest model of human gait consists of a subject moving in the sagittal plane as shown in Figure 3-3. Human gait is a cyclic motion that begins and ends with the heel strike of the right leg. The gait is divided into two phases namely, a stance phase (the foot is on the ground and supports the weight of the body), and a swing phase (foot is in the air).

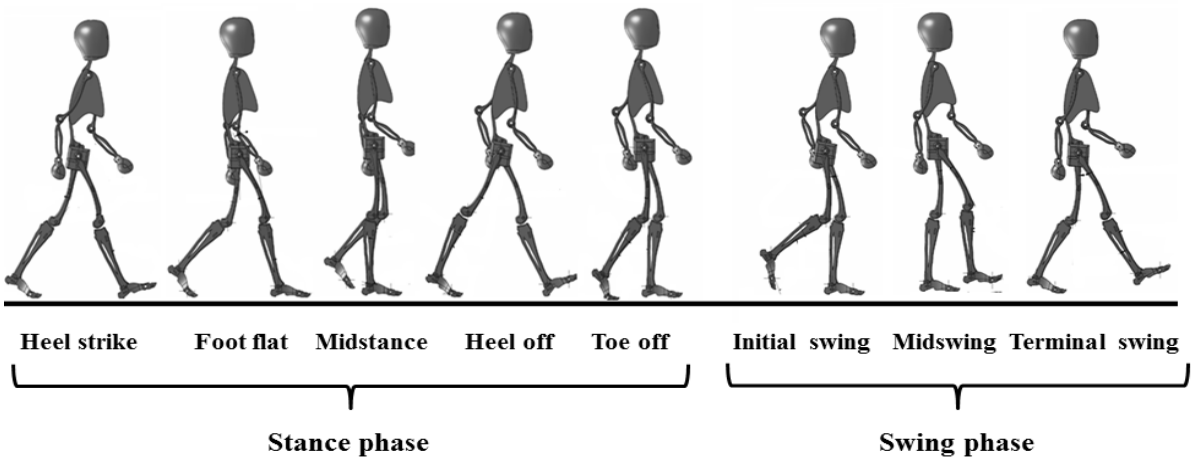

Figure 3-3: Human gait model in sagittal plane illustrated via Solid Works

The stance phase consists of approximately 60% of the gait cycle during normal walking and it is subdivided into five phases namely, heel strike, foot flat, midstance, heel off and toe off. The swing phase consists of approximately 40% of the cycle during normal walking and it is subdivided into three phases namely, initial swing, midswing and terminal swing. Double stance

(two lower limbs support) occurs when one leg is finishing and the other is starting the stance phase. This occurs twice during a gait cycle as shown in Figure 3-3.

3.2 ANTHROPOMETRIC MODEL

For powered lower limb prostheses, size and mass are critical design requirements. Due to symmetry of the human body, balance has to be considered when designing a replacement to an amputated limb. A successful prosthesis should reproduce the mass and inertial characteristics of a sound human limb. Thus, for a transfemoral amputee, the mass of the prosthesis should be approximately the same as a biological lower limb. According to [**54**], the mass of each segment of the lower limb is expressed as a function of the total body weight *BW* as shown in Table 3-1.

Table 3-1: Lower limb segments mass

Anatomical Segments	**Weight**
Foot	0.0145*BW*
Lower leg	0.0465*BW*
Upper leg	0.1000*BW*

According to Table 3-1 and assuming a subject of 75 kg of body mass, transfemoral prosthesis should not surpass the lower leg mass of approximately 3.5 kg. This is a substantial design challenge for powered prostheses which include an actuator(s) and a power supply. Moreover, the moment of inertia of the prosthesis about the hip joint should be equivalent to anthropometric norms to prevent additional work at the hip. The gravity center depends on the mass, the form and the length of each body part. With respect to the lower leg, its gravity center G_{LG} is located at a distance of 0.42 L_{LG} from the proximal end of the lower leg at the rear side of the shinbone, where L_{LG} is the length of the lower leg. Using anthropometric data from Figure A3.1 [**55**], a graphically illustration of the lower limb via Solid Works is shown in Figure 3-4.

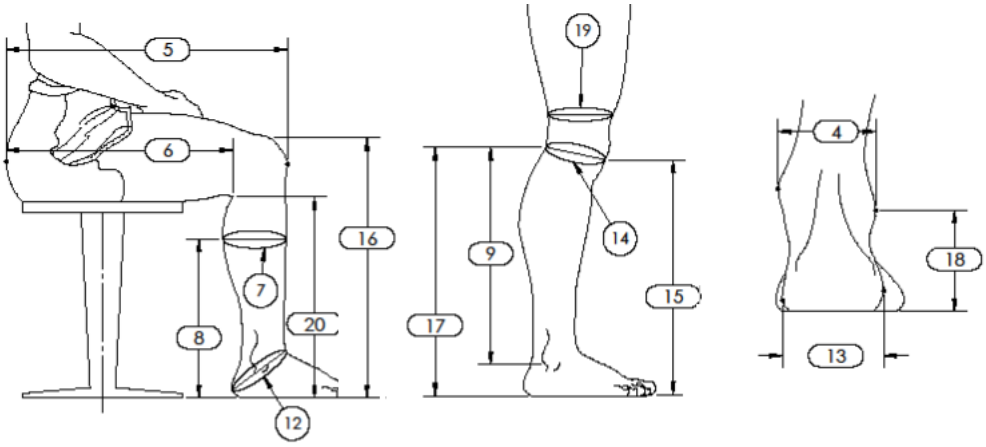

Figure 3-4: Standard male adult calf and foot geometry illustrated via Solid Works

With reference to Figure A3.1 and Figure 3-4, a female and male subject with a height of 1.75 meters would have a calf link length (#9 in Figure 3-4) of 40.04 and 43.45cm, respectively, a calf circumference(#7 in Figure 3-4) of 35.24 and 37.8cm respectively, and a heel breadth (i.e. #13 in Figure 3-4) of 6.3 and 7.01cm, respectively. This would imply that powered lower limb prostheses can be no longer than approximately 40cm in length and 11cm in diameter.

3.4 KINEMATICS OF THE KNEE

Kinematics is the study of body motion with no consideration to mass or forces. The relative motion of the knee joint is a combination of rolling and sliding that is achieved in the three anatomical planes as shown in Figure 3-1. The knee joint has six degrees of freedom; however, the most significant amount of motion occurs in the sagittal plane. Angular displacement range in this plane ranges from 0^o to 140^oor from maximum extension to maximum flexion, respectively. Thus, this justifies the replication of knee motion by prostheses designers using mostly a hinge type of joint. The range of motion of the knee joint during level walking for all three anatomical planes is shown in Figure 3-5 .

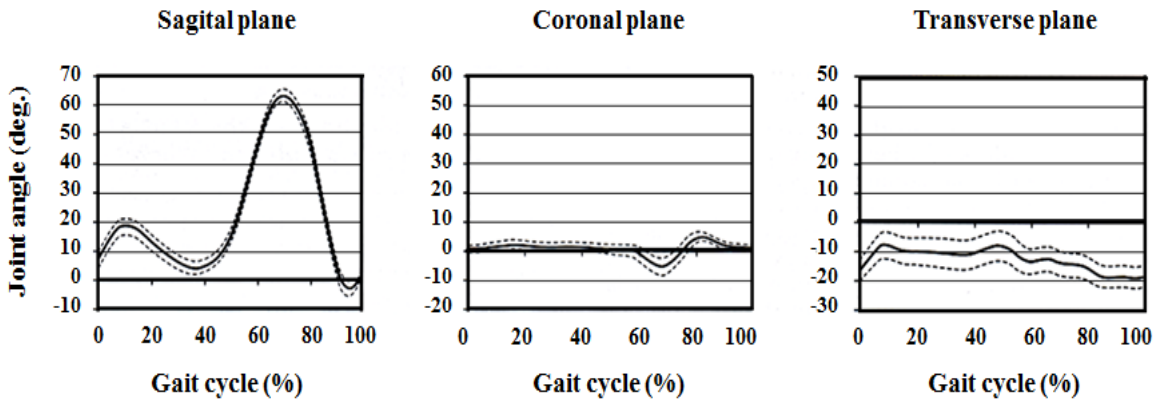

Figure 3-5: Knee range of motion during level walking. Sagittal plane: extension >0°, flexion <0°.Coronal plane: adduction>0°, abduction <0°.Transverse plane: internal rotation >0°, external rotation <0°. [**56**].

A human knee range of motion is a function of the performed activity and speed. As shown in Table 3-2, the maximum knee flexion occurs when the person is lifting an object but for typical daily activities, the knee joint requires no less than 117°of flexion [**56**].

Table 3-2: Range of knee motion in the sagittal plane throughout typical activities **[**56**]**

Activity	Range of motion from extension to flexion
Walking	0 - 67°
Climbing stairs	0 - 83°
Descending stairs	0 – 90°
Sitting down	0 – 93°
Tying a shoe	0 – 106°
Lifting an object	0 – 117°

Any restriction in the knee joint is compensated by the increase of motion in other joints. As shown in **Error! Reference source not found.**, the increment in speed requires increment of motion or more flexion in the knee joint [**56**].

Table 3-3: Amount of knee flexion during stance phase of walking and running **[**56**]**

Activity	Knee flexion during stance phase
Walking	
- Slow	0 – 6°
- Free	6 – 12°
- Fast	12 – 18°
Running	18 – 30°

Having identified that the angular displacement of a knee joint for typical daily activities is 117^{o}, the contraction distance of the quadriceps muscle can be determined as a function of the distance between the center of rotation of the knee and the patella-femoral contact. Measurements of this distance which also corresponds to the moment arm are typically obtained from radiological imaging. Figure 3-6 shows the relationship between the moment arm and flexion angle of the knee joint. The variation of knee moment of arm provides the knee the ability to produce a large knee moment during mid-flexion angle (30 to 60^{o}) and achieve a large angular displacement during other phases. This behaviour minimizes the required force and contraction distance produced by the quadriceps muscles.

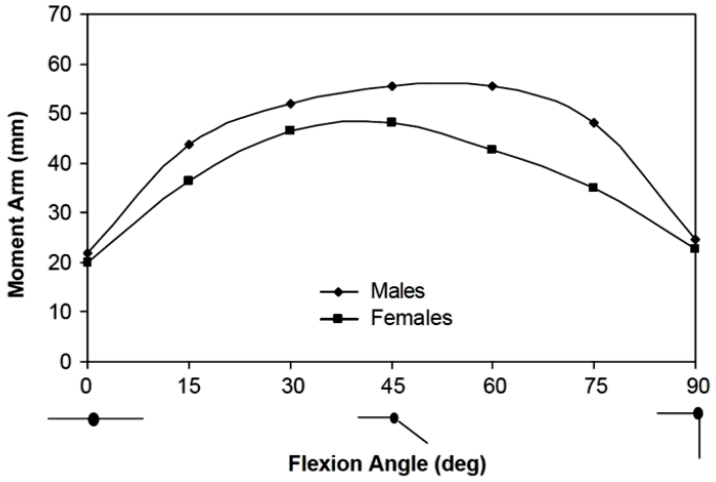

Figure 3-6: Knee moment arm versus knee flexion angle from male and female adults [**57**]

With reference to Figure 3-6, the moment arm of the patellar tendon is measured in three dimensions; however, according to [**57**], similar results are also found when the moment arm is only measured in the sagittal plane. Using GetData Graph Digitizer, Figure 3-6 is digitized such that the graph data is extrapolated to identify the values of moment arms as a function of the knee flexion angle. These results are presented in TableA3.1 (Appendix A). The identification of the range of motion of the knee, coupled with the prosthesis design criteria will dictate the contraction distance that is required by the PAM.

3.5 KINETICS OF THE KNEE

Kinetics is the portion of biomechanics that studies the motion of a body when considering the mass and forces. This study includes static and dynamic analysis of forces and the movements resulting from the application of those forces. Whereas experimentally measured moments about the knee consider the dynamics of the subject, in this research, a quasi-static force analysis is employed to determine the kinetic requirements of the PAM. This assumption is valid during high energy activities such as sit to stand movement or ascending stairs where the speed of the subject is relatively slow.

To perform a static force analysis of a subject during gait, a free body diagram that illustrates the dimension and external forces must first be drawn. Using SolidWorks, a three-dimension model of a human subject is created using anthropometric data from [**58**] and [**55**]. Thus, the dimensions of the model shown in Figure 3-7 are proportional to a standard human body height.

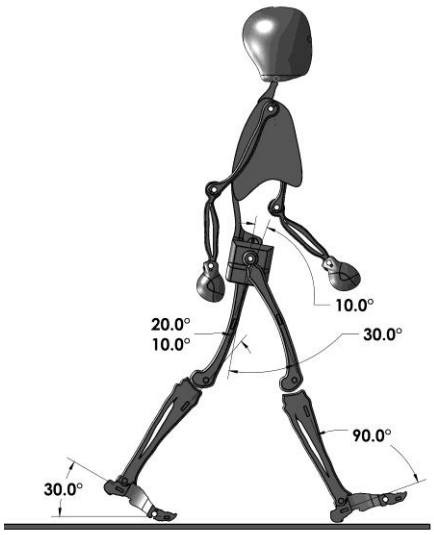

Figure 3-7: three-dimension model of a human subject in double stance phase

This Solid Works model of the subject facilitates the illustration of subject position and automatically determines the geometrical properties for each of the study cases namely, walking, ascending stairs and sit to stand movement. Whereas a static analysis throughout the gait for each study case is possible, in the following section, static force analysis is only performed at peak knee moment that coincides with the highest demand of muscle forces during the stance phase.

As for most biomechanics analysis, each of the study cases would result in a static indeterminate system. However, relying on anatomical and physiological knowledge, additional unknown variables such as muscle forces, friction forces, ligament forces and anatomical distances can be either eliminated or determined. Thus, for each study case, there will be no more than three force vectors, namely one active muscle force, the body weight and a joint contact force.

3.5.1 Static analysis during walking

The static force analysis during walking is achieved by considering a two-dimensional sagittal free body diagram. With reference to [**56**][**45**], the peak knee flexion angle through the stance phase occurs at approximately 16.5 % of the gait cycle which corresponds to the loading response or flat foot phase as shown in Figure 3-3 and Figure 3-8. This phase of the gait also corresponds to the maximum moment produced about the knee.

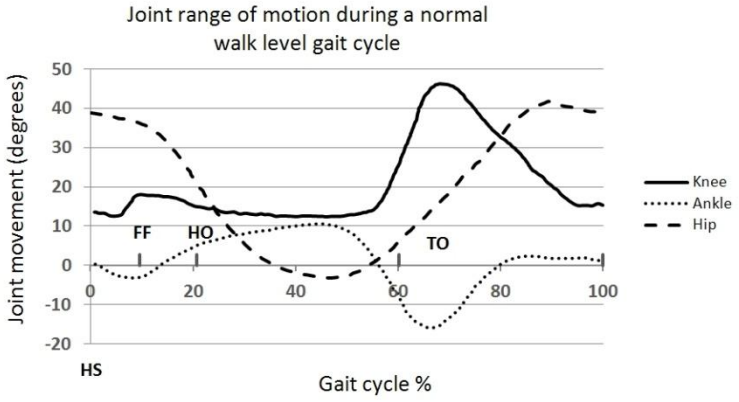

Figure 3-8: Joint range of motion during normal level walk gait cycle adapted from [**56**][**45**]

From Figure 3-8, at 16.5 % of gait cycle, the hip, knee and ankle joints are found at 29^{o}extension, 17^{o}flexion, and 12^{o}dorsiflexion, respectively. Using this information and the anthropometric data presented earlier, two-dimensional sagittal free body diagrams are drawn in SolidWorks as shown in Figure 3-10.The first free body diagram Figure 3-10(a) consists of the entire subject and two external forces namely, the body weight *W*, and the ground reaction force F_g. For static equilibrium, the body weight force is aligned with the ground force reaction and the body weight does not generate any moment about the center of pressure. Thus, the ground friction force is null. As shown in Figure 3-10(b), the second free body diagram consists of the entire subject with exception of the lower leg and foot with three external forces namely, the

femoral-tibial contact force *J*, the quadriceps femoris muscle force vector *Q* and the body weight minus the lower leg and foot W_G. During a single stance of the gait cycle, one foot supports the entire body weight and the weight of the foot and lower leg do not contribute to the moment about the knee joint.

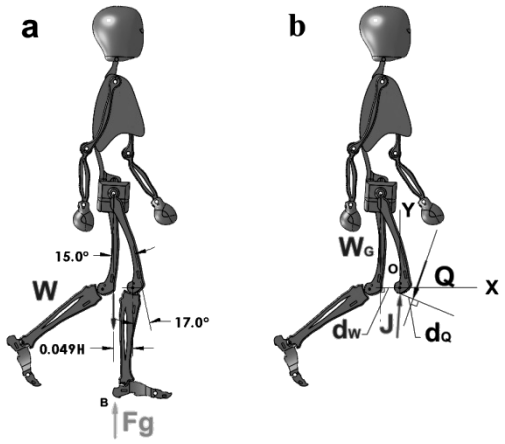

Figure 3-9: Free body diagram of subject during walking

With reference to Figure 3-9(b), *O* corresponds to the femoral-tibial contact point and the center of rotation of the knee joint, d_W is the perpendicular distance between the vector force W_G and point *O* and d_Q is the perpendicular distance between the vector force *Q* and point *O*. Using the Solid Works model of the subject, the location of the center of mass, orientation of quadriceps muscle and perpendicular distances between *Q* and *O* and between *W* and *O* are automatically determined. According to [**59**], the center of gravity of the lower leg and foot is located at 61% of the length of the leg measured from the knee joint. Applying an equilibrium condition at this instant of the gait, the quadriceps femoris muscle force is subsequently determined:

$$W_g = BW - W_L \tag{3-1}$$

Where *BW* is the total body weight and W_L is the weight of the lower leg and foot. From Table 3-1

$$W_L = 0.061BW \tag{3-2}$$

$$or\ W_g = 0.939BW \tag{3-3}$$

From Solid Works model, d_{Wg} is 0.0436H where H is the total height of the body. According to Figure 3-6 and its digitized data in TableA3.1, d_Q is equivalent to 45.54 mm for a knee flexion of 17^o. Applying equilibrium conditions about point O with positive moments in the clockwise direction:

$$\Sigma M = 0 \tag{3-4}$$

$$Q \times d_Q - W_g \times d_{wg} = 0$$

$$Q = \frac{W_g \times d_{wg}}{dq} = \frac{0.939BWx\ 0.049H}{0.02679H}$$

$$\boldsymbol{Q = 1.72\ BW}$$

The above result represents the quadriceps femoris muscle force as a function of body weight that is required to maintain this static position while standing on one leg with 17^o of knee flexion. Applying this result to a subject of 1.7 meters height and 736 Newton (75 Kg) body weight, the required quadriceps force is:

$$Q = 1.72\ BW$$

$$\boldsymbol{Q = 1{,}263.1N} \tag{3-5}$$

The moment contributed to the knee joint by the quadriceps during this instance of the gait is:

$$\boldsymbol{M} = Q \times d_Q$$

$$M = 1{,}263.1\ N \times 0.02679\ H$$

$$\boldsymbol{M = 57.52\ Nm} \tag{3-6}$$

Performing clinical gait analysis using a 3-D musculoskeletal model, Kim [**60**] experimentally determined the knee joint moment throughout the gait as shown in Figure 3-10. For these results, the subject is a 27 year old male with a height of 1.78m and weight of 83kg.

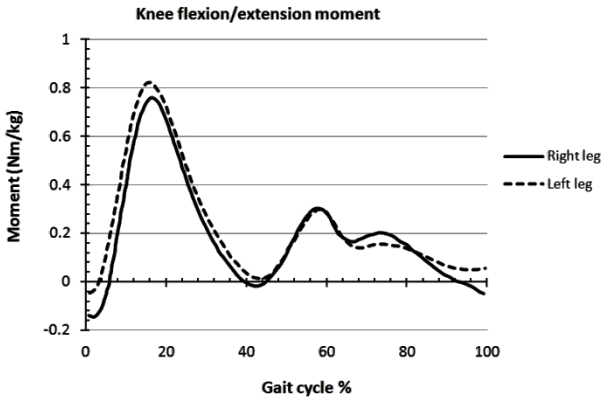

Figure 3-10: Knee moment experimentally obtained as a function of the total body weight **[**60**]**

According to Figure 3-10, for a subject of 736N body weight (75 kg), the moment about the knee joint is 56.89 Nm at 16.49% of the gait cycle, 11% greater than the moment determined from the static analysis. This discrepancy is attributed to the many assumptions made in the static analysis. The static calculation gives an approximation of the force applied by the quadriceps muscle during walking in the sagittal plane; however, this is a three dimensional problem where forces change continually and are affected by several factors such as friction in the joint, friction between the foot and ground, muscle line of pull, momentum as well as movement possessed by the body.

3.5.2Static analysis during stair ascent

Similar to the static analysis during walking, a two-dimensional sagittal free body diagram is considered for analyzing stair ascent. The range of motion for the hip, knee and ankle joint during stair climbing are shown in Figure 3-11 but only the stance phase is considered to determine the maximum quadriceps force.

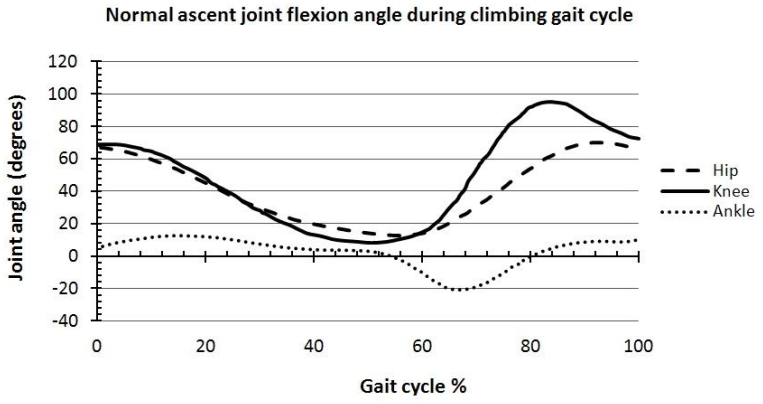

Figure 3-11: Hip, knee and ankle during the stair gait cycle [**45**]

According to [**45**], at maximum knee moment, the joint angles are 49^{o} extension for the hip, 53^{o} flexion for the knee and 12.5^{o} plantar flexion for the ankle. For this instance, Figure 3-12 shows two free body diagrams which include external forces during a single stance stair ascent. During this phase of the movement, the leading lower limb supports and lifts the body to the next step. Assuming static equilibrium, the center of mass of the subject is aligned with the ground force reaction and as such the body weight does not generate any moment and thus the ground friction force is null.

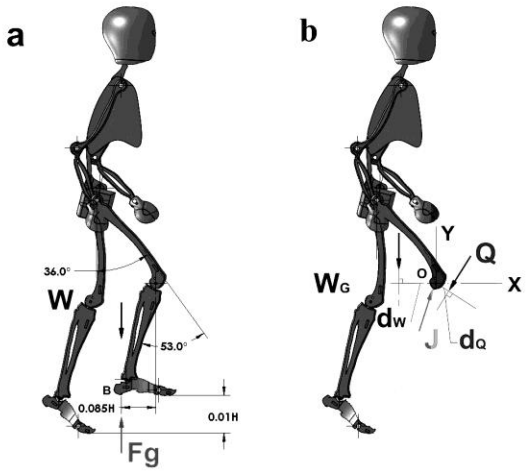

Figure 3-12: (a) Free body diagram 1 of the subject during stair ascent **(b)** Free body diagram 2 of the subject during stair ascent

Using the Solid Works model, at a knee flexion angle of 49°, the perpendicular distance d_{Wg} is equivalent to 0.106*H*. According to Figure 3-6 and its digitized data in TableA3.1, d_Q is equivalent to 36.6 mm (0.0331*H*) for a knee flexion of 53°.

During stair ascent, there are two forces resulting in a moment about the knee. The body weight produces a flexion moment while the quadriceps force produces a counter balancing extending moment. Applying the equilibrium condition, the sum of moments about the femoral-tibial contact point is equal to zero.

$$\sum M = 0$$

$$Q \times d_q - W_g \times d_{wg} = 0$$

$$Q = \frac{W_g \times d_{wg}}{d_q} = \frac{0.939BW \times 0.085H}{0.0331\text{H}}$$

$$\boldsymbol{Q = 2.411\, BW} \tag{3-7}$$

Applying this result to a subject with 1.7 meters height and 736 Newton body weight, the required quadriceps force for ascending stairs at 53° knee flexion is:

$$Q = 2.411 \times 736\text{N}$$

$$\mathbf{Q = 1,773.4N} \tag{3-8}$$

Or the moment contributed to the knee joint by the quadriceps during this instance of the gait is

$$\boldsymbol{M} = Q \times d_Q$$

$$M = 1{,}773.4\, N \times 0.0331H\, m$$

$$\boldsymbol{M = 99.8\, Nm} \tag{3-9}$$

Figure 3-13 displays experimental results for the knee moment during a normal stairs gait cycle expressed as a percentage of the total body weight. According to these results, the maximum knee moment is 1.008BW and occurs at 17.6% of the cycle during the weight acceptance phase.

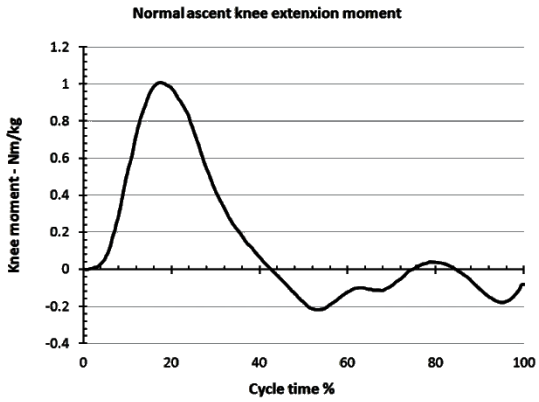

Figure 3-13: Knee Moment during the stairs gait cycle [**45**]

Applying this proportional value to a 75 kg subject, the maximum knee moment is

$$M = \frac{1.008Nm}{kg} \times 75kg$$

$$\boldsymbol{M = 75.6\ Nm}$$

Similar to the previous static analysis, discrepancy between the theoretical and experimental results is attributed to the assumptions made for the static analysis.

3.5.3 Static analysis during sit to stand

During a sit to stand movement, the body weight produces a flexion moment about the knee which is counter balanced by the quadriceps femoris muscle. Figure 3-14shows two free body diagrams which include external forces during a double stance sit to stand movement at a knee flexion angle of 90^o. At this instance, both lower limbs support and lift the body from a sitting to a standing position. The body weight is assumed to be equally distributed on the two lower limbs. Assuming static equilibrium, the center of mass of the subject is aligned with the ground force reactions and as such the body weight does not generate any moment and thus the ground friction force is null.

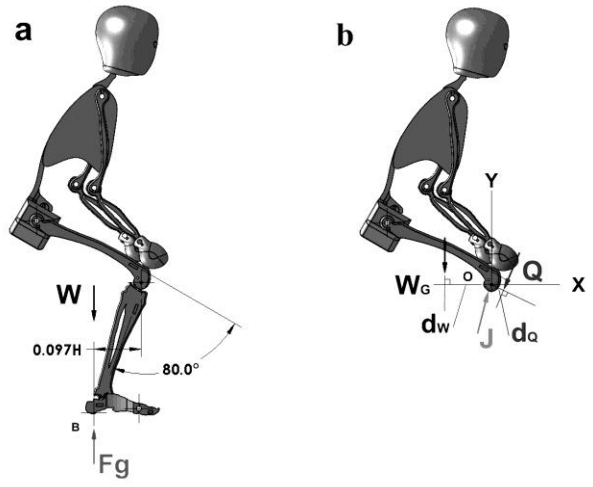

Figure 3-14: (a) Free body diagram 1 of subject during sit to stand **(b)** Free body diagram 2 of subject during sit to stand

For static analysis, if the body weight is equally distributed to both lower limbs, then the load acting over each knee joint is:

$$W_{G1} = \frac{BW}{2} - 0.061BW$$

$$W_{G1} = 0.439BW \tag{3-10}$$

$$W_{G2} = W_{G1} \tag{3-11}$$

Using the Solid Works model for a knee flexion angle of 90^o, the perpendicular distance d_{Wg1} or d_{Wg2} is equivalent to 0.097H. According to Figure 3-6 and its digitized data in TableA3.1, d_Q is equivalent to 41.48 mm (0.0244H) for a knee flexion of 80^o.

Applying the equilibrium condition about the femoral-tibial contact point gives:

$$\sum M = 0$$

$$Q \times d_q - W_g \times d_{wg} = 0$$

$$Q = \frac{W_g \times d_{Wg}}{dq} = \frac{BW \times 0.439 \times 0.097H}{0.0244H}$$

$$\boldsymbol{Q = 1.745BW} \tag{3-12}$$

Applying this result to a subject of 1.7 meters height and 736 Newton body weight, the required quadriceps force for sit to stand at 90^{o} knee flexion is:

$$Q = 1{,}745 \times 736\text{N}$$

$$\boldsymbol{Q = 1{,}283.5N} \tag{3-13}$$

The moment contributed to the knee joint by the quadriceps during this instance of the gait is

$$\boldsymbol{M} = Q * d_Q$$

$$M = 2448\, N \times 0.0244H$$

$$\boldsymbol{M = 53.2\, Nm} \tag{3-14}$$

Experimentally determined knee joint moments during the sit to stand phase are shown in Table 3-4. The maximum torque value of the knee joint was 0.72Nm/kg during the sit-to-stand stage using a walker and the maximum torque value of the knee joint was1.20Nm/kg during the sit-to-stand stage with no constraints in sagittal plane.

Table 3-4: Knee moment during sit to stand condition [60]

Type	Knee Torque (Nm/kg)
Without Arm Support	0.88
With Arm Support	0.77

Similar to the previous static analysis, discrepancy between the theoretical and experimental results is attributed to the assumptions made for the static analysis. Moreover, the theoretical values obtained are significantly affected by the kinetics and position of the arms, head and trunk. The position of these parts of the body can alter the body center of mass which in turn determines the location of the center of pressure and finally the counterbalanced moment or the quadriceps force.

Chapter 4

PNEUMATIC MUSCLE DESIGN

4.1 PAM DESIGN REQUIREMENTS

Subsequent to the findings presented in Chapters 2 and 3, five PAM design requirements have been identified for powered lower limb prostheses: (i) PAM pulling force F_m to achieve the required knee moment, (ii) PAM contraction distance ΔL to achieve the required knee angular displacement, (iii) PAM weight W_m to limit the weight of the prosthesis, (iv) PAM diameter D and (v) PAM length L to limit the size of the prosthesis.

Based on anthropometric data of the human body, lower limb prostheses can be no more than approximately 40cm in length, 11cm in diameter and 3.5kg in weight. Given that a PAM expands radially by approximately 200% when it is fully contracted and assuming an antagonistic muscle setup design as shown in Figure 2-18**,** the maximum PAM diameter is limited to approximately 4cm. Thus, the maximum unstressed diameter of the PAM is about 2cm.Assuming a hinge type of joint for the knee prosthesis and a maximum moment arm that is similar to a biological knee, the maximum PAM length is limited to approximately 30cm.

Whereas the mass constraint of the PAM depends on the final design of the prosthesis, based on known masses of existing passive prostheses, the proposed PAM should not surpass a mass of 250g. These requirements determine the PAM size and weight constraints for powered lower prostheses, shown in Table 4-1.

Table 4-1: PAM size constraints

Max. PAM length	Max. PAM diameter	Max. PAM weight
30cm	4cm	250g.

As determined in Chapter 3, the angular displacement of a knee joint for typical daily activities such as walking and ascending/descending stairs is approximately 117^o. According to TableA3.1, throughout this angular displacement, the knee moment arm varies from 2.5 to 5.6cm. This variation of moment arm provides the knee with the ability to produce large knee moments and angular displacements, while minimizing the knee size. Consequently, this optimizes the required force and contraction distance produced by the quadriceps muscles.

Assuming a hinge type of joint for the knee prosthesis and a moment of arm of 5.6cm, this would require a PAM contraction distance of:

$$\Delta L = \theta * r = \frac{117^o}{180}\pi * 5.6 = 11.44\ cm$$

Assuming a PAM length that is equivalent to the maximum PAM length as defined in Table 4-1, this would yield a PAM contraction ratio C_r of

$$C_r = \frac{\Delta L}{L_o}$$

$$C_r = \frac{11.44}{30} = 38.12\ \%,$$

where ΔL is the PAM contraction distance and L_o is unstressed PAM length. Though a muscle contraction of 38.12% is unattainable by the PAM, an eccentric design of a pulley mechanism can increase the moment arm while keeping the overall diameter of the knee prosthesis within limits. Assuming an average moment arm of 4.1cm for the eccentric pulley, this yields

$$\Delta L = \theta * r = \frac{117^o}{180}\pi * 4.1 = 8.37\ cm$$

$$or\ contraction\ radio = \frac{8.37}{30} = 27.9\%$$

Based on the static analysis in Chapter 3, to replicate the quadriceps muscle during daily activities, the PAM must achieve a maximum knee moment M_k of 99.8 N-m. Assuming a

moment arm that is similar to the average moment arm of 4.1cm for the eccentric pulley, the PAM must produce a maximum pulling force F_m of

$$F_m = \frac{M_k}{R_k} \tag{4-1}$$

$$F_m = \frac{99.8\ Nm}{0.041m} = 2434.1\ N \tag{4-2}$$

Combined with the previous results, this yields the PAM kinetic and kinematic constraints for powered lower limb prostheses, shown in Table 4-2.

Table 4-2: PAM kinetic and kinematic constraints for powered lower limb prostheses

Maximum PAM force	Maximum PAM contraction
2434.1N	8.37cm

Considering a PAM having an unstressed PAM length of 30cm, an unstressed PAM diameter D_o of 2cm and an unstressed PAM braiding angle$\theta_o$of 20^o, then from equation (2-1), the uncoiled fiber length L_{ym} is given by

$$L_{ym} = \frac{D\pi n}{sin\theta}$$

$$L_{ym} = 40.9\ cm$$

Using equation (2-3), to achieve a force of 2434.1N while restricting the unstressed muscle diameter to 2cm, the pressure should be:

$$F = -P\left[\frac{L_{ym}^2 - 3L^2}{4\pi n^2}\right]$$

$$-P = \frac{F4\pi n^2}{L_{ym}^2 - 3L^2}$$

$$-P = 3{,}403N \times 4 \times 3.1416 \times \frac{6.35}{1{,}670 - 4{,}332} = -163\frac{N}{cm^2}$$

$$P = 1.63\ \ (236\ psi)$$

Thus, to achieve a muscle force of 2434.1N that is required by powered lower limb prostheses while confining the size of the PAM, an operating pressure of 1.63 MPa is required. Currently, the maximum operating pressure of existing PAMs is limited to 0.83 MPa. Thus existing PAMs would fail to satisfy powered lower limb prosthesis requirements and consequently a new PAM design must be developed to sustain this higher pressure.

4.2 END FIXTURES DESIGN

The PAM is a device that converts gas pressure into a high pulling force. It mainly consists of three components, the internal flexible tube or bladder, the braided sleeve and the end fixtures. Whereas each muscle component is important to the performance of the PAM, it was deemed important to focus the design effort on the end fixtures, since this has been the weakest link of existing PAM designs. During high operating pressures, the end fixtures must sustain high mechanical loads while connecting the muscle components together and sealing the high pressure gas inside the muscle.

The muscle end fixture has many functions, connecting the muscle membrane to the end fixture, connecting the end fixture to the apparatus, transferring muscle force to the apparatus, sealing internal pressurized gas and acting as a conduit for gas flow. With the goal of getting the final design, it was necessary to go through a series of conceptual designs that gradually led to the final solution. The first concept, illustrated in Figure 4-1, is a simple cylindrical arrangement of three parts numbered as No. 1, 2 and 3. Part 1 has an external cone to hold the bladder and the sleeve together and a centered longitudinal hole acting as a conduit to inflate and deflate the muscle. Part 2 has a hexagonal external shape to ease the process of assembly and an internal cone that serves to press the bladder and sleeve together. Part 3 is a commercial nut used to exert the initial force on part 2.

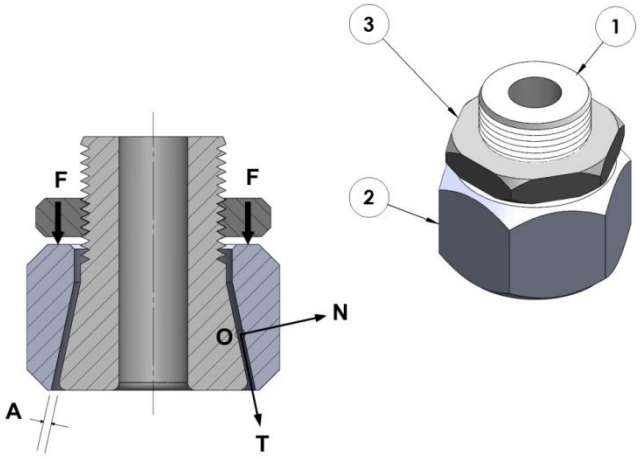

Figure 4-1: End fixtures design 1

The braided sleeve and the internal tube have the same length and are held together with the end fixture in section A, located between the two conical and parallel surfaces of part 1 and part 2. When the nut (part 3) is tightened, the generated force F_n moves part 2 toward part 1 and consequently increases the normal force$N$which acts perpendicularly to the sleeve and bladder, see Figure 4-1. The static friction coefficient (μ) is constant and thus the friction force F_f is a function of the normal force *N* as follows:

$$F_f = \mu N. \tag{4-3}$$

To avoid slippage in the end fixtures, the frictional force must be greater than or equal in magnitude and opposite in direction to the sleeve and bladder tension *T*.

$$F_f \geq T$$

One important aspect of this design is the self-retaining feature that holds the fixtures, sleeve and bladder together. This functions when the muscle is pressurized (or pulled) and the frictional force, which opposes the sleeve-bladder tension, tends to move part 2 along part 1. This displacement increases the normal force *N* which consequently increases the frictional force and improves the holding and sealing capacity of the end fixtures.

With the intention of increasing the contact area between the sleeve-bladder and the end fixtures and ultimately increasing the load capacity of the muscle, a variation of the first design is

proposed in Figure 4-2. Design 2 consists of successive waved chambers in section*A*which accumulates material and restricts it at the periphery of each cavity. This eliminates relative motion of the sleeve bladder material between parts 1 and 2. Consequently, design 2 retains higher tension loads in section *A*, but the fabrication of these chambers makes it more complex and thus its manufacturing cost would be higher. Figure 4-2 shows the geometric details of design 2, part 2.

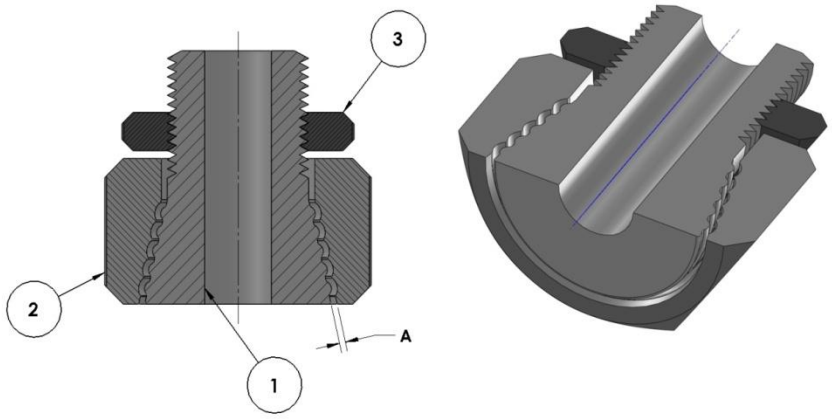

Figure 4-2: End fixtures design 2

To reduce the manufacturing cost in Design 2but also maintain its characteristics, a third design is proposed to reduce the number of circular cavities and add a hexagonal form at the end of part 1. As illustrated in Figure 4-3, Design 3 keeps the self-retaining feature of Design 1 and the circular cavity from Design 2, which acts as a high pressure ring where the force ***F*** is longitudinally perpendicular to the sleeve-bladder surface. The hexagonal external forms in Parts 1 and 2 are used as a means of holding the end parts when assembling the end fixtures.

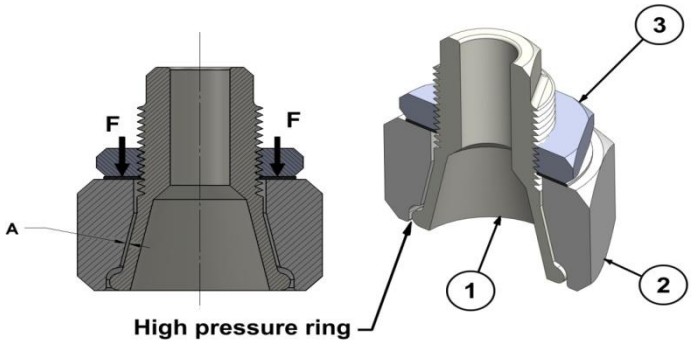

Figure 4-3: End fixtures design 3

Figure 4-4 displays an alteration to part 1, where the hexagonal shape is replaced with two parallel faces to simplify the fabrication process. The transversal hole at the top of Part 1 is used for assembly purposes and the lateral blind hole at the center is used to connect the gas supply to the PAM.

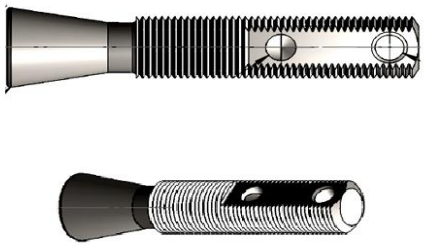

Figure 4-4: Design alteration to Part 1

Figure 4-5displays assembled parts of the end fixtures for both sides of the muscle. Side 1 is the part of the muscle that supplies and releases the gas while Side 2 is completely sealed and usually connected to the load. Both sides share Parts 2, 3 and 4 (gas connector), but the central component ofPart1 differs to accommodate for gas flow connection and conduit. Figure 4-6 shows the assembled PAM prototype in Solid Works.

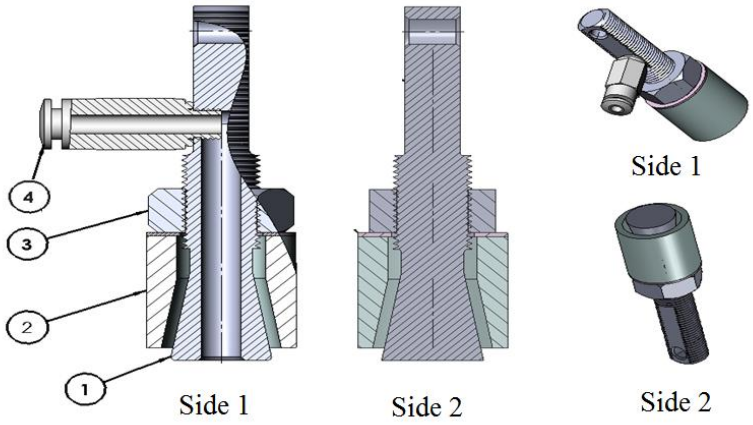

Figure 4-5: End fixtures assembly

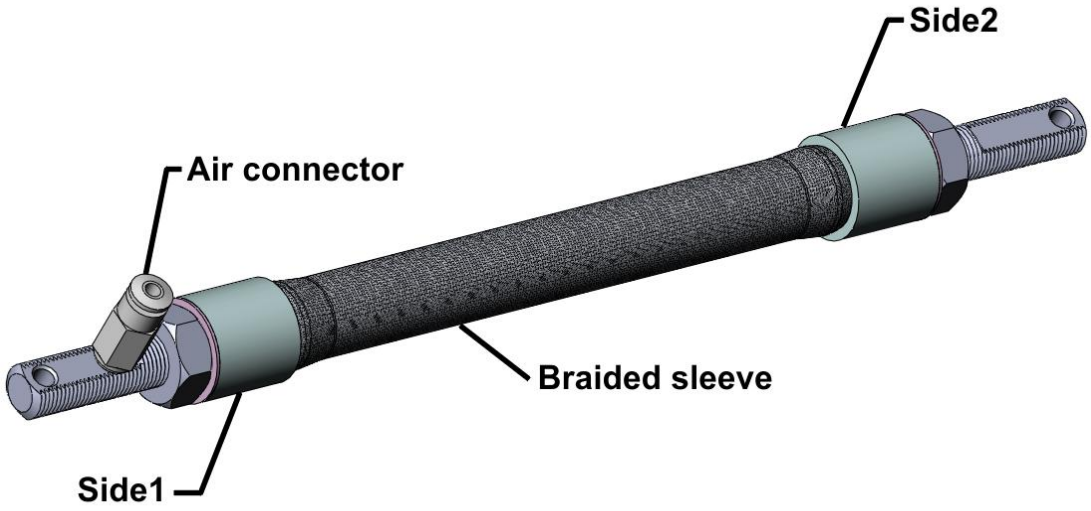

Figure 4-6: 3D model of the PAM prototype using the first end fixtures prototype

4.3 PAM PROTOTYPE TESTING

The first prototype consisted of a bladder made of natural latex rubber and a FlexoPet braided sleeve, as shown in Figure 4-7. The prototype was first tested for gas pressure retention over a period of five days. Experimental results showed that the PAM pressure remained constant at 0.62 MPa, which confirms the sealing properties of the joint that is achieved by the end fixtures.

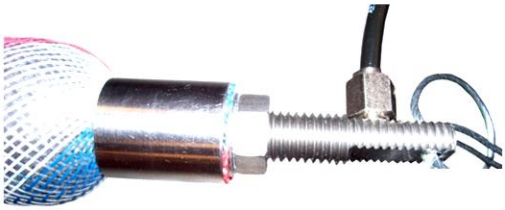

Figure 4-7: Gas retention test for PAM prototype

The second prototype test consisted of an isometric PAM contraction used to determine the capacity of the end fixtures to retain the sleeve-bladder when the muscle is loaded. Figure 4-8 illustrates the experimental setup achieved with an Instron tensile machine which will be described in detail in Chapter 5.

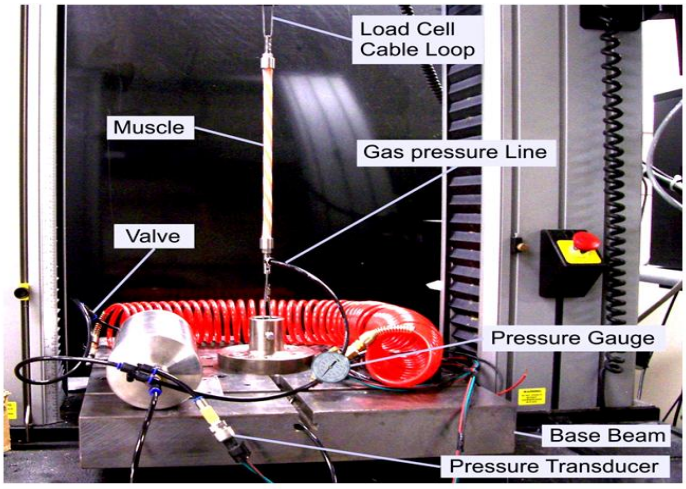

Figure 4-8: Load retention test for PAM prototype

For this test, the muscle was installed at its unstressed length and consequently pressurized to increment the pulling force generated by the PAM until the muscle failed. Whereas a maximum pulling force of 3700 N was achieved, PAM failure occurred when its membrane slipped out of the end fixtures. Thus, the end fixtures were not able to hold the braided sleeve to material failure. This prompted an alteration to the fixtures design as illustrated in Figure 4-9

Figure 4-9: Alteration for end fixtures design

To eliminate PAM membrane slipping from the end fixtures at high pulling load, a small cup form was added between Parts 2 and 3. Moreover, part 2 was machined to match the surface of the new part (cup) as shown in Figure 4-9. The cup purpose is to increase the sleeve grabbing area and break the continuity of the slipping path. Figure 4-10displays the failure of the braided sleeve after sustaining a pulling load that is beyond 6000N. As can be seen, the end of the sleeve is in good condition which demonstrates that the fixtures can withstand forces that are larger than the ultimate strength of the sleeve and bladder materials combined together.

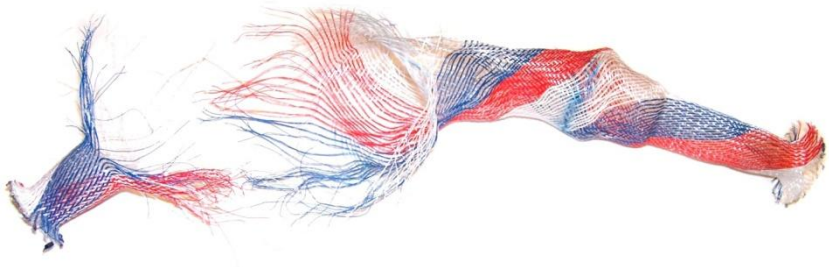

Figure 4-10: Ruptured braid in the new end fixtures design

Throughout these experiments, it was observed that high elasticity of the bladder material had a critical contribution to the premature failure of the muscle. As the muscle contracts, muscle radial expansion occurs which results in a hemispherical deformation at the end of the muscle. This deformation leads to an accumulation of fibers and sleeve fabric distortion which result in uneven and larger trapezoidal spaces between the sleeve fibers at the end of the muscle. For highly elastic material such as the rubber bicycle tube, it was observed that the bladder material tends to bulge out from the braided sleeve and this, results in premature bladder rupture at high

operating pressures. To prevent the sleeve fabric deformation, a coat of liquid rubber (Shoe GOO Adhesive) was applied on the muscle covering the hemisphere area at each of its ends. As shown in Figure 4-11 this creates an elastic film that maintains the symmetry and uniformity of the fabric in the hemisphere critical area.

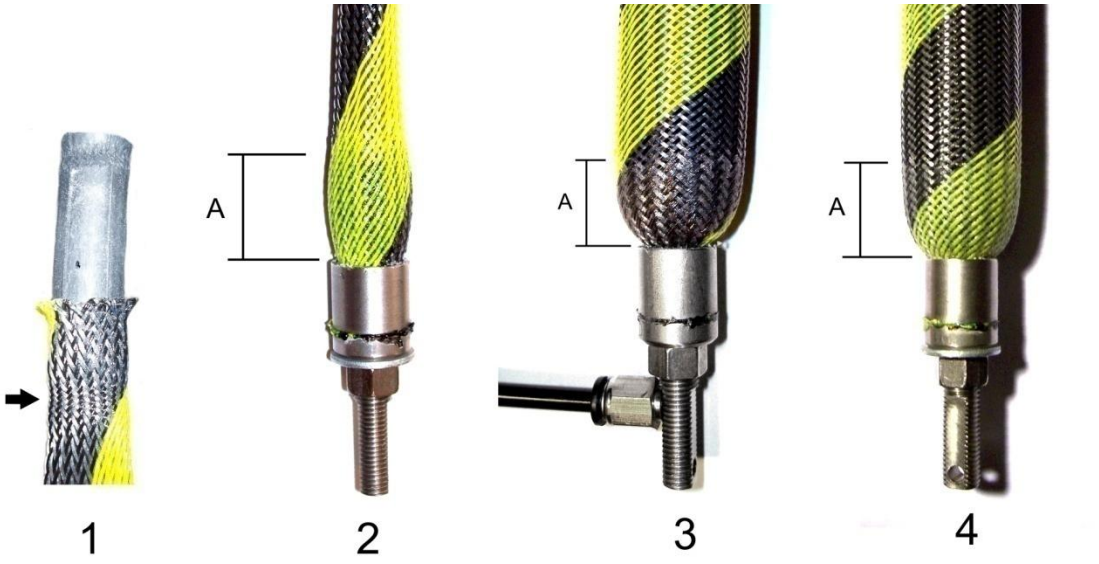

Figure 4-11: PAM prototype coated with an elastic film at its ends

With reference to Figure 4-11, part (1) shows the end side of a tested muscle that failed by bulging of bladder material through the sleeve fabric. The black arrow points to the braid jamming at the end fixture area, which induced the failure. Figure 4-11, part (2) displays a PAM prototype with coated liquid rubber at the area of section A, at an unstressed muscle state. Parts 3 and 4 present the sleeve fabric uniformity and symmetry in the muscle pressurized at 2.1MPa (300 psi) in part 3 and after 100 cycles in part 4.

4.4 PAM PROTOTYPE ASSEMBLY

The PAM assembly is relatively simple, but it is important to consider some details for the proper functionality of the muscle. After determining the required diameter and length of the PAM and fabricating all components, it is important to ensure that all the parts are in good condition. Any imperfection, especially in the braided sleeve or in the bladder, could induce premature failure.

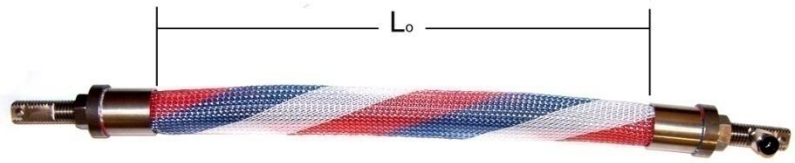

Figure 4-12: Pneumatic artificial muscle at rest position

To assemble the actuator, the flexible inner tube and braided sleeve are arranged concentrically and the end of the bladder is cleared for the end fixtures installation. The conical and cylindrical surfaces of Parts 1 and 5, Figure 4-8, are inserted at each side of the bladder as shown in Figure 4-13A. For easy installation of the muscle, it is important to keep parallel the flat surface of both parts when they are inserted in the bladder. Consequently, the braided sleeve is aligned with the inner tube, Figure 4-13C, and both are pressed with Part 2 by the nut, Part 3, Figure 4-13 B.

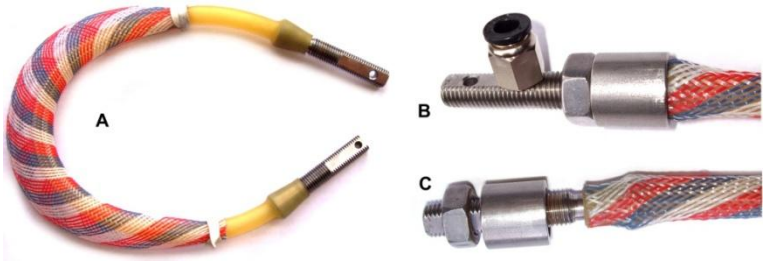

Figure 4-13: PAM first model assembly

Finally, the gas connector is installed in Part 1 and the actuator is pressurized to 0.69MPa (100 psi) to press fit all components against each other and the nut is tightened again to make the actuator ready for testing. This design is adequate for pressures that are no higher than 0.86 MPa (125 psi) and a maximum pulling force of 2000 N. Thus, this design can be used in small sizes where low pressure and small pulling forces are required.

After selecting the bladder and braided sleeve length, the PAM is assembled as displayed in Figure 5-5. First, part 1 is inserted in the bladder and mesh (Figure 4-14 a) then part 2 is inserted over the mesh (Figure 4-14 b). The extended braid section over part 1 is bent backward (Figure 4-14 c) and the cup adaptor, washer and nut are installed (Figure 4-14 d). Finally the air connector is mounted and the excess of braided sleeve is cut (Figure 4-14 e). similar to the

previous design, the prototype is pressurized to 0.69 MPa (100 psi) to press fit all component against each other and the nut is tightened again to make the actuator ready for testing.

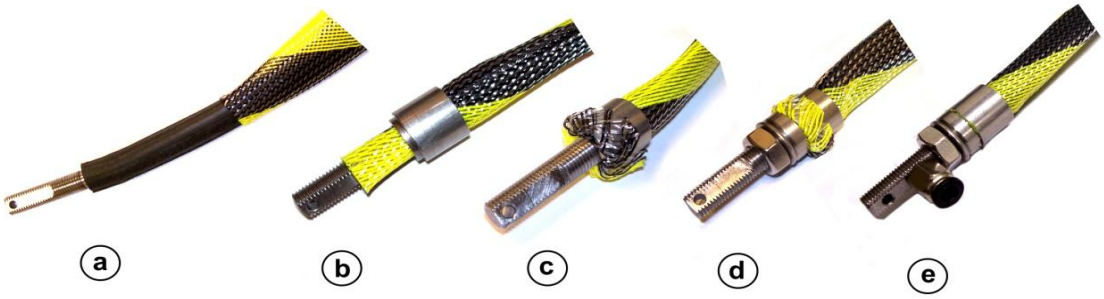

Figure 4-14: Corrected PAM end fixtures, assembly progression

For PAM assembly, an adaptor (Figure 5-6) was fabricated to protect the fixtures and ensure correct assembly of the muscle. Moreover, this component served as a connection between the muscle and the Instron machine.

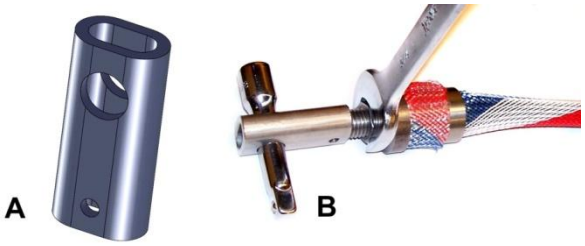

Figure 4-15: Adaptor used in the muscle assembly

4.5 PAM MATERIALS

4.5.1 Bladder materials

Unlike the end fixtures, the fabrication of the PAM membrane was based on the availability of commercially available materials that offer adequate mechanical properties. For the inner flexible tube of the PAM, three different materials were used namely, bicycle tube rubber, silicon rubber and latex rubber.

Figure 4-16: Bladder materials for the PAM

Made from Polyisobutylene, the bicycle inner tube is a doughnut shaped bladder that holds air pressure inside a bicycle tire. It is inexpensive, durable and offers low air diffusion over time. The selected rubber bicycle tube is the "INNOVA", size 700 x 19/23CF/V48MM. This is an ideal candidate for PAM during low operating pressures (0.69MPa or 100psi). The second type of material used is natural latex rubber. This is a highly elastic rubber material commonly used in party balloons and surgical gloves. The main advantage of this material is its high elasticity, or its ability to be stretched by large amounts and return to its unstressed state with very little hysteresis, or energy loss. Natural latex rubber was found to be adequate for moderate operating pressures (1.38 MPa or 200 psi). Silicone rubber was the third material used to make the bladder of the PAM. This material is an elastomer commonly used in industry with many different formulations. For this research, TYGON 3350 silicone tubing Silicone rubber was selected. It is generally non-reactive, stable, and retains its mechanical properties through extreme environments and temperatures. This is an ideal candidate for PAM during high operating pressures (2.76 MPa or 400 psi)

4.5.2 Braided sleeve materials

With respect to the braided sleeve materials, previous studies by[**10**] showed that Polyethylene Terepthalate braided sleeves are the best candidates for the PAM. Manufactured by several companies in different sizes and configurations, they are flexible, resistant, inexpensive and offer an open mesh configuration which results in a large contraction distance by the PAM. More importantly, the resistance or load capacity of the PAM can be increased by selecting a higher number of filaments within the sleeve or a larger filament diameter such as the "Flexo Heavy Wall" by Techflex, as shown in Figure 4-17.

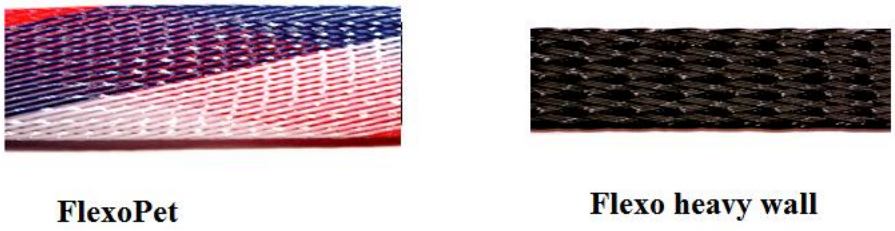

Figure 4-17: Distinct braided sleeve materials used in the PAM construction

4.5.1 End fixtures material selection

In line with the muscle design requirements, mechanical strength and good wear resistance, stainless steel AISI/SAE 304 was selected as the candidate material for fabricating the end fixtures of the PAM. For mass production of lighter PAM, an aluminum alloy with good mechanical strength and wear resistance could also be a candidate material.

Chapter 5

EXPERIMENTAL VALIDATION OF PAM DESIGN

This Chapter presents the experimental testing results for the PAM design presented in Chapter 4. These experimental tests validate the kinetic as well as the kinematic behaviour of the newly developed PAM for powered lower limb prostheses requirements. Moreover, this chapter includes the design and development of the experimental setup for testing the PAM prototypes.

5.1 EXPERIMENTAL SETUPS

To evaluate the PAM prototypes, three experimental setups were designed and built. These setups were designed according to the requirements of three different types of muscle contraction achieved by a skeletal muscle: 1)Isometric muscle contraction takes place when the muscle generates force, but its length remains constant, 2) eccentric muscle contraction occurs when the force generated by the muscle is inefficient to hold the applied load and thus the muscle length extends during contraction, 3)concentric muscle contraction happens when the muscle force is greater than the applied load and thus the muscle length decreases as the muscle contracts.

The isometric contraction test and eccentric contraction test were performed using the experimental setup presented in Figure 5-1. The PAM was installed in the Instron 4482 tensile testing machine and extended at a specific length between the load cell at the moving crosshead and the base beam. For isometric contraction, the PAM was restrained to a specific length and then inflated to a specific pressure. The muscle pressure and the muscle force are measured by a pressure transducer and by the Instron machine load cell, respectively. These measurements were recorded using a data acquisition system (LABVIEW) that running on a Personal Computer (PC).

For the eccentric contraction, the PAM was initially inflated at a specific pressure and then mounted in the tensile testing machine at its maximum contraction length. While retaining a constant muscle air mass during the test, the muscle was gradually pulled at a speed rate of 10 mm/min until it reached the muscle unstressed length L_o. PAM length elongation resulted in a decrease in muscle volume and thus an increase in muscle pressure. The muscle force and the muscle length were measured by the Instron machine load cell and displacement sensor, respectively. Moreover, the muscle pressure was measured by a pressure transducer and all measurements were recorded using a data acquisition system (LABVIEW).

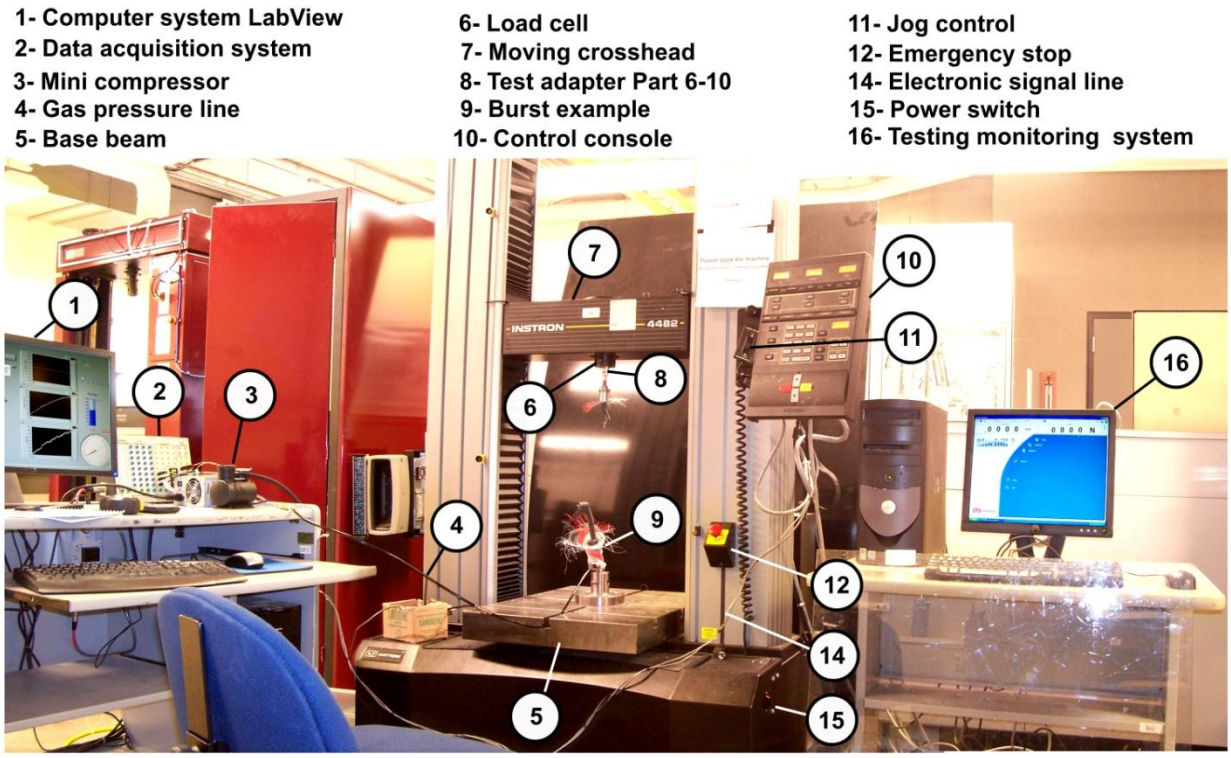

Figure 5-1: Experimental setup for isometric and eccentric muscle contraction test

The PAM concentric contraction test was carried out by the experimental setup shown in Figure 5-2. In this case, the muscle was suspended vertically while being fixed at one end and attached to a mass at its other end. As the muscle was inflated, muscle contraction lifted the weight until it reached force equilibrium or the maximum contraction distance of the PAM prototype. The muscle contraction distance was monitored using a rotary potentiometer mounted on the pulley or by a Linear Variable Displacement Transducers (LVDT) sensor. The concentric contraction

setup was controlled by a software program using Laboratory Virtual Instrumentation Engineering Workbench (LabVIEW) running on a PC. Also, the same program acted as the data acquisition system for the muscle parameters. The sampling time for LabVIEW was 0.1 seconds. The design process and detailed construction drawings of this experimental setup are presented in Appendix C. Moreover, finite element analysis shows the ability of this experimental setup to support a load is shown in Figure C-17 and Figure C-18 (Appendix C).

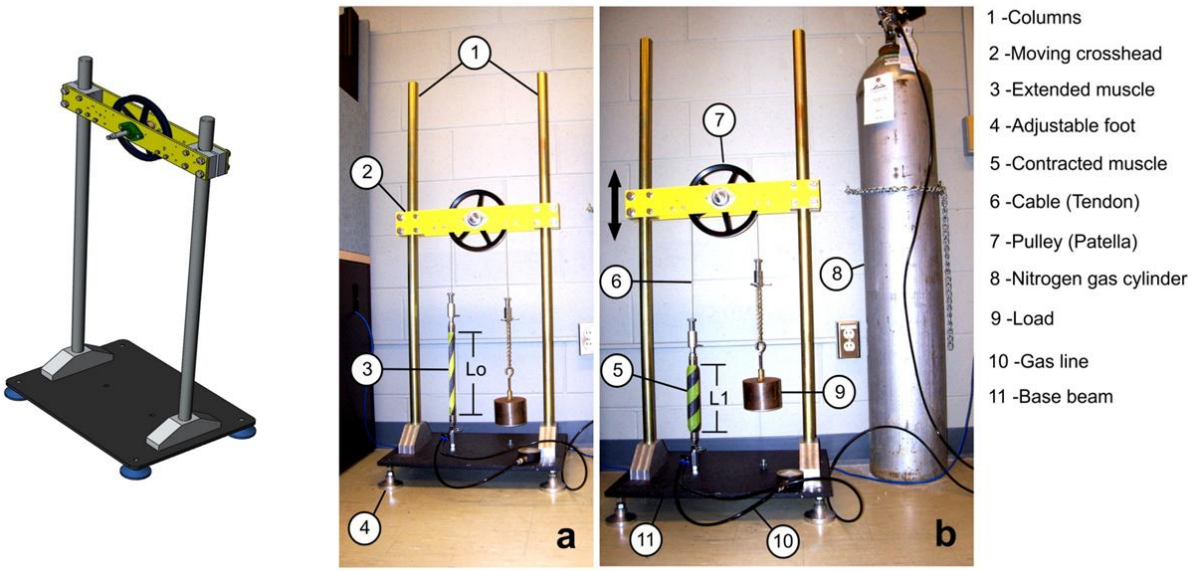

Figure 5-2: Antagonistic experimental setup used for concentric contraction tests

To inflate the PAM prototypes in the course of these experiments, different pneumatic power sources were used. For the low gas pressure test, the air pressure supply system of the laboratory was used (0.69MPa or 100psi). For the medium gas pressure test, a portable electric mini compressor was used to supply a pressure up to 1.38MPa (200 psi). For the high gas pressure test, 20.7MPa (3000 psi) nitrogen gas cylinder with a pressure regulator was used to supply a pressure up to 4.14MPa (600 psi), Figure 5-3.

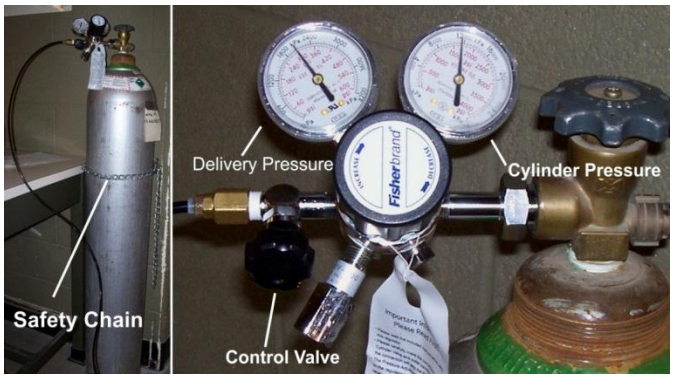

Figure 5-3: Nitrogen cylinder regulator and tank installation

5.2 PAM IDENTIFICATION

For the experimental analysis, PAM prototypes of different materials and sizes were built in the laboratory. The prototypes were of the same design and consisted of a braided sleeve, a bladder and the end fixtures. To identify the PAM prototype, a designation code was established and described in Table 5-1.

Table 5-1: PAM prototype designation code

14P-10S-L300		
14	Unstressed sleeve diameter (mm)	14 mm
P	Sleeve material	PET
10	Bladder internal diameter (mm)	10 mm
S	Bladder material	Silicone
R	Bladder material	Rubber
L	Bladder material	Latex
L300	Unstressed muscle length (mm)	300 mm

5.3 PAM EXPERIMENTAL RESULTS

5.3.1 Concentric contraction

For the concentric muscle contraction test, two PAM prototypes (14P-10S-L300 &14P-12R-L300) were constructed. The unstressed prototype length of 300mm and sleeve diameter of 14mm were intentionally selected to satisfy the PAM size constraint of the lower limb prostheses defined in Table 4-1.As shown in Figure 5-2, the PAM prototypes were connected to a constant

load through a steel cable which wraps around the pulley to generate a torque and an angular displacement when the muscle contracts. The prototypes were inflated to a pressure of 1.42MPa (200 psi) and contracted from an unstressed muscle length L_o of 300 mm to the maximum contraction distance, 69% of L_o. Table 5-2 presents the unstressed and contracted parameters of the tested prototypes.

Table 5-2: Concentric contraction test results of the muscles 14P10S-L300 and 14P12R-L300

	Unstressed muscle		**Contracted muscle**		**Contraction**		**Pressure**
PAM Prototype	Length(L_o)	Diameter (D_o)	length (L)	Diameter (D)	Distance	%	MPa
14P-10S-L300	300	13	204	32.87	90	32	1.38
14P-12R-L300	300	14	199	33.54	101	33.8	1.38

Results in Table 5-2 show the ability of the PAM to achieve a contraction distance and ratio of 90 mm and 32 % respectively, which exceed the kinematic requirements for powered lower limb prostheses as defined in Table 4-1.

5.3.2 Isometric contraction

For the isometric muscle contraction test, two prototypes (14P-10S-L300 & 14P-12R-L300) were constructed. As shown in Figure 5-1, the PAM prototypes were restrained at specific lengths in the Instron tensile testing machine and then inflated to a maximum pressure of 1.42MPa (200 psi). Figure 5-4 displays the isometric contraction test results of the muscle 14P-10S for a range of contracted muscle length of 200 to 300 mm.

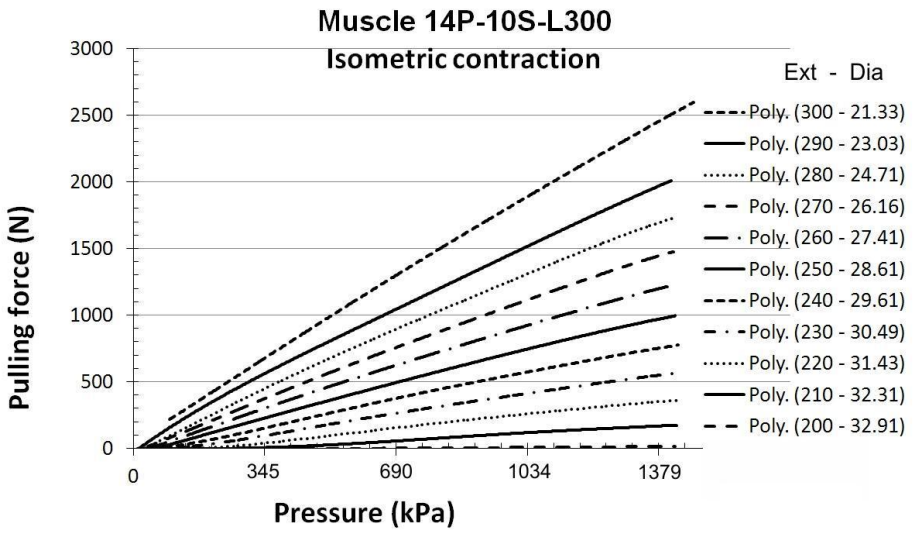

Figure 5-4: Isometric contraction results of the muscle 14P-10S-L300

Experimental results in Figure 5-4 show the ability of the PAM to generate a pulling force as a function of its contracted length. A maximum muscle force of 2700N was obtained at an operating pressure and contracted muscle length of 1.42MPa and 300mm, respectively. As the PAM contracted length reached the maximum contraction distance, the muscle force became approximately zero.

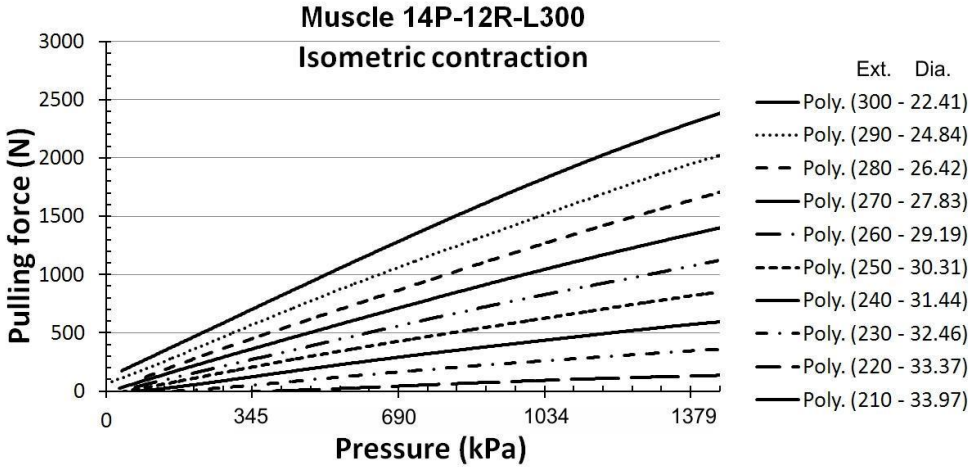

Figure 5-5: Isometric contraction results of the muscle 14P-12R-L300

With reference to Figure 5-4, the column at the right of the picture displays the extension (*L*) and the diameter of the PAM prototype at each state. Similar experimental results were also achieved

for the PAM prototype 14P-12R as shown in Figure 5-5.Whereas the bicycle inner tube material is more flexible, the maximum muscle force was 2400N- 300 N less than the prototype with the silicone bladder (14P-10S). The two muscles were tested several times in isometric contraction mode and the results showed similar behaviour. This occurrence was attributed to the uneven and rough surface of the bicycle inner tube bladder which increases the bladder-sleeve friction and temperature of the muscle.

Results in Figure 5-4 and Figure 5-5 show the ability of the newly designed PAM prototype to exceed the kinetic requirements for powered lower limb prostheses, as determined in Table 4-2.

5.3.2 Eccentric contraction

For the eccentric muscle contraction test, the prototype 14P-10S was constructed. As shown in Figure 5-1, the PAM was restrained at its maximum contraction distance in the tensile testing machine and then while retaining a constant muscle air mass during the test, the muscle was gradually pulled until it reached its unstressed length L_o. Figure 5-6 shows the eccentric contraction test results for the PAM prototype 14P-10S. For this test, the prototype was initially inflated at six different pressures (345, 517, 690, 862, 1034 and 1207 KPa) and then elongated.

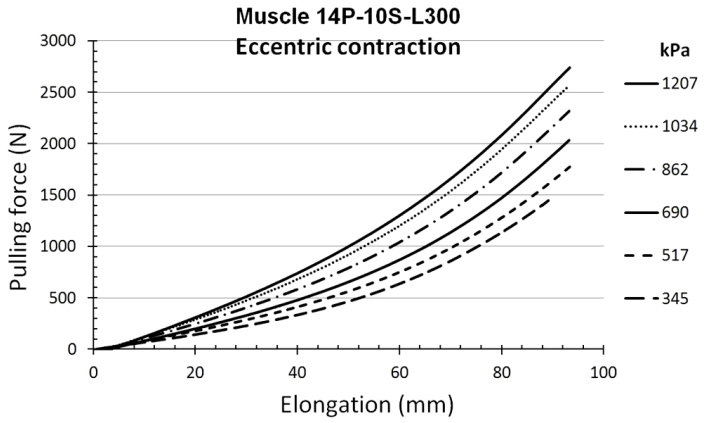

Figure 5-6: Eccentric contraction results of the muscle 14P-10S for six different initial pressures

With reference to Figure 5-6, the right column presents the muscle initial test pressure. The elongation of the muscle decreases its volume which leads to an increase of muscle pressure and thus a higher pulling force. Figure 5-7 displays the elongation and pressure relationship of the

tested muscle 14P-10S. Similar to the previous test, the muscle was tested in six different initial pressures.

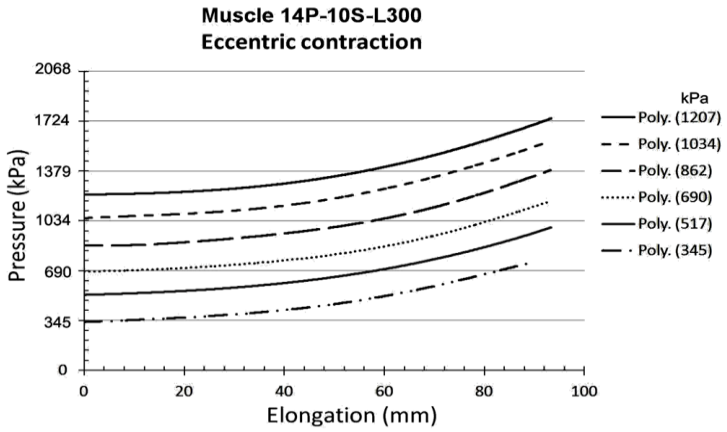

Figure 5-7: Eccentric contraction results of the muscle 14P-10S-L300

Figure 5-8 displays the experimental results of muscles 14P-12R and 14P-10S tested in eccentric contraction mode. In this test, results of the silicone example did not differ with respect to those previously found. However, in contrast to the results of the previous test mode, the bicycle inner tube model presented an exerted pulling force of 3230N, 530N more than the others. This discrepancy is attributed to the inelasticity of the rubber material as the muscle operates and thus increases the muscle pulling force.

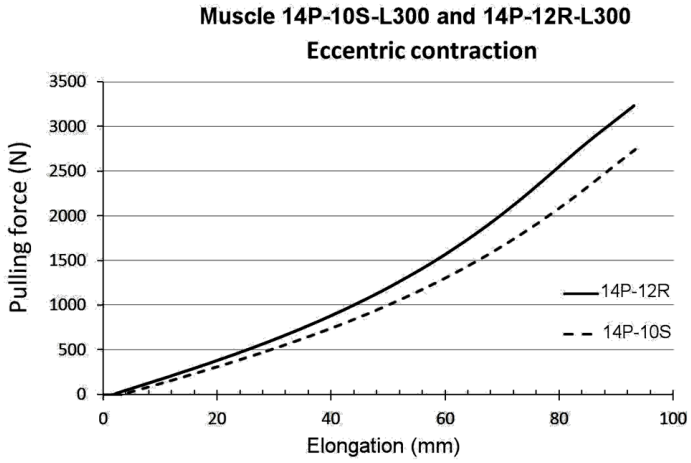

Figure 5-8: Eccentric contraction results of the muscles 14P10S-L300 and 14P12R-L300

Similar to the results obtained in isometric contraction tests, Figure 5-4 and Figure 5-5 demonstrate the ability of the newly designed PAM prototype to exceed the kinetic requirements for powered lower limb prostheses, as determined in Table 4-2.

In conclusion, the experimental results of this investigation present a pneumatic artificial muscle of 14mm diameter and 120g weight that is able to exert a pulling force of more than 2700N suitable for powered lower limb prostheses.

Chapter 6

CONCLUSIONS AND FUTURE WORK

6.1 CONCLUSION

Presently, in spite of technological advancement, the lack of powered lower limb prostheses prohibits millions of transfemoral amputees worldwide from regaining their mobility and thus quality of life. The purpose of this thesis was to propose an innovative and validated PAM design which would offer an actuation solution for powered lower limb prostheses.

A literature survey was first conducted to identify and analyze previous research achievements. This included a historical background review of PAM as well as an analysis of currently available PAM designs and models. Moreover, this chapter covered a review of current lower limb prostheses and their limitations. In particular, it was noted that the current lower limb prostheses lack an effective actuation solution. This led the research to a complete study of knee biomechanics to characterize the actuation requirements for lower limb prostheses. Using Solid Works and anthropometric data, a three-dimension model of a human subject was created to achieve full understanding of human gait and also to perform a static force analysis of a subject during high energy movement namely, walking, ascending/descending stairs and sit to stand movements.

Having identified the actuation requirements for powered lower limb prostheses, it was clear that no currently available PAM would meet these criteria. This led to the design of new end fixtures and a novel combination of braid and bladder material that permits the muscle to operate at a very high pressure while withstanding extreme muscle pulling forces.

One of the important aspects of the new PAM design is the self-retaining feature that holds the fixtures, sleeve and bladder together. This functions when the muscle is pressurized (or pulled) and the frictional force, which opposes the sleeve-bladder tension, tends to increase and thus enhance the holding and sealing capacity of the PAM.

Subsequent to finalizing the design of the new PAM, numerous prototypes were fabricated, tested and validated. Moreover, experimental setups for testing the muscle prototypes through three type of muscle contraction were developed. Experimental testing results revealed that the new PAM design exceeded the kinetics and kinematics requirement for powered lower limb prostheses. The PAM prototype 14p-10S-L300 has achieved a pulling force and a contraction distance of 2700N and 32%, respectively. Table 6-1 displays a comparison between the pneumatic artificial muscle requirements presented in chapter four and the achieved parameters of the PAM prototype proposed in this thesis.

Table 6-1: Comparison between the PAM required and achieved parameters

	Length	**Contraction**	**Diameter**	**Weight**	**Max. force**	**Max. pressure**
	cm	**cm**	**cm**	**g**	**N**	**MPa (psi)**
Required	30	8.4	4	250	2434	-----
Achieved	**30**	**9.3**	**1.4**	**150**	**3887**	**2.53 (367)**

Finally, the result of this investigation presents a PAM that satisfies the knee kinetics and kinematics throughout a normal gait, stairs ascending and descending as well as sit-to-stand movements. Moreover, the proposed PAM conforms to the size and weight constraint of a human leg, giving a significant advance to the development of powered lower limbs prostheses.

6.1 FUTURE WORK

Whereas the gas source of the PAM was not part of this study, the successful application of the PAM for powered lower limb prostheses would depend on the existence of an adequate source of energy. Thus, it is recommended that further research be undertaken in the subject of monopropellant (hot gas) technology to investigate the feasibility of such systems to provide adequate pressurized gas during a practical period of time throughout the normal use of powered lower limb prostheses.

This dissertation has demonstrated that the end fitting design and the selection of material for the body of the muscle completely match the PAM design requirements. However, further research on its service life, reliability and components degradation needs to be undertaken.

More broadly, research is also needed to determine the effect of lubricants on the efficiency and performance of the muscle, affected by the high bladder-sleeve frictional effect and also to establish the most suitable lubricant considering the stability of the muscle materials and the lubricant operation.

REFERENCES

[1] Education, Labor, and Pensions Senate Committee on Health, "Insurance Fairness for Amputees Act of 2011," United State Congress, Bill S. 773, 2011.

[2] M. Owings and L. Kozak , "Ambulatory and inpatient procedures in the United States, 1996," *tal Health Statistics*, vol. 13, no. 139, pp. pg. 1 - 119, 1998.

[3] C Nielsen. (2012, Feb.) American Academy of Orthotists and Prosthetists. [Online]. www.oandp.org

[4] Amputee Coalition of America. (2012, May) Amputation statistics by cause limb loss in the United States. [Online]. http://www.amputee coalition.org/fact_sheets/amp_stats_cause.html

[5] Robert L. Waters and Sara Mulroy, "The energy expenditure of normal and pathologic gait," *Gait & Posture*, vol. 9, no. 3, pp. 151-240, July 1999.

[6] F. Sup, A. Bohara, and M. Goldfarb, "Design and Control of a Powered Transfemoral Prosthesis ," *International journal of rehabilitation research*, vol. 27, no. 2, pp. pp. 263–273, February 2008.

[7] GK Klute , jM Czerniecki, and B. Hannaford , "Artificial muscles: Actuators for biorobotic systems," *International journal of robotics*, vol. 21, no. 4, pp. pp. 295–309, 2002.

[8] GS Sawicki , KE Gordon, and DP Ferris, "Powered lower limb orthoses: applications in motor adaptation and rehabilitation," in *IEEE 9th International Conference on Rehabilitation Robotics*, Chicago, IL, 2005.

[9] Darwin G. Caldwell, G. A. Medrano-Cerda, and C. J. Bowler, "Investigation of bipedal robots locomotion using pneumatic muscle actuators," in *IEEE International Conference of Robotics and Automation*, vol. 1, New Mexico, 1997, pp. 799-804.

[10] Marc Doumit, "Characterization, modeling, and design of the braided pneumatic muscle ," University of Ottawa, Ottawa, PhD Thesis 2009.

[11] Marc D Doumit, Michael Munro, and Atef Fahim, "Analytical Modeling and Experimental Validation of the Braided Pneumatic Muscle," *IEEE Transactions on Robotics*, vol. 25, no. 6, pp. 1282-1291, 2009.

[12] Glenn K. Klute, M. Joseph Czerniecki, and Blake Hannaford, "McKibben artificial muscles: pneumatic actuators with biomechanical intelligence," in *IEE International Conference on Advanced Intelligent Mechatronics*, Atlanta, 1999.

[13] Charles R. Johnson and Robert C. Pierce, "Expansible cover," 2238058, April 15, 1941.

[14] Hugh De Haven, "Tensioning device for producing a linear pull," 2483088, September 27, 1949.

[15] Richard H. Gaylord, "Fluid acutated motor system and stroking device," 2238058, July 22, 1958.

[16] V. Nickel and A. Garrett, "Development of useful function in the severely paralysed hand," *The Journal of Bone and Joint Surgery*, vol. 45, no. 5, pp. 933-952, 1963.

[17] K. Inoue, "Rubbertuators and applications for robots," in *Robotics Research: The 4th International Symposium*, Cambridge, 1988, pp. 57-63.

[18] F Daerden and D Lefebe, "The concept and design of pleated pneumatic artificial muscles," *International Journal of Fluid Power*, vol. 2, no. 3, pp. 41-50, 2001.

[19] D Bergemann, B Lorenz, and A Thallemer, "Actuating Means," 6349746, February 26, 2002.

[20] K. Kawashima et al., "Development of robot using pneumatic artificial rubber muscles to operate construction machinery," *Journal of Robotics and Mechatronics*, vol. 16, no. 1, pp. pp. 8-16, 2004.

[21] M. Mayuko, K. Suzumori, M. Takahashi, and T. Hosoya, "Very High Force Hydraulic McKibben Artificial Muscle with a p-Phenylene-2, 6-benzobisoxazole Cord Sleeve," *Advanced Robotics*, vol. 24, no. 1-2, pp. pp. 233-254, 2010.

[22] Shadow Robot Company Ltd. Shadow Robot Comapany. [Online]. www.shadowrobot.com

[23] Shadow Robot Company Ltd. (2012, July) Shadow Robot. [Online]. http://www.shadowrobot.com/airmuscles/

[24] Festo Inc. Festo. [Online]. www.festo.com

[25] SymBiotechs USA. (2012, January) SymBiotechs. [Online]. http://www.symbiotechsusa.com/

[26] P.C. Tang et al., "Let Them Walk! Current Prosthesis Options for Leg and Foot Amputees ,"

Journal of the American College of Surgeons, vol. 206, no. 3, pp. pp. 548 - 560, 2008.

[27] JW. Michael, "Modern prosthetic knee mechanisms. Clin Orthop Relat Res 1999;361:39–47," *Clinical orthopaedics and related research*, vol. 361, pp. pp 39-47, 1999.

[28] B. Kelly. (2012, july) Lower Limb Prosthetics. [Online]. http://emedicine.medscape.com/article/317358-overview

[29] Össur Americas. (2012, July) Össur Americas. [Online]. http://www.ossur.com/?PageID=12644

[30] Otto Bock. (2012, July) Otto Bock. [Online]. http://www.ottobock.ca/

[31] Johansson J. L., D. M. Sherrill, and P.O. Riley, "A clinical comparison of variable-damping and mechanically passive prosthetic knee devices," *American journal of physical medicine & rehabilitation* , vol. 84, no. 8, pp. pp. 563-575, 2005.

[32] A. Boonstra, J. Schrama, W. Eisma, L. Hof, and V. Fidler, "Gait analysis of transfemoral amputee patients using prostheses with two different knee joints ," *Archives of Physical Medicine and Rehabilitation*, vol. 77, no. 5, pp. pp. 515-20, 1996.

[33] A. M. Boonstra, J. M. Schrama, W. H. Eisma, A. L. Hof, and Fidler V., "Gait analysis of transfemoral amputee patients using prostheses with two different knee joints," *Archives of Physical Medicine and Rehabilitation*, vol. 77, no. 5, pp. pp. 515 - 520, 1996.

[34] C. Sjodahl, G. B. B. Jarnlo, B. Soderberg, and B. M. Persson, "Pelvic motion in transfemoral amputees in the frontal and transverse plane before and after special gait re-education," *Prosthetics and orthotics international*, vol. 27, no. 3, pp. pp. 227 - 237, 2003.

[35] Osssur. (2012, July) The Power Knee, Technical Manual. [Online]. http://www.ossur.com/lisalib/getfile.aspx?itemid=22244

[36] Waycaster G. C., "Design of a powered above knee prosthesis using pneumatic artificial muscles in the Department of Mechanical Engineering In the Graduate School of The University of Alabama, 2010," University of Alabama, Tuscaloosa , thesis 2010.

[37] Ossur, "Bionic technology by ossur," Instruction for use power Knee report 2009.

[38] B. G. A. Lambrecht, "Design of a Hybrid Passive-Active Prosthesis for Above-Knee Amputees," University of California, Berkeley, Berkeley, Thesis 2008.

[39] Ossur. (2012, July) Ossur. [Online]. http://www.ossur.com/?pageid=15748

[40] W. F. Flowers, "A Man-Interactive Simulator System for Above-Knee Prosthetics ," Massachussetts Institute of Technology, Cambridge, thesis 1972.

[41] W. C. Flowers and R. W. Mann, "Electrohydraulic knee-torque controller for a prosthesis simulator ," *ASME Journal of Biomechanical Engineering*, vol. 99, no. 4, pp. pp. 3-8, 1977.

[42] G. K. Klute, J. Czerniecki, and B. Hannaford, "Development of powered prosthetic lower limb," in *Proceedings of the 1st National Meeting, Veterans Affairs Rehabilitation Research and Development Service*, Washington, 1998.

[43] G. K. Klute, J. Czerniecki, and B. Hannaford, "Muscle-Like pneumatic actuators for below-knee prostheses," in *Proceedings the 7th International Conference on New Actuators*, Bremen, 2000, pp. pp. 289 - 292.

[44] D. A. Winter, *The Biomechanics and Motor Control of Human Gait: Normal, Elderly and Pathological Waterloo*, 2nd ed. Waterloo: University of Waterloo Press, 1991.

[45] R. Riener, M. Rabuffetti, and C. Frigo, "Stair ascent and descent at different inclinations. Gait and Posture 2002;15(1):32–44.," *Gait and Posture*, vol. 15, no. 1, pp. pp. 32 - 44, 2002.

[46] F. Sup, H. A. Varol, J. Mitchell, T. J. Withrow, and M. Goldfarb, "Self-contained powered knee and ankle prosthesis: initial evaluation on a transfemoral amputee," in *IEEE 11th Int. Conf. on Rehabilitation Robotics*, 2009, pp. pp. 638-44.

[47] R. Versluys et al., "IPPAM: Intelligent Prosthesis actuated by pleated Pneumatic Artificial Muscles," in *Proceedings of the 9th international conference on climbing and walking robots*, Brussels, , 2006.

[48] R., Desomer, A. Versluys et al., "A biomechanical transtibial prosthesis powered by pleated pneumatic artificial muscles," *International journal of modelling, identification and control*, vol. 4, no. 4, pp. pp. 394-404, 2008.

[49] T. J. Yeh, M. Wu, T. Lu, F. Wu, and C. Huang, "Control of McKibben pneumatic muscles for a power-assist, lower-limb orthosis," *Journal of Mechatronics*, vol. 20, no. 6, pp. pp. 686 - 697, 2010.

[50] G. Waycaster, S. Wu, and X Shen, "Design and control of a pneumatic artificial muscle actuated above-knee prosthesis," *Journal of Medical Devices* , vol. 5, no. 3, September 2011.

[51] E. N. Marieb and K. Hoehn, *Human Anatomy & Physiology* , 8th ed.: Benjamin Cummings, 2010.

[52] Shi U., "Finite element analysis ot total knee replacement considering gait cycle load and malalignment ," University of Wolverhampton, Thesis 2007.

[53] P. Rasch, M. Grabiner, R. Gregor, and J Gaarhamme, *Kinesiology & Applied Anatomy*, 7th ed. Philadelphia, United States: Lea & Febiger, 1989.

[54] P. Grimshaw, A. Lees, N. Fowler, and A. Burden, *Sport and Exercise Biomechanics*. New York: Taylor & Francis, 2006.

[55] C. Gordon et al., "1988 Anthropometric Survey of U.S Army Personnel: Methods and Summary Statistics," Anthropology Research Project NATICK/TR-89/044, 1989.

[56] Nordin M. and V. Frankel, *Basic biomechanics of the musculoskeletal system*, 2nd ed. United States: Lippincott Williams & Wilkins, 2001.

[57] Spoor C. W. and Van Leeuwen J. L., "Knee muscle moment arms from MRI and from tendon travel Journal of Biomechanics," *Journal of Biomechanics*, vol. 25, no. 2, pp. pp. 201–206, February 1992.

[58] D. Bartel, D. Davy, and T. Keaveny, *Orthopaedic Biomechanics: Mechanics and Design in Musculoskeletal Systems*, 1st ed. United States: Prentice Hall, 2006.

[59] A. Oatis, *Kinesiology: The mechanics and pathomechanics of human movement*, 2nd ed. United States: Lippincott Williams & Wilkins, 2009.

[60] S. M. KIM, S. Y. LEE, H. C. KANG, and J. H. JEONG, "Study of Knee and Hip Joints' Moment Estimation by Biomechanical Simulation During Various Motion Changes," *Directory of Open Access Journals*, pp. pp. 785 – 788, 2009.

[61] Department of Intelligent Mechanical Systems Okayama University. (2012, April) Intelligent machine control lab. [Online]. http://mcrlab.mech.okayama-u.ac.jp/study_e.htm

[62] S. Davis and Darwin G. Caldwell, "Braid effects on contractile range and friction modeling

in pneumatic muscle actuators," *The international journal of robotics research*, vol. 25, no. 4, pp. 359-369, 2006.

[63] Frank K. Ko, Christopher M. Pastore, and Andrew A. Head, *Handbook of industrial braiding*.: Atkains & Pearce, 1988.

[64] Blaine W, Andersen, *The analysis and design of pneumatic systems*. Huntington: Robert E. Krieger publishing company, 1976.

[65] K. Zelik. (2011, May) Active vs. passive. [Online]. http://www-personal.umich.edu/~kzelik/Active_vs_Passive_Devices.html

[66] T Chin et al., "Comparison of different microprocessor controlled knee joints on the energy consumption during walking in transfemoral amputees: intelligent knee prosthesis vs. c-leg," *Prosthet. Orthot. Int.*, vol. 30, no. 1, pp. 73-80, April 2006.

[67] B. Dellon and Y. Matsuoka, "Prosthetics, exoskeletans, and rehabilitation," *IEEE Robotics & Automation Magazine*, pp. 30-4, March 2007.

[68] W. Ko. (May, 2002) Sensors and actuators for prosthetic systems. [Online]. http://ieeexplore.ieee.org/

[69] E. Levy. (2011, May) The history of prosthetics: Artificial limbs past and present. [Online]. http://www.disaboom.com/amputations-information/

[70] D. G. Caldwell, N. Tsagarakis, G. Medrano-Cerda, J. Schofield, and s. Brown, "Development of a pneumatic muscle actuator driven manipulator rigfor nuclear waste retrieval operations," in *IEEE International Conference Robotics and Automation*, vol. 1, Detroit, 1999, pp. 525-530.

[71] K. Kaufman, S. Frittoli, and C. Frigo, "Gait asymmetry of transfemoral amputees using mechanical and microprocessor-controlled prosthetic knees," *Clinical Biomechanics*, January 2012.

[72] I. Clements. (2011, May) How amputations work. [Online]. http://orthopedics.about.com/od/anatomy/g/lowerextremity.htm

[73] NLLIC Staff. (2008, May) Diabetes and lower extremitis amputations. [Online]. http://www.amputee-coalition.org/fact_sheets/diabetes_leamp.html

[74] J. Rose and J.G. Gamble, *Human Walking*. Baltimore, United States: Williams & Wilkins.

APPENDICES

APPENDIX A

Figure A3-1: Standard dimensions of lower leg and foot geometry for male and female standard adults illustrated via Solid Works

Lower Leg and Foot Geometry			
No	Description	Dimensions in cm	
		Female	Male
1	Stature	162.94	175.58
2	Ball Of Foot Circumference	22.35	24.85
3	Ball Of Foot Length	17.94	19.6
4	Bimalleolar Breadth	6.44	7.28
5	Buttock-Knee Length	58.89	61.64
6	Buttock-Popliteal Length	48.17	50.04
7	Calf Circumference	35.24	37.81
8	Calf Height	31.61	35.34
9	Calf Link	40.04	43.45
10	Foot Breadth, Horizontal	8.97	10.06
11	Foot Length	24.44	26.97
12	Heel Ankle Circumference	30.48	33.9
13	Heel Breadth	6.3	7.01
14	Knee Circumference	36.52	38.64
15	Knee Height, Midpatella	45.87	50.48
16	Knee Height, Sitting	51.54	55.88
17	Lateral Femoral Epicondyle Height	46.11	50.15
18	Lateral Malleolus Height	6.06	6.71
19	Lower Thigh Circumference	37.75	39.18
20	Popliteal Height	38.94	43.41
21	Popliteal - Knee Length	10.72	11.6

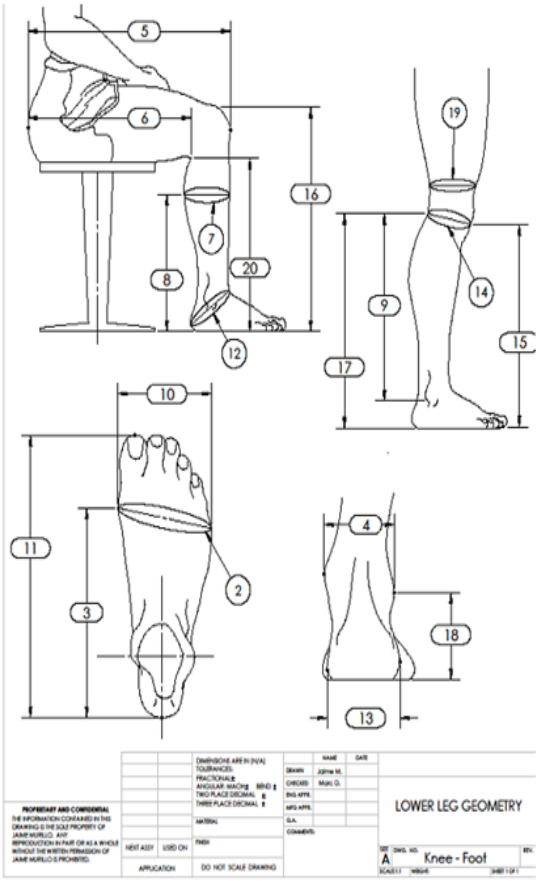

Table A3.1: Knee moment arm (mm) versus knee flexion angle (deg.) from male and female adults **[**57**]**

Flexion Angle	Moment Arm	Flexion Angle	Moment Arm	Flexion Angle	Moment Arm	Flexion Angle	Moment Arm
0.0215517	23.0799	20.3448	47.9988	46.6272	55.8827	72.9526	50.0766
0.786638	23.0946	21.056	48.4114	47.3922	56.0448	73.6207	49.5167
1.33621	23.7872	21.7996	48.7504	48.1681	56.1627	74.278	48.9567
1.8319	24.6124	22.5323	49.0893	48.9332	56.2216	74.903	48.323
2.33836	25.4229	23.2543	49.4282	49.7091	56.2511	75.4849	47.6452
2.86638	26.2039	23.9978	49.7524	50.4741	56.2806	76.0668	46.9525
3.3944	26.9702	24.7414	50.0619	51.25	56.2806	76.6595	46.2599
3.91164	27.7513	25.4741	50.3861	52.0259	56.2658	77.2306	45.5379
4.39655	28.5765	26.2069	50.6955	52.8017	56.2658	77.4138	45.3168
4.88147	29.4017	26.9612	50.9608	53.5776	56.2658	77.9957	44.6095
5.37716	30.2269	27.7155	51.2113	54.3534	56.2806	78.5668	43.9022
5.85129	31.0669	28.4591	51.4766	55.1293	56.2806	79.0948	43.1359
6.32543	31.9069	29.1918	51.786	55.9052	56.2364	79.5905	42.3106
6.82112	32.7321	29.9353	52.0808	56.681	56.1332	80.0754	41.4854
7.34914	33.5279	30.6897	52.3165	57.4461	56.0301	80.5711	40.6602
7.86638	34.3089	31.444	52.5376	58.222	55.9269	81.0453	39.8202
8.38362	35.0899	32.1875	52.8176	58.9871	55.7795	81.5194	38.9803
8.90086	35.8856	32.9418	53.127	59.7522	55.6174	81.9935	38.1403
9.4181	36.6667	33.6853	53.3923	60.528	55.4848	82.5	37.3445
9.93534	37.4624	34.4504	53.5396	61.3039	55.3669	83.028	36.5635
10.4418	38.2582	35.2047	53.7607	62.069	55.2196	83.5022	35.7235
10.9806	39.0245	35.9591	53.967	62.8341	55.0722	83.9763	34.8836
11.5409	39.7613	36.7349	54.1438	63.5991	54.8806	84.4504	34.0436
12.1336	40.4391	37.5	54.3059	64.3534	54.6154	84.9246	33.1889
12.7478	41.0875	38.2651	54.4385	65.097	54.3059	85.4095	32.3637
13.3513	41.7654	39.0302	54.5712	65.8405	54.0112	85.9052	31.5385
13.9224	42.458	39.7953	54.748	66.5841	53.7312	86.4009	30.728
14.4935	43.1506	40.5496	54.9396	67.3384	53.4807	86.875	29.9027
15.097	43.8137	41.3147	55.1017	68.0819	53.2154	87.3491	29.0922
16.2608	44.9632	42.0905	55.2343	68.8147	52.9207	87.8448	28.2818
16.9073	45.5379	42.8556	55.3669	69.5474	52.5818	88.3297	27.4271
17.597	46.0242	43.6207	55.4553	70.2586	52.1544	88.8039	26.5134
18.2974	46.4957	44.3858	55.4701	70.9375	51.6681	89.3534	25.8355
18.9871	46.982	45.1293	55.529	71.6164	51.1524	90.1185	25.865
19.6659	47.4978	45.8728	55.6911	72.2953	50.6219		

APPENDIX B

PAM SOLIDWORKS DRAWINGS & MECHANICAL PROPERTIES

End fixture size S

Part – S1

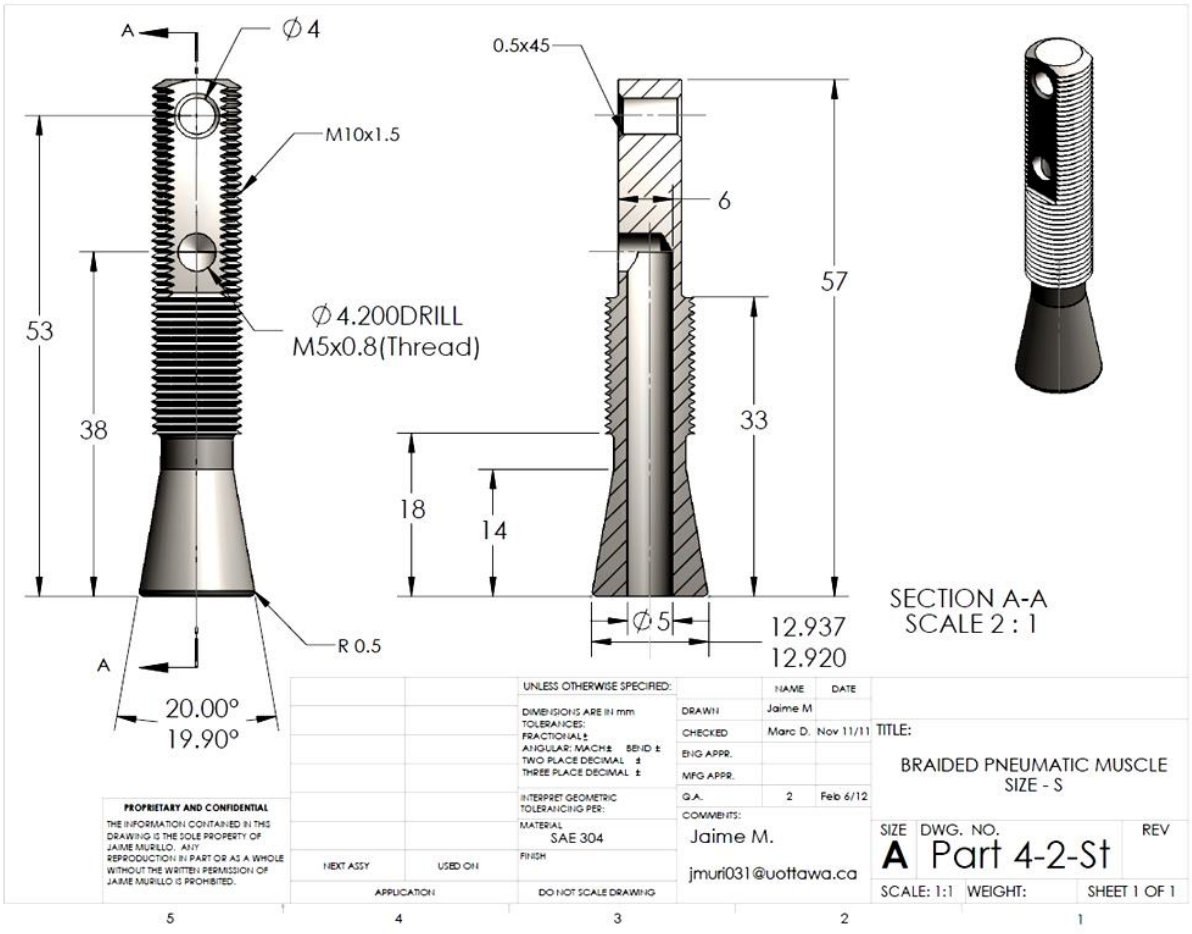

Figure B-1: Construction Drawing 4-2 – Part S1

Figure B-1 shows a detailed fabrication drawing of part S1.The most important aspect in the construction of this component to ensure that design requirements are met (20^o angle and its

maximum diameter). The angle must be the same angle of part S2 to certify that the metallic surfaces in contact with the sleeve-bladder are parallel and the pressure on its material is uniform. In static installations the elastic tube needs a flattening deformation between 12% and 25% to seal the muscle, in this design it is estimated that with a bladder flattening of 40% of the thickness the contact area between sleeve-bladder and the end fitting is around 500 mm^2. Variations in the cone angle or its maximum diameter could considerably reduce this contact area decreasing the service life of the muscle or making the end fitting inoperable. To prevent this problem it is recommended to fabricate the part using a CNC lathe machine which can eliminate machining errors. With this process it is possible to obtain an exact result every single time that is very important in standardized and interchangeable parts.

For this study, all of the components were manufactured in the machine shop of the Mechanical Engineering Department in University of Ottawa.

Part – S2

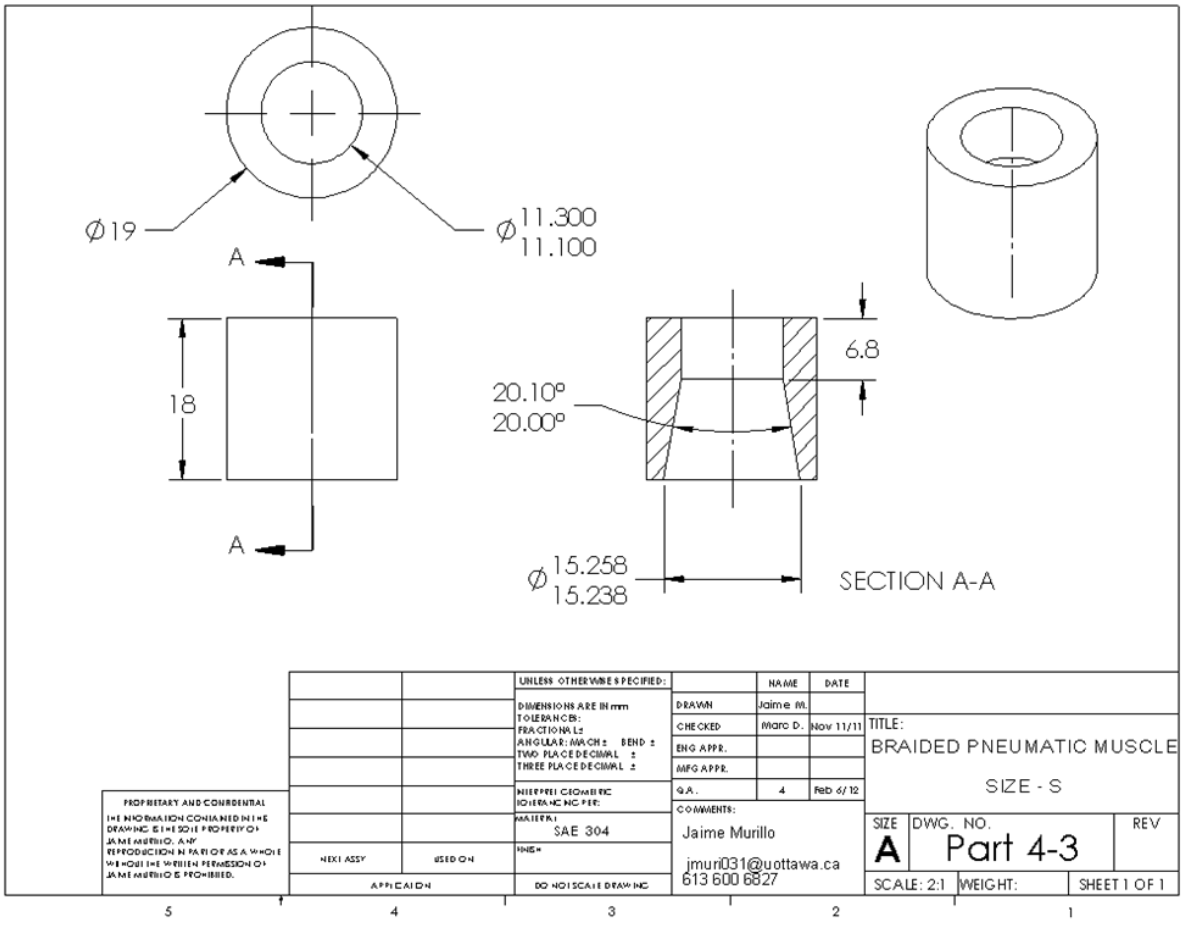

Figure B-2: Construction drawing 4-3 – Part S2

Figure B-2 illustrates the detailed construction drawing number 4-3 of part S2. Similar to part S1, the most important aspect of this component is related to the internal cone dimensions, missing these tolerances could ruin the end fitting and for this reason, as it was explained previously, it is recommended to manufacture the part using the CNC lathe machine process.

Part – S3

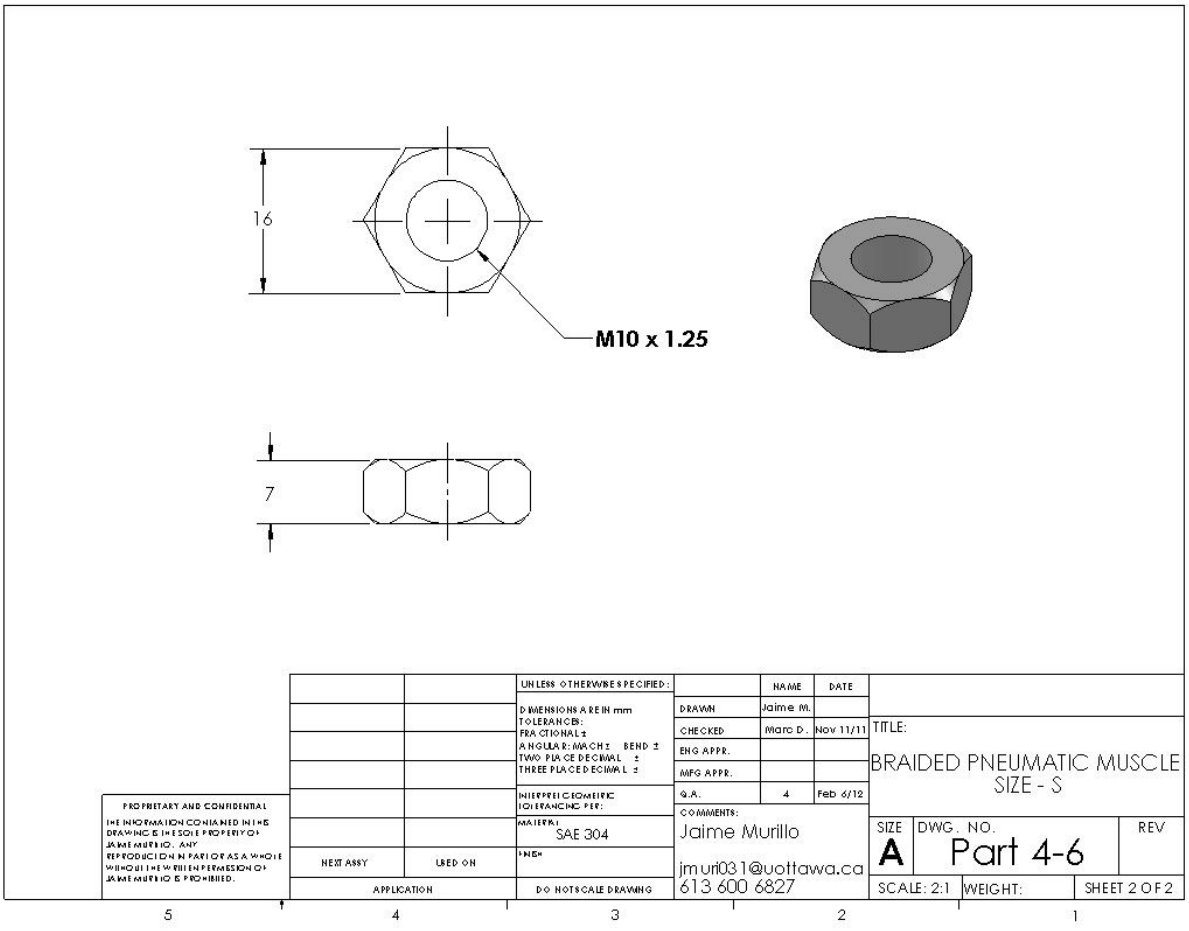

Figure B-3: Construction Drawing 4-6 – Part S3

Figure B-3 shows the detailed construction drawing number 4-6 of part S3. This part is a 10 mm commercial nut, but due to the inconsistence in the external diameter and thickness of nuts from different providers, it is important to establish the dimensions required for this end fitting. Keeping at minimum the variation of dimensions is important to use the minimum number of tools to assemble the muscle.

Part – S4

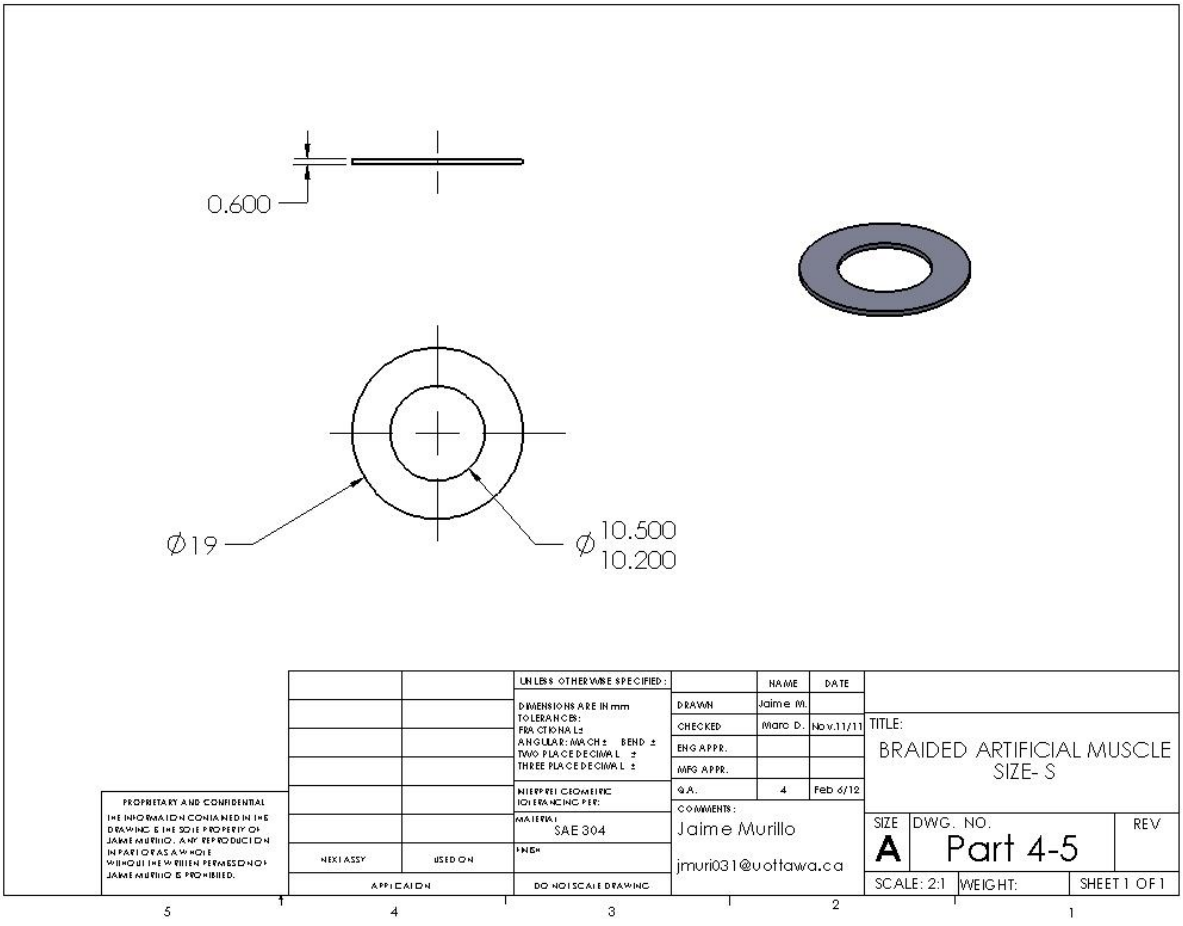

Figure B-4: Construction Drawing 4-5 – Part S4

Figure B-4 presents detailed construction drawing 4-5 of part S4. This component is an M10 commercial washer, but due to incongruence between dimensions of commercial parts, using the same reference is not guaranty of geometric equality. The minimum diversity of dimensions between parts makes easier to assemble the muscle. Usually the standard measure of the washer is only the central measure and the external dimension and thickness could vary considerably. It could not affect the performance of the muscle if the external diameter of the washer is smaller than 19 mm, but it would be different if it is bigger, any part out of the body of the muscle could easily collide during the expansion and contraction displacement.

Part – 5S

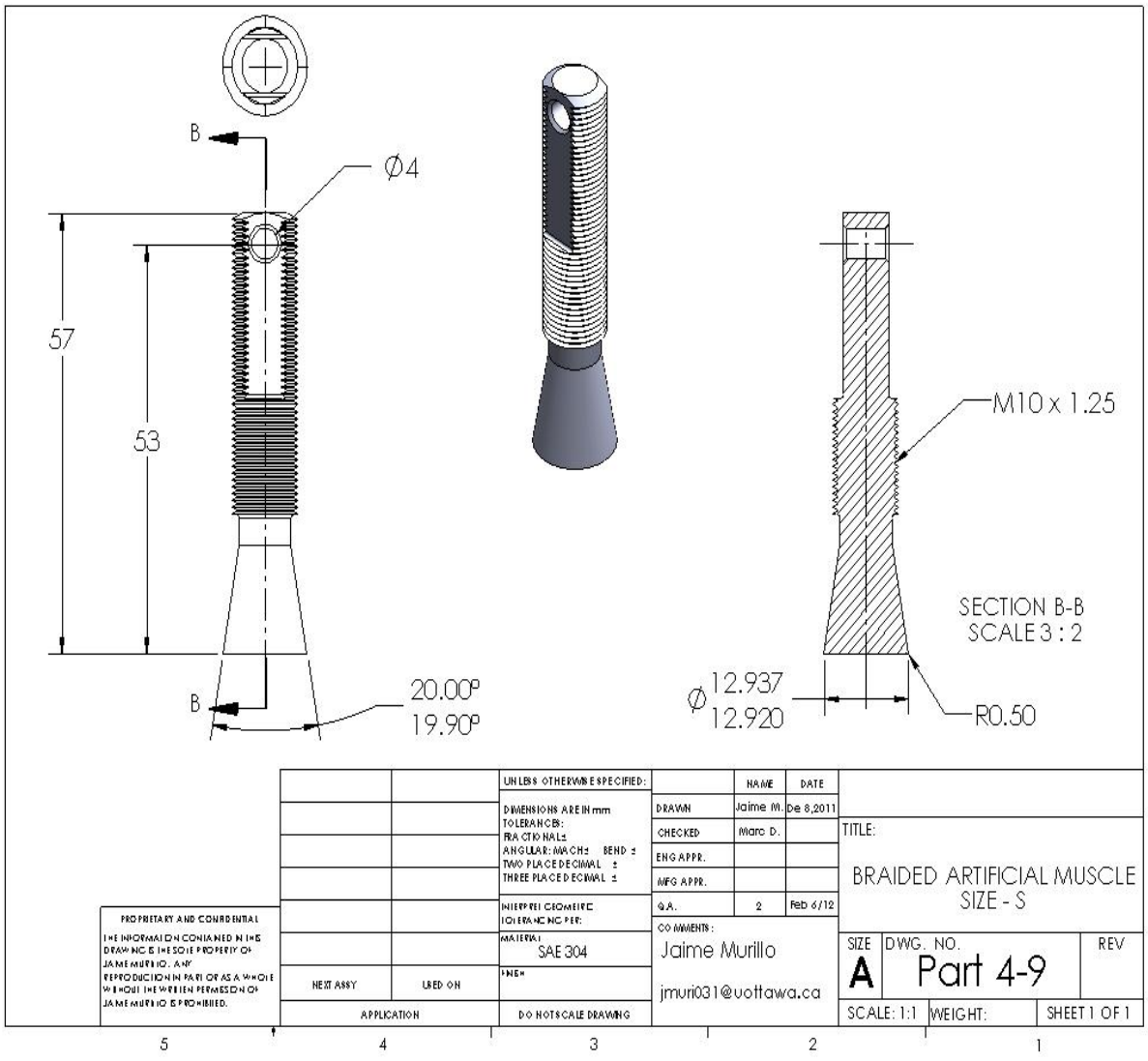

Figure B-5: Construction Drawing 4-9 – Part 5S

Figure B-5 displays the detailed construction drawing number 4-9 of part S5. This part has the same characteristics and geometry of part S1 without the gas pressure connection. For the construction, this element has the same warning about the angle dimensions and same recommendation on the subject of its construction.

.

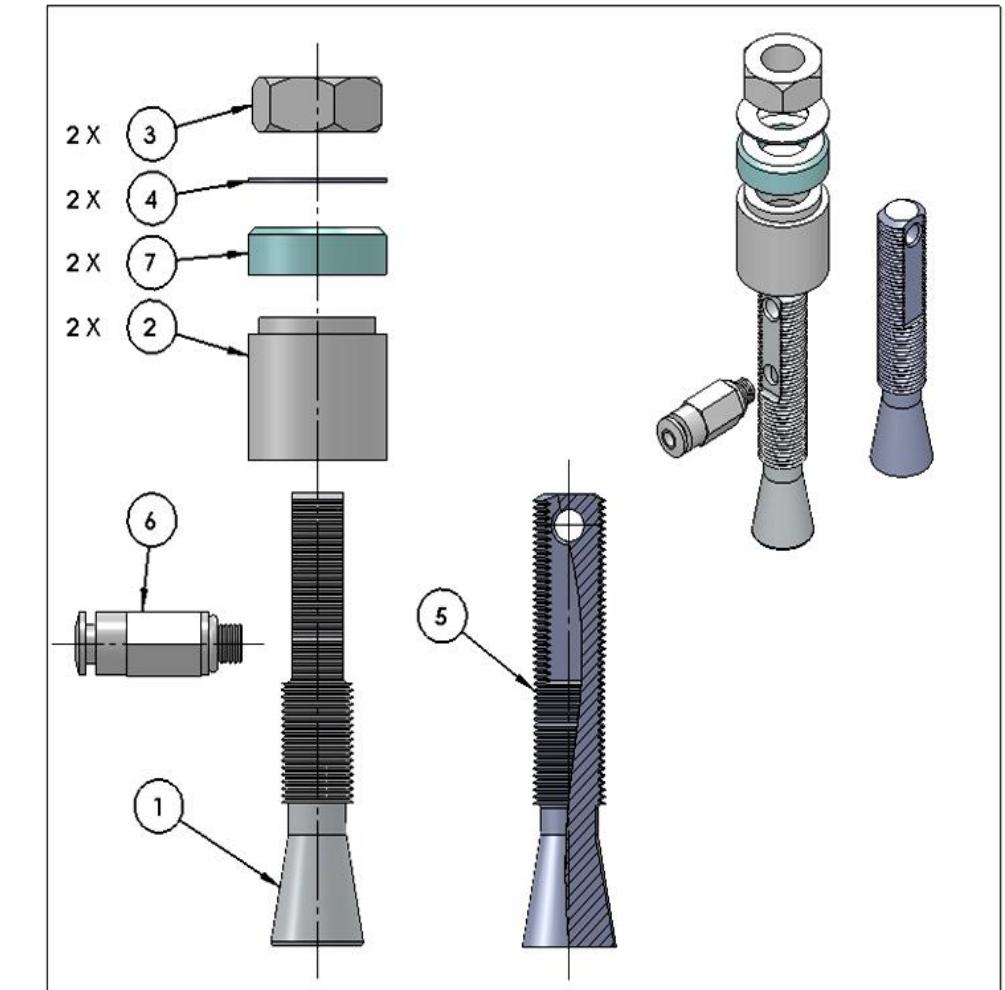

ITEM NO.	PART NUMBER	DESCRIPTION	MATERIAL	QTY.
1	Part 4-2	0.5" Round Bar - 2" Length	SAE 304	1
3	Part 4-6	Metric Hex Nut M10x1.5	SAE 304	2
6	Part 4-4	Straight Adaptor ΦD 0.25" - M5x0.8	Brass	1
2	Part 4-3 MOD	0.75" Round Bar - 1.0" Length	SAE 304	2
4	Part 4-5	10 mm Washer	SAE 304	2
7	Part 4-5 MOD	0.75" Round Bar - 0.3" Length	SAE 304	2
5	Part 4-9	0.5" Round Bar - 2" Length	SAE 304	1

Figure B-6: End Fitting Size S - Assembly and BOM table

Part – 2SM

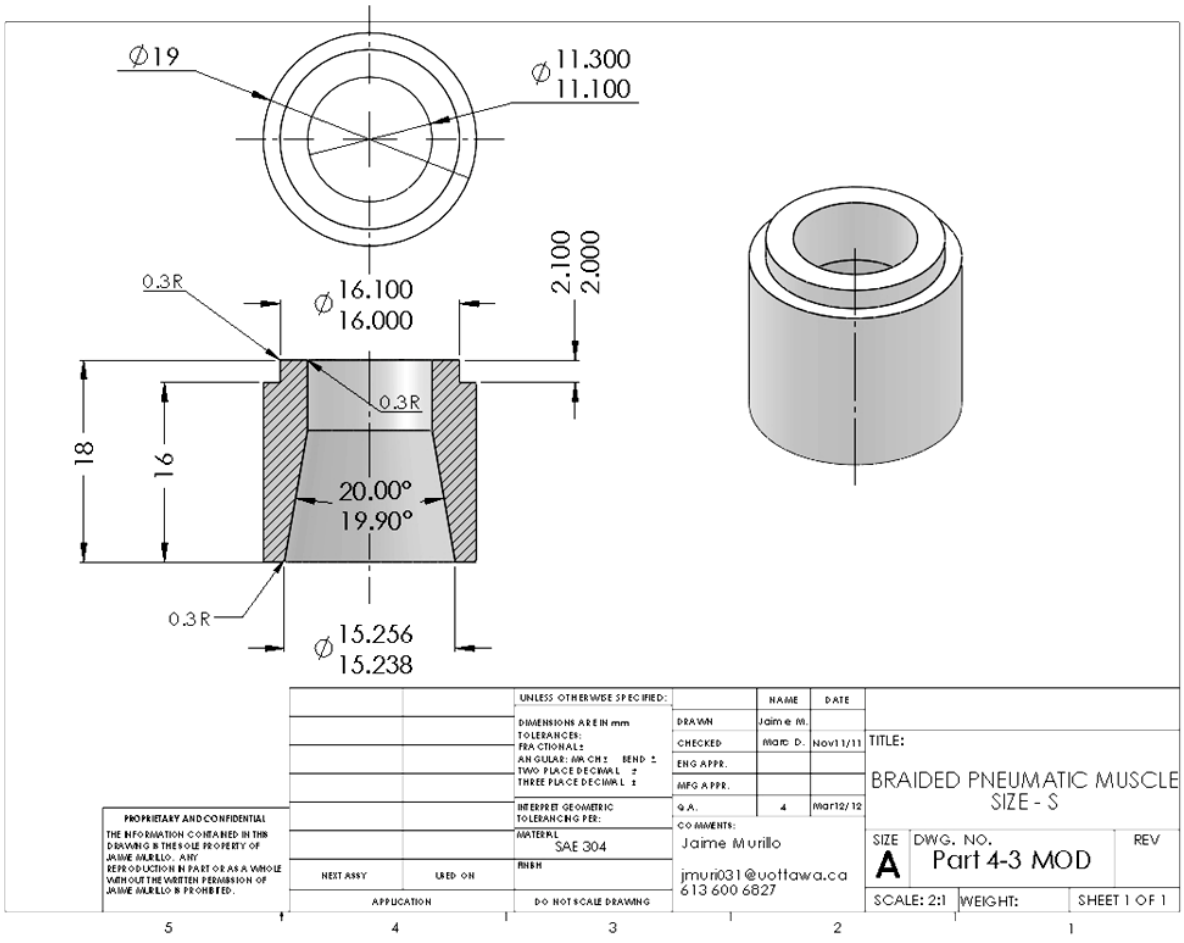

Figure B-7: Construction Drawing 4-3MOD - Part S2M

Figure B-7 is the detailed construction drawing 4-3MOD of part S2M which replaces the initial drawing number 4-3. The difference between this part and the initial part lies essentially in the top of the component that in the new part was machined to grab the sleeve in combination with part 7S. The tolerance in the 16 mm diameter is important to permit the correct pressure between the two parts and the sleeve fabric. These dimensions were calculated in base of the thickness of the sleeve we are using for this study, the sleeve material is flexible and small changes in the thickness do not affect the junction performance, but for differences higher than 30% it is recommended to recalculate the tolerances at this point of part 2 and part 7. Other important

measures in this component are the cone angle and its diameter that how it was explained in the initial design the part would be useless if these measures are out of limit.

Part – 7SM

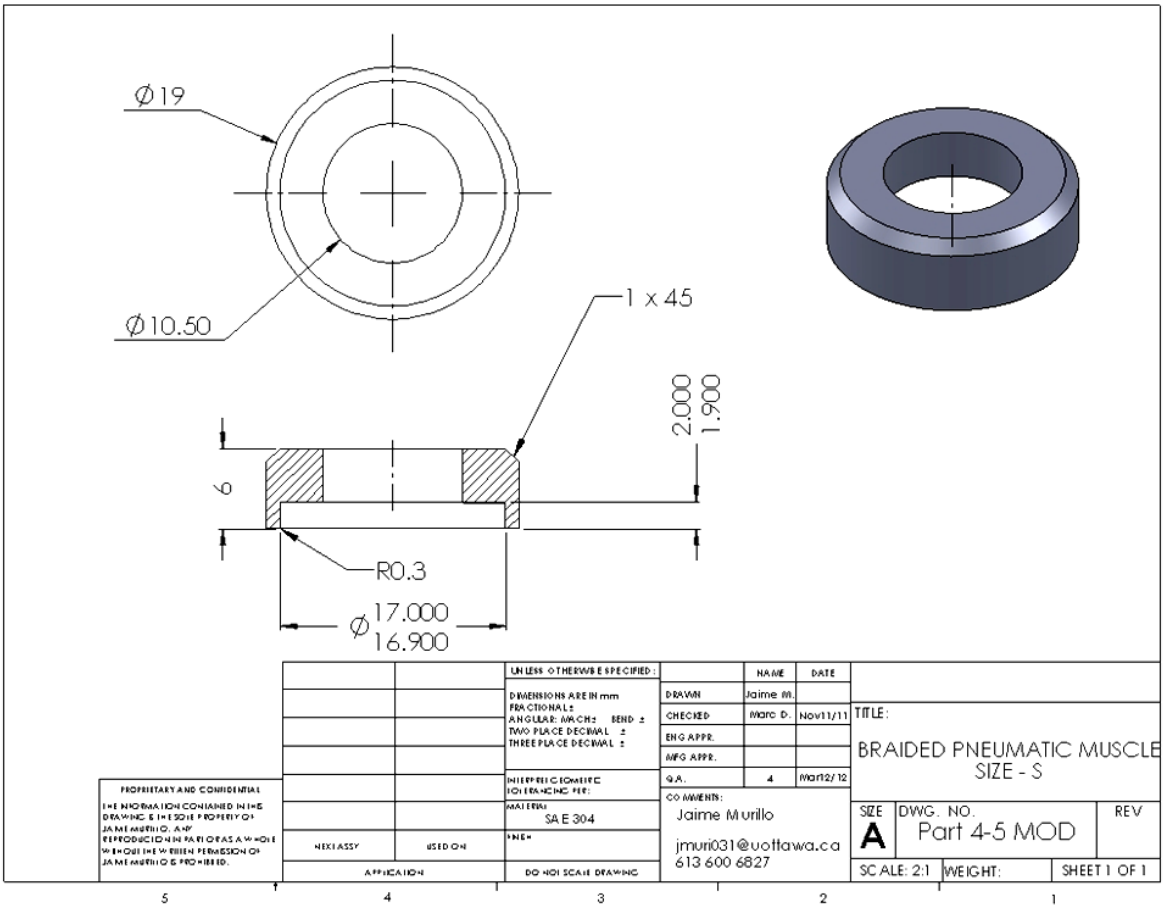

Figure B-8: Construction Drawing 4-5MOD - Part S7MOD

Figure B-8 illustrates the detailed construction drawing 4-5MOD of the part 7S. With this modification the sleeve is pressed vertically by the new part and pressed horizontally by part2 when the nut 3 is tightened. Similar to the part 2S, keeping tolerances ensure a good performance of the fitting. Dimensions of this part were calculated according the braided sleeve thickness and variations of this measure over 30% could involve new calculation of the part to prevent malfunction of the system.

Mechanical properties of part S1

In the end fitting the part 1 is the longest and most important component. This element supports the muscle pulling force and transversal forces due to the gas pressure. Also, it has to withstand additional stresses during assembly and installation. Because the part1 is the most demanded part, additional analyzes were made to validate the capacity and corroborate these results with testing laboratory work.

Density = 8.00 grams per cubic centimeter

Mass = 23.47 grams

Volume = 2933.30 cubic millimeters

Surface area = 3225.49 mm^2

Center of mass:

X = 0.02 mm

Y = 26.47 mm

Z = 0.00 mm

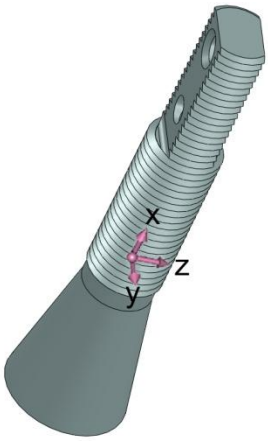

Principal axes of inertia and principal moments of inertia: (grams * square millimeters)
Taken at the center of mass

Ix = (0.00, 1.00, 0.00)	**Px** = 327.67
Iy = (0.00, 0.00, 1.00)	**Py** = 7441.07
Iz = (1.00, -0.00, -0.00)	**Pz** = 7469.35

Moments of inertia: (grams * square millimeters)
Taken at the center of mass and aligned with the output coordinate system.

Lxx= 7469.34	**Lxy** = 4.93	**Lxz** = 0.00
Lyx = 4.93	**Lyy** = 327.67	**Lyz**= 0.00
Lzx = 0.00	**Lzy** = 0.00	**Lzz**= 7441.07

Moments of inertia: (grams * square millimeters)

Taken at the output coordinate system

Ixx = 23905.60	**Ixy** = 16.16	**Ixz** = 0.00
Iyx = 16.16	**Iyy**= 327.68	**Iyz** = -0.00
Izx= 0.00	**Izy** = -0.00	**Izz** = 23877.34

Finite Element Analysis - Simulation of Part S1 Results

For this simulation, the highest pressure and forces were used in mechanical testing laboratory, the gas pressure and pulling force were 2964745.63N/M2 and 2,000 N, respectively.

Table B1: Finite element simulation

Solid Bodies			
Document Name and Reference	Treated As	Volumetric Properties	Document Path/Date Modified
Chamfer1 	**Solid Body**	Mass:0.0235296 kg Volume:2.9412e-006 m^3 Density:8000 kg/m^3 Weight:0.23059 N	D:\MASTER\ANTAGONISTIC PNEUMATIC MUSCLE JOINT\Phase II\Drawings -Fittings\Design 4\Part 4-2.SLDPRT **Feb 13 12:07:22 2012**

Table B2: Finite element simulation

Model Reference	Properties		Components
	Name:	AISI 304	Solid-Body 1(Chamfer1)(Part 4-2)
	Model type:	Linear Elastic Isotropic	
	Default failure criterion:	Unknown	
	Yield strength:	2.06807e+008 N/m^2	
	Tensile strength:	5.17017e+008 N/m^2	

Loads and Fixtures

Table B3: Finite element simulation

Fixture name	Fixture Image	Fixture Details	
Fixed-1	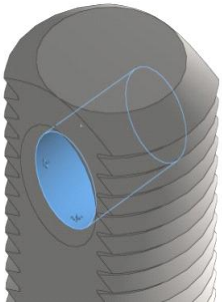	Entities: Type:	**1 face(s)** **Fixed Geometry**

Load name	Load Image	Load Details	
Force-1	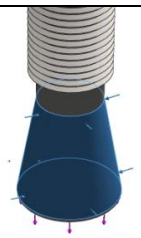	Entities: Type: Value:	**1 face(s)** **Apply normal force** **500 N**

Pressure-1	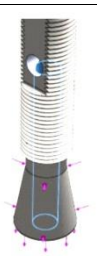	Entities: Type: Value: Units:	**1 face(s)** **Normal to selected face** **2.96475e+006** **N/m^2**

Force-2	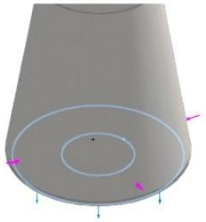	Entities: Type: Value:	**1 face(s)** **Apply normal force** **-2000 N**

Table B4: Mesh Information

Mesh type	Solid Mesh
Mesher Used:	Standard mesh
Automatic Transition:	Off
Include Mesh Auto Loops:	Off
Jacobian points	4 Points
Element Size	0.716685 mm
Tolerance	0.0358343 mm

Mesh Quality	High

Table B5: Mesh information details

Total Nodes	184722
Total Elements	123211
Maximum Aspect Ratio	20.872
% of elements with Aspect Ratio < 3	84.8
% of elements with Aspect Ratio > 10	0.188
% of distorted elements(Jacobian)	0
Time to complete mesh(hh;mm;ss):	00:00:17
Computer name:	0110S070

Table B6: Study results

Name	Type	Min	Max
Stress	VON: von Mises Stress	171629 N/m^2 Node: 148029	2.343e+008 N/m^2 Node: 130388
Model name: Part 4-2 Study Name: Simulation Xpress Study Plot Type: Static nodal stress Deformation Scale: 381.812			

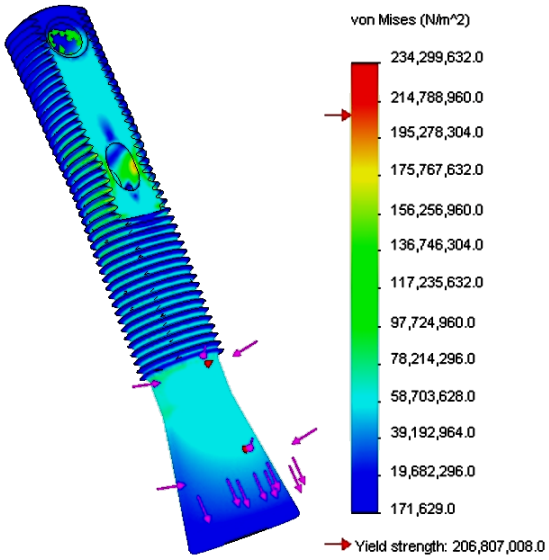

Model name: Part 4-2

Study Name: Simulation Xpress Study

Plot Type: Deformed Shape Deformation

Deformation Scale: 381.812

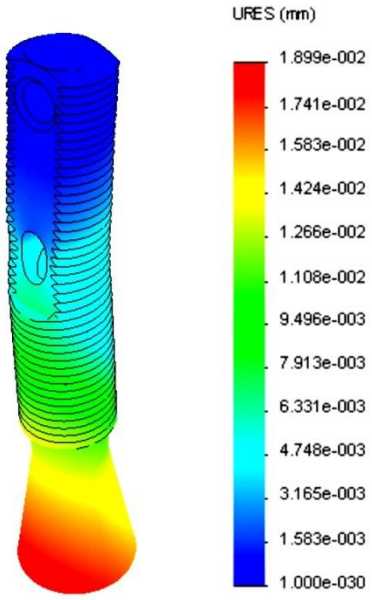

Part 4-2-SimulationXpress Study-Displacement-Displacement

Name	Type
Deformation	Deformed Shape

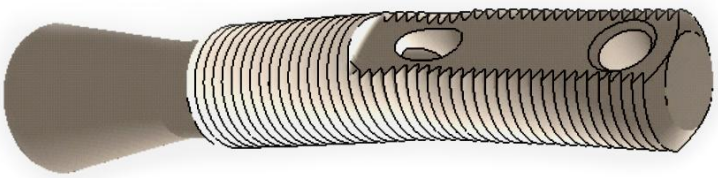

Model name: Part 4-2

Name	Type	Min	Max
Factor of Safety	Max von Mises Stress	0.88266 Node: 130388	1204.97 Node: 148029

Model name: Part 4-2

Study Name: Simulation Xpress Study

Plot Type: Factor of Safety

Criterion: Max von Misses Stress

Red<FOS=1.5<Blue

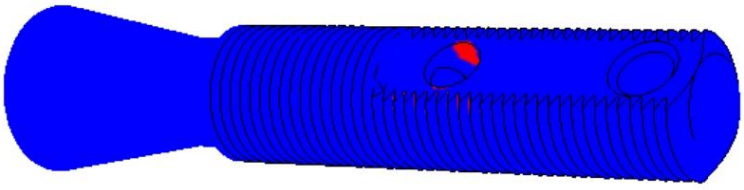

Part 4-2-SimulationXpress Study-Factor of Safety-Factor of Safety

Conclusion

The simulation showed the expected deformation and the critical point of the part at the air pressure connection. Simulation and Laboratory Analysis results indicated that the design makes the part safe and strong enough to be used in the pneumatic artificial muscle with forces around 2000 N. For different application where the puling force generated by muscles using this size of end fitting, the factor of safety FOS can be easily increased reducing the internal diameter dimension of the longitudinal hole in the center of the part.

END FITTING SIZE - L

Size L was designed for a 14 mm bladder diameter and a 32 mm sleeve diameter. Similar to the previous design, the flexibility of the bladder and braided sleeve permit assembling several different muscle sizes with size of end fitting. The part number column in the table makes reference to the number of the construction drawing of the part, and the description column refers to the raw material necessary for construction of the component.

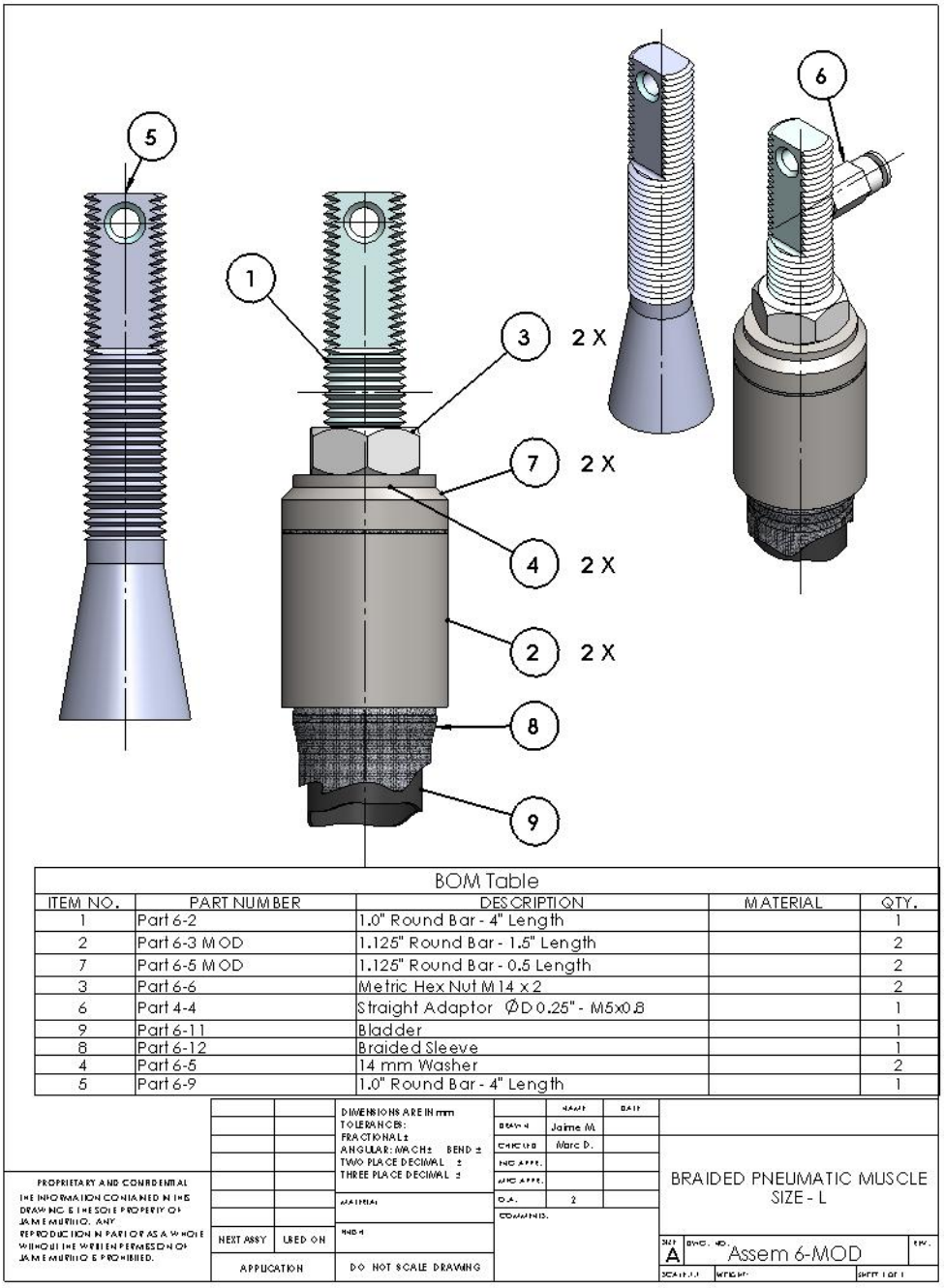

BOM Table

ITEM NO.	PART NUMBER	DESCRIPTION	MATERIAL	QTY.
1	Part 6-2	1.0" Round Bar - 4" Length		1
2	Part 6-3 MOD	1.125" Round Bar - 1.5" Length		2
7	Part 6-5 MOD	1.125" Round Bar - 0.5 Length		2
3	Part 6-6	Metric Hex Nut M 14 x 2		2
6	Part 4-4	Straight Adaptor ØD 0.25" - M5x0.8		1
9	Part 6-11	Bladder		1
8	Part 6-12	Braided Sleeve		1
4	Part 6-5	14 mm Washer		2
5	Part 6-9	1.0" Round Bar - 4" Length		1

Figure B-9: End fixture size L, Assembly and BOM table

Figure B-9 displays assembly of the end fitting size L with all components necessary for the muscle and the BOM table which includes drawing part number, raw material and parts quantity.

Part- L1

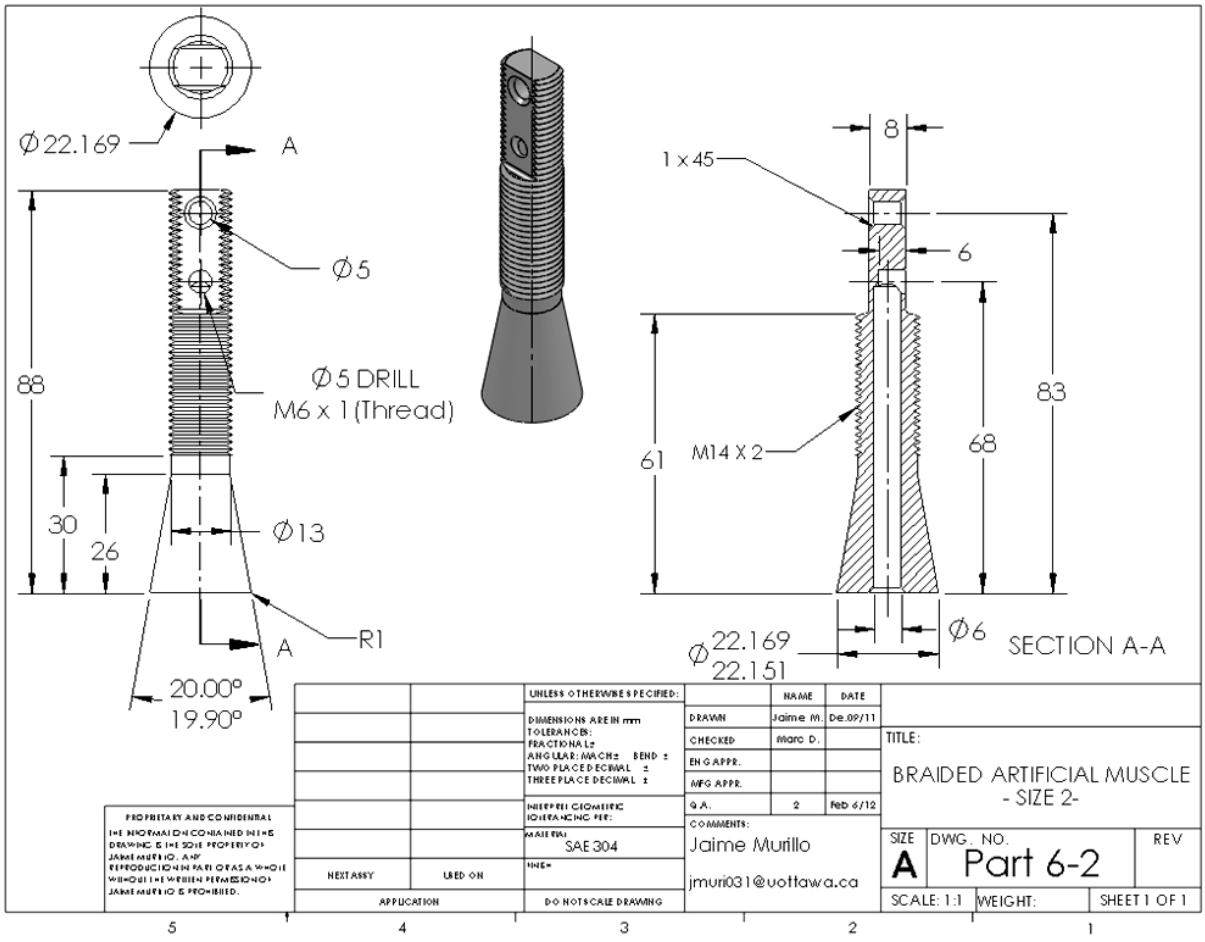

Figure B-10: Construction Drawing 6-2 - Part L1

Figure B-10 illustrates detailed construction drawing of the part L1. For the construction of this component the same advice and recommendations given for the part S1 apply.

Part - L2

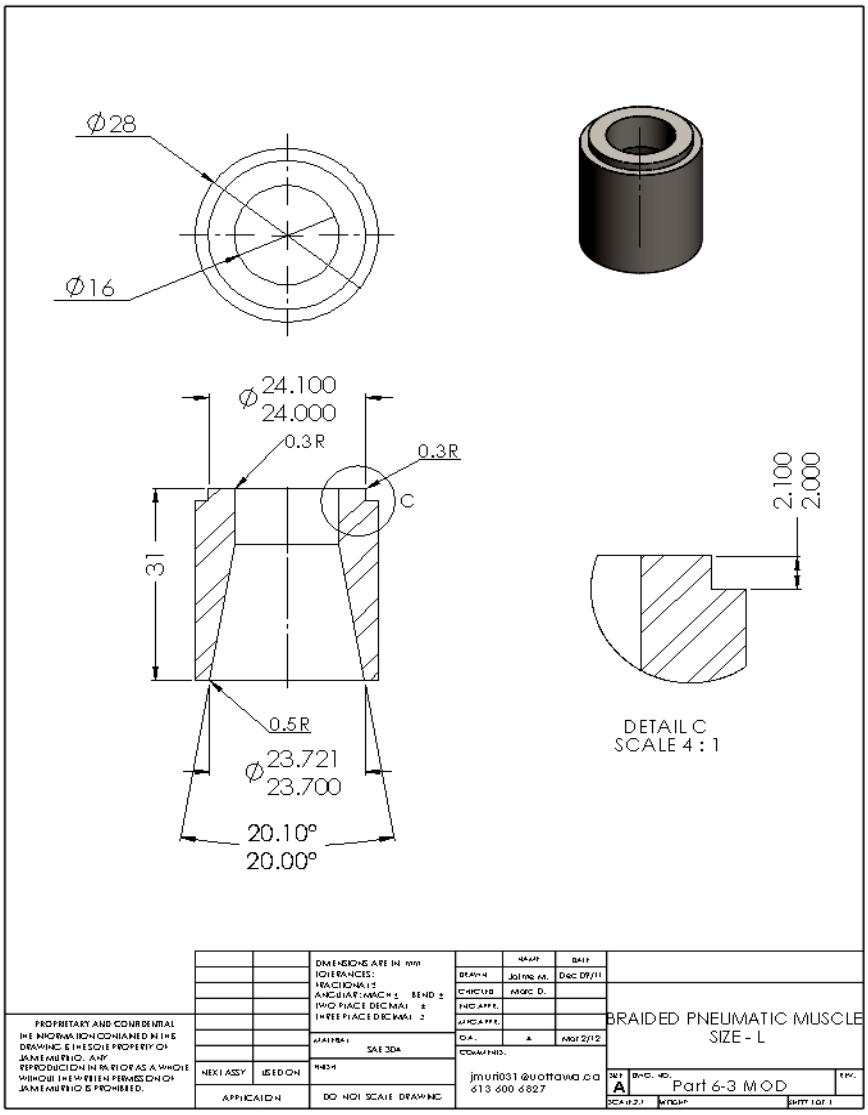

Figure B-11: Construction Drawing 6-3MOD - Part L2

Figure B-11 displays the detailed construction drawing of part L2. For the construction of this part it is recommended to see the advice related about tolerances and angle measures given in part S2

Part - L3

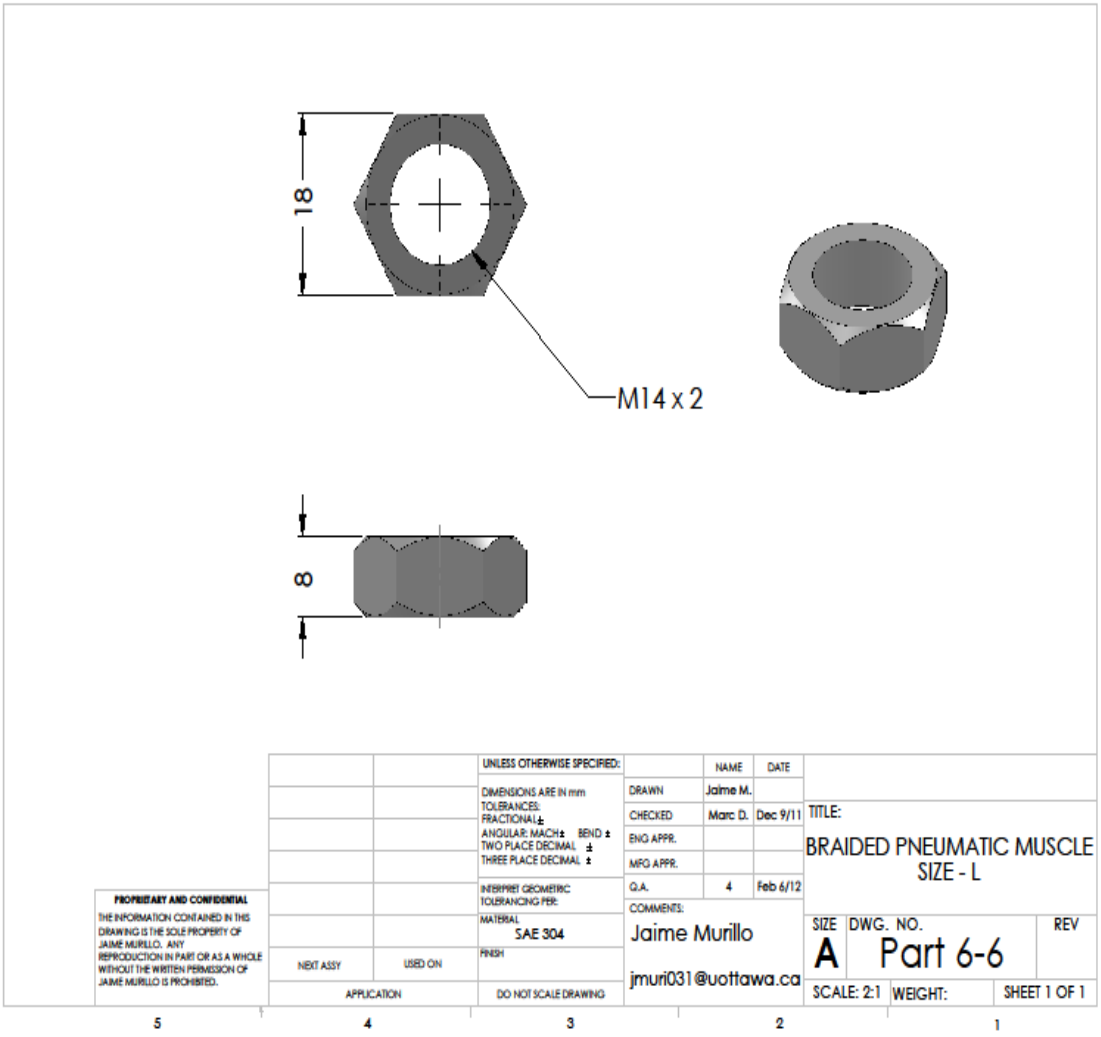

Figure B-12: Construction Drawing 6-6 - Part L3

Figure B-12 shows the detailed construction drawing of part L3. This component is an M14 x 2 metric hexagonal commercial nut and this drawing indicates the dimensions required for this end fitting.

Part - L4

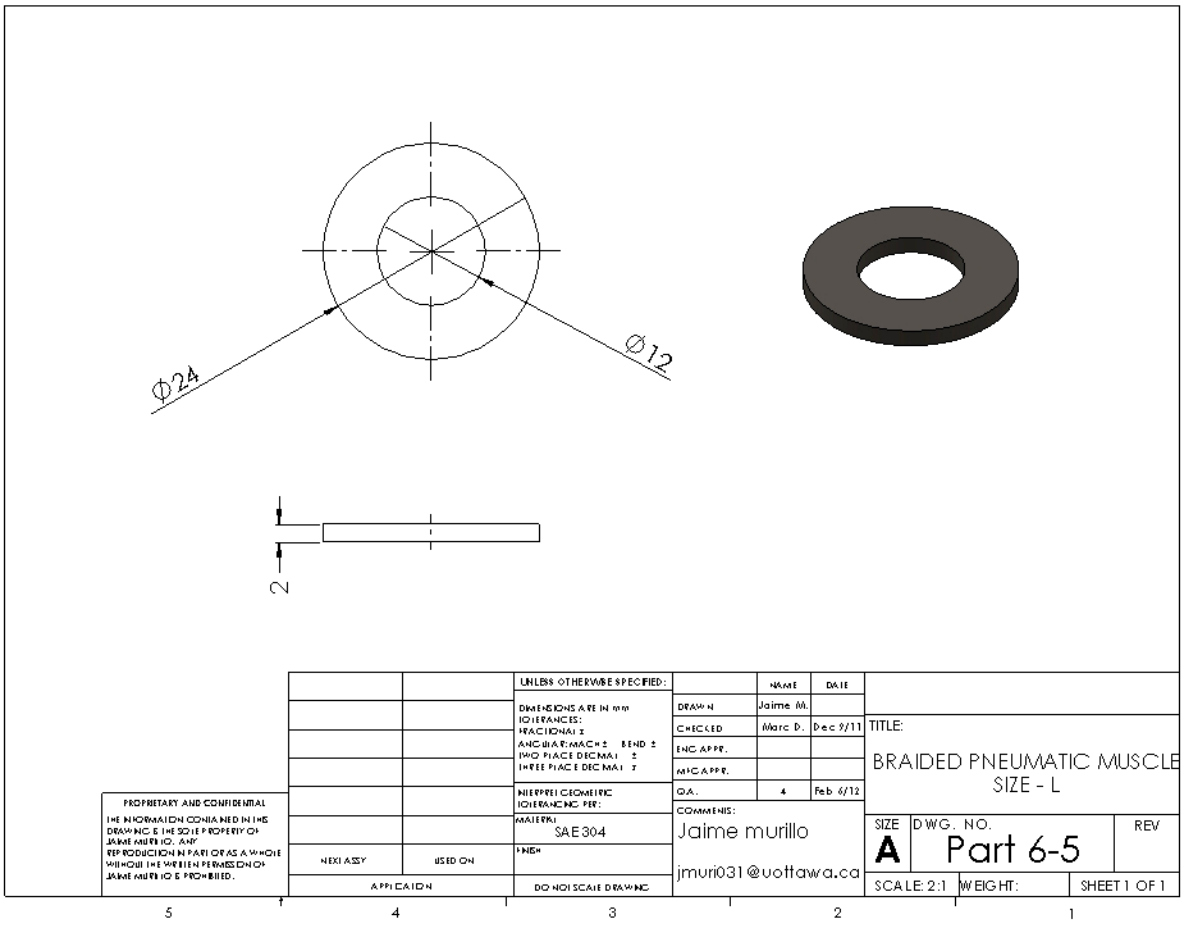

Figure B-13: Construction Drawing 6-5 - Part L4

Figure B-13 displays the construction drawing of the part L4 with the dimensions recommended for the fitting. The external diameter could be smaller with no incidence in the performance of the muscle, but bigger diameters could interfere with the smooth displacement of the fitting.

Part – L5

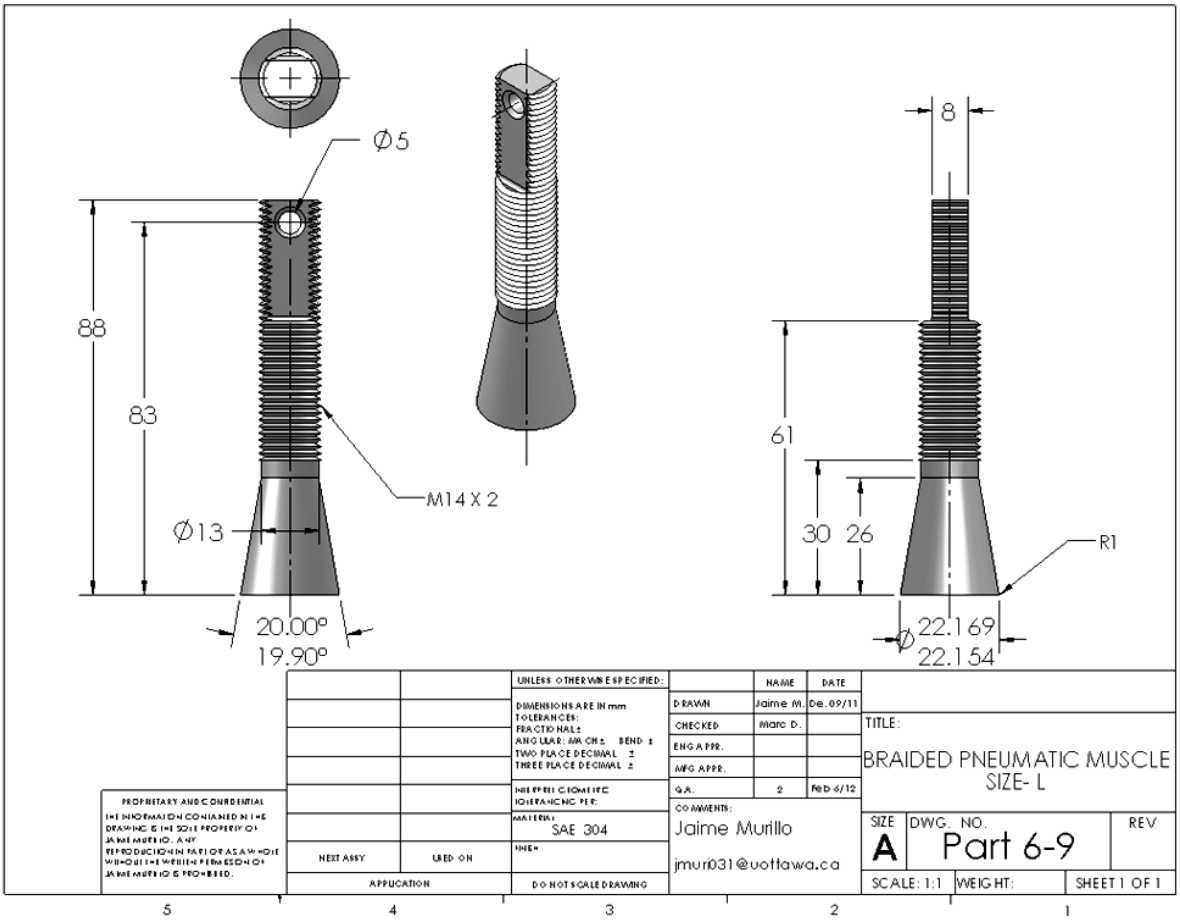

Figure B-14: Construction Drawing 6-9 - Part L5

Figure B-14 displays the detailed construction drawing of the part L5. This is the most important component of the end fitting and recommendations in connection with its construction are shown in part S1.

Part – L7

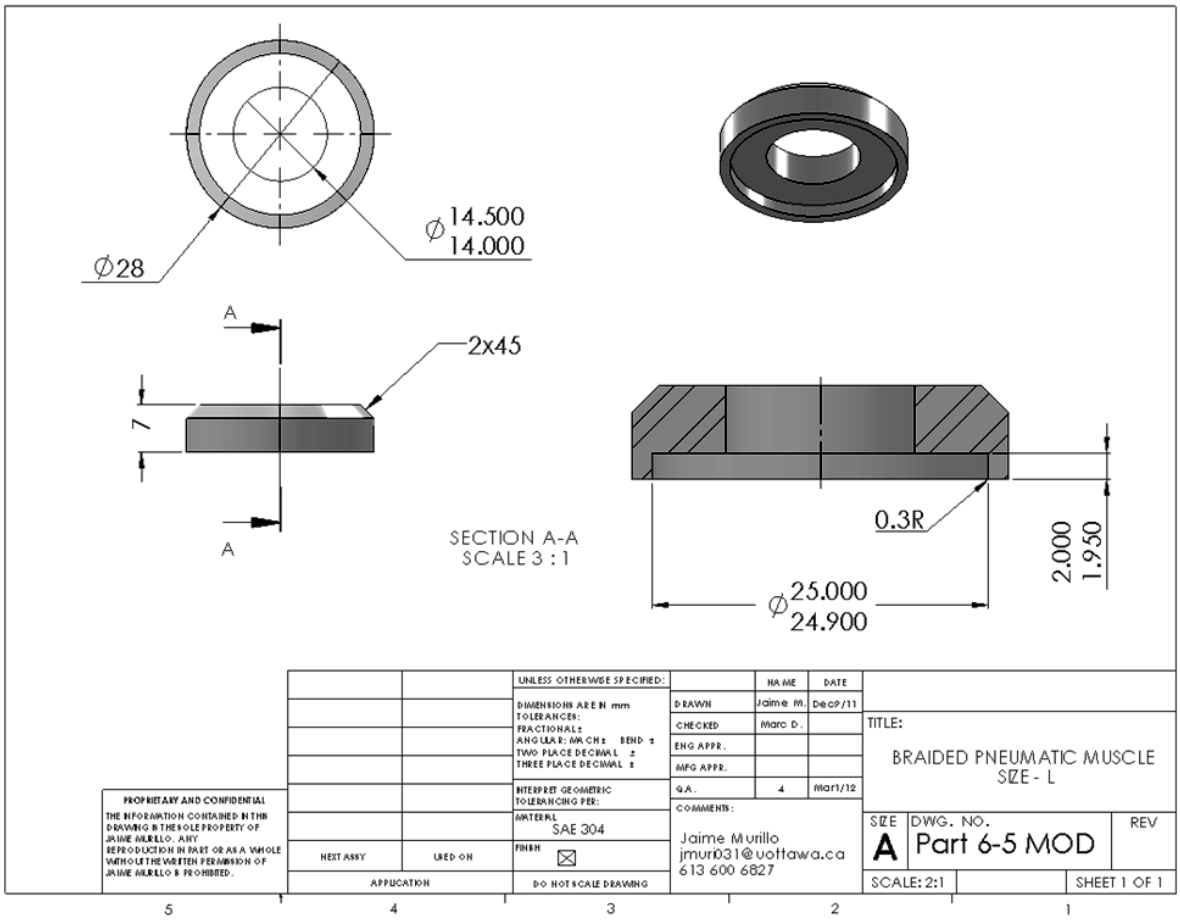

Figure B-15: Construction Drawing 6-5MOD - Part L7

Figure B-15 shows the detailed construction drawing of part L7. This part, similar to part S7, was designed to enhance the holding capacity of the end fitting putting additional pressure on the braided sleeve.

Mass properties of Part L1

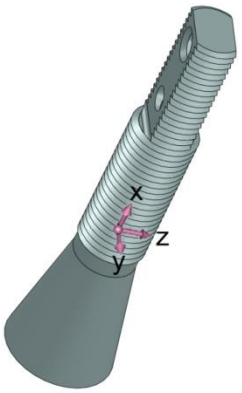

Density = 0.01 grams per cubic millimeter

Mass = 90.39 grams

Volume = 11299.13 cubic millimeters

Surface area = 7427.55 mm^2

Center of mass:

X = 0.00 mm
Y = 32.67 mm
Z = 0.01 mm

Principal axes of inertia and principal moments of inertia: (grams * square millimeters)

Taken at the center of mass

Ix = (0.00, 1.00, 0.00)	**Px**= 3215.04
Iy = (-1.00, 0.00, 0.00)	**Py** = 63415.51
Iz = (0.00, -0.00, 1.00)	**Pz**= 63564.75

Moments of inertia: (grams * square millimeters)

Taken at the center of mass and aligned with the output coordinate system.

Lxx = 63415.51	**Lxy** = 0.00	**Lxz** = -0.00
Lyx= 0.00	**Lyy** = 3215.05	**Lyz**= 29.98
Lzx = -0.00	**Lzy** = 29.98	**Lzz** = 63564.74

Moments of inertia: (grams * square millimeters)

Taken at the output coordinate system

Ixx = 159867.00	**Ixy** = 0.01	**Ixz**= -0.00
Iyx = 0.01	**Iyy** = 3215.06	**Iyz**= 57.57
Izx = -0.00	**Izy**= 57.57	**Izz** = 160016.22

Mass properties of Part 4-2

Density = 0.01 grams per cubic millimeter

Mass = 23.47 grams

Volume = 2933.30 cubic millimeters

Surface area = 3225.49 millimeters^2

Center of mass:

X = 0.02 mm
Y = 26.47 mm
Z = 0.00 mm

Principal axes of inertia and principal moments of inertia: (grams * square millimeters).

Taken at the center of mass.

Ix = (0.00, 1.00, 0.00)	**Px** = 327.67
Iy = (0.00, 0.00, 1.00)	**Py**= 7441.07
Iz = (1.00, -0.00, -0.00)	**Pz**= 7469.35

Moments of inertia: (grams * square millimeters)

Taken at the center of mass and aligned with the output coordinate system.

Lxx = 7469.34	**Lxy**= 4.93	**Lxz**= 0.00
Lyx = 4.93	**Lyy** = 327.67	**Lyz** = 0.00
Lzx= 0.00	**Lzy** = 0.00	**Lzz** = 7441.07

Moments of inertia: (grams * square millimeters)

Taken at the output coordinate system.

Ixx = 23905.60	**Ixy** = 16.16	**Ixz** = 0.00
Iyx = 16.16	**Iyy** = 327.68	**Iyz** = -0.00
Izx = 0.00	**Izy**= -0.00	**Izz** = 23877.34

BRAID AND BLADDER MATERIAL

Bladder Materials - Rubber Bicycle Tube

In this study three different materials were used for the inner flexible tube of the muscle. The first material was a Rubber Bicycle Tube "INNOVA", size 700 x 19/23CF/V48MM. This inner tube is a doughnut shaped "bladder" that goes inside a bicycle tire to hold the air pressure. The most common material in the fabrication of this inner tube is butyl rubber ("Polyisobutylene").

Key Properties and Characteristics

Durometer (Shore A)	40-80
Specific Gravity (Polymer)	0.92
Tensile Strength Max-psi (MPa)	2000 (13.8)
Low Temperature Brittle Point (C/F)	(-58)/(-70)
Resilience	P
Compression Set	F
Heat Aging	G to E
Abrasion Resistance	G
Tear Strength	G
Flame Retardant Properties	P
Weathering Characteristics	G to E
Oxidation Resistance	E
Ozone Resistance	G to E
Oil Resistance	P
Acid Resistance	E
Resistance to Alkali Substances	E

Low gas permeability BIIR & CIIR offer improved cure characteristics

Legend: **P**=Poor; **F**=Fair; **G**=Good; **E**=Excellent

This rubber is used for the inner tubes and linings of pneumatic tires and in vacuum and high pressure applications due to the very high impermeability to gases. This material shall not be used in contact with mineral oils.

Pros:
Inexpensive; Good air pressure retention – low air diffusion over time; Durable

Cons:
it is relatively inelastic – higher losses from flexing;

Bladder Materials - Natural Latex rubber

The second type of material was natural Latex rubber. This is more specialized material and is typically used in “high performance” tubular tire models. It is available for use in clincher tires and is a form of natural rubber known as latex. This highly elastic rubber material is the same type of material used in common party balloons and some types of surgical gloves. The main advantageous feature of this material is it's elasticity, or its ability to be stretched, or deflected by large amounts and return to its unloaded state with very little hysteresis, or energy losses.

Natural Rubber Latex Tubing Specification Sheet:

Chemical Resistance:

Strong Alkalies	Fair
Weak Alkalies	Good
Strong Acids	Poor
Weak Acids 100%	Good
Petroleum	Poor
Ozone Resistance:	Poor
UV Resistance:	Fair
Physical Properties:	
Tensile Strength (psi)	3500 min

Ultimate Elongation	750% min
Hardness (Shore A)	35 ± 5
Modulus (psi)	125max
Specific Gravity	0.97max

Maximum Recommended Operating Temperature

212°F Intermittent - 158°F Continuous Primeline's natural rubber latex tubing meets or exceeds the physical properties of Commercial Item Description A-A-52047C Type I Class 1, 2, and 3, Type III, Type IV, and Type V Class 1, 2, and 3 which replaced Federal Specification ZZ-T-831D.

Standard Tolerances: Inside diameter is ± 0.015 inch on sizes up to 3/8 inch, proportionately greater on larger sizes. Wall thickness is 1/32 inch (0.8 mm) and 3/64 inch (1.2 mm) ± 0.007 inch, 1/16 inch (1.6 mm) and 5/64 inch (2.0 mm) ± 0.010 inch, 3/32 inch (2.4 mm) and 1/8 inch (3.2 mm) ± 0.015 inch. Wall thickness over 1/8" is estimated on the outside diameter tolerance.

Pros:
Highly elastic – low energy losses from deflection; Good resistance to flats from impacts ("snakebite" flats)

Cons:
Relatively expensive – typically 2X-3X the cost of butyl; higher air diffusion – need to check pressures more; more sensitive to installation technique for clinchers [2].

Bladder Materials - Silicone rubber

Silicone rubber was the last material used to make the bladder of the PAM for this study. This material is an elastomer made of a polymer containing silicon together with carbon, hydrogen, and oxygen commonly used in the industry with many different formulations. Silicone rubber is generally non-reactive, stable, and resistant to extreme environments and temperatures between −55 and +300 °C keeping its properties. In extreme environments some properties like the tensile

strength, elongation, tear strength and compression sets are normally higher than in conventional rubbers. On the other hand, silicone robber has low tensile strength compared with natural rubber and is sensitive to fatigue from cyclic loading. The formulation used in the muscle was TYGON 3350 silicone tubing. This platinum-cured silicone tubing resists temperature extremes, ozone, radiation, moisture, compression sets, weathering and chemical attack.

TYGON 3350 Typical Physical Properties

Property	ASTM Method	Value or Rating
Durometer Hardness		
Shore A, 15 Sec	D2240	50
Color		Translucent
Tensile Strength		
Psi (MPa)	D412	1,450 (10)
Ultimate Elongation, %	D412	770
Tear Resistance	D624	200 (35)
Lb.-f/inch (KN/m)	Die B	
Specific Gravity	D792	1.14
Water Absorption, %		
24 hrs. @ 23°C	D570	0.11
Compression Set	D395-89	
Constant Deflection, %	Method B	
@ 158°F (70°C) for 22 hrs.		7
@ 347°F (175°C) for 22 hrs.		35
Brittleness by Impact		
Temp., °F (°C)	D746	-112 (-80)
Maximum Recommended		
Operating Temp., °F (°C)		400 (204)
Dielectric Strength		

v/mil (kV/mm) ----------	D149-93----------	480(19.0)
Tensile Modulus, @ 200%		
Elongation, psi (MPa) ----------	D412-92----------	280 (1.9)

Braided Sleeve Materials

Previous studies showed that the sleeve of the muscle made of Polyethylene Terepthalate [4], that is manufactured by several companies, is one of the best options to make the braided sleeve of the pneumatic artificial muscle. It is flexible, resistant and relatively cheaper compared with any other sleeve specially manufactured for this analysis.

The resistance or load capacity of the muscle can be increased using more external tubs or sleeves as desired. Also, it can be achieved changing some characteristics of the braid such as the thickness of the fabric or its number of filaments.

FlexoPet (PT)

FlexoPet (PT) grade is mainly found in electric and electronic applications where cost efficiency and durability are important. The special fabric and its expandability make the sleeve easy to install. The fabric is braided from 10 mil polyethylene Terepthalate (PET) monofilament yarns and the material can operate at wide range of temperatures. Additionally, it is resistant to chemical degradation, UV radiation, and abrasion. It is Halogen Free, Resists Gasoline, Engine Chemicals and Cleaning products.

Figure B-16: Five distinct braided sleeve examples used for the PAM construction

Figure B-16 shows the five different dimensions of braided sleeves used for this study. These examples were measured in the mechanical laboratory using an electronic caliper and a digital representation of the braided sleeve took using SolidWorks design software. Every model was also mechanically tested using the Instron testing machine as it is presented in Chapter 5.

Physical Properties

Monofilament Thickness (ASTM D-204) ----------	**0.01(0.25 mm)**
Flammability Rating----------	UL-94
Recommended Cutting----------	Hot Knife
Colors----------	35

Wall Thickness----------	0.025 (0.63 mm)
Tensile Strength - Yarn (ASTM D-2265) lbs. ----------	**7.5**
Abrasion Resistance----------	Medium
Specific Gravity----------	1.38
Moisture Absorption % (ASTM D-570) ----------	0.1 - 0.2
Hard Vacuum Data (ASTM E-595 at 10-5 torr)	
TML----------	0.19
CVCM----------	0
WVR----------	0.16
Smoke D-Max (ASTM E-662) ----------	56
Out gassing----------	Medium
Oxygen Index (ASTM D-2863) ----------	21
Operating Temperatures	
Minimum Continuous----------	94°F/-70°C
Maximum Continuous (MIL-I-23053) ----------	257°F/125°C
Melt (ASTM D-2117) ----------	482°F/250°C

Flexo Heavy Wall[7]

Extreme abrasion protection braided sleeve, ideal for contact with rough and abrasive surfaces.

Monofilament Diameter (ASTM D-204) ----------	**0.015 (0.38 mm)**
Flammability Rating----------	UL94
Recommended Cutting----------	Hot Knife
Colors----------	3
Wall Thickness----------	0.038 (0.96 mm)
Tensile Strength (Yarn) (ASTM D-2256) Lbs. ----------	**10**
Specific Gravity (ASTM D-792) ----------	1.38
Moisture Absorption % (ASTM D-570) ----------	0.1-0.2
Hard Vacuum Data ASTM E-595 at 10-5 torr	
TML----------	0.19
CVCM----------	0.00
WVR----------	0.16

Smoke D-Max ASTM E-662	56
Out gassing	Med
Oxygen Index ASTM D-2863	21
Abrasion Resistance	Medium
Abrasion Test Machine	Taber 5150
Abrasion Test Wheel	Calibrase H-18
Abrasion Test Load	500g
Room Temperature	80°F
Humidity	72%
Two Broken Strands	200 Test Cycles
Braid Worn Through In One Direction, In Several Places	700 Test Cycles
Material Destroyed -Braid Worn Through In Both Directions	950 Test Cycles
Pre-Test Weight	5,262.7 mg
Post-Test Weight	4,979.9 mg
Test End Loss of Mass Point of Destruction	239.3 mg
Melt Point ASTM D-2117	482°F (250°C)
Maximum Continuous Mil-I-23053	257°F (125°C)
Minimum Continuous	-94°F (-70°C)

End Fixture Materials

Following the muscle design requirements, mechanical strength, good wear resistance, machinability low cost and others, an excellent and the most suitable material for the artificial muscle end fitting was the stainless steel AISI/SAE 304 which physical, mechanical, electrical and thermal properties are shown below.

Figure B-17: PAM end fitting small size made of stainless steel SAE 304

Component Wt. %

C----------	Max 0.08
Cr----------	18 - 20
Fe----------	66.345 - 74
Mn----------	Max 2
Ni----------	8 - 10.5
P----------	Max 0.045
S----------	Max 0.03
Si----------	Max 1

SAE 304 Physical Properties	Metric (English)
Density	8 g/cc (0.289 lb. /in³)

Mechanical Properties

Hardness, Brinell	123 123	Converted from Rockwell B hardness.
Hardness, Knoop	138 138	Converted from Rockwell B hardness.
Hardness, Rockwell B	70 70	
Hardness, Vickers	129 129 109	Converted from Rockwell B hardness.

Tensile Strength, Ultimate	505 MPa (73200 psi)
Tensile Strength, Yield	215 MPa (31200 psi) at 0.2% offset
Elongation at Break	70 % (70 %) in 50 mm
Modulus of Elasticity	193 - 200 GPa (28000 - 29000 kip/si)
Poisson's Ratio	0.29(0.29)
Charpy Impact	325 J (240 ft-lb)
Shear Modulus	86 GPa (12500 kip/si)

Electrical Properties

Electrical Resistivity	7.2e-005 ohm-cm (7.2e-005 ohm-cm) at 20°C (68°F); 1.16E-04 at 650°C (1200°F)
Magnetic Permeability	1.008 (1.008) at RT

Thermal Properties

CTE, linear 20°C	17.3 µm/m-°C (9.61 µin/in-°F) from 0-100°C
CTE, linear 250°C	17.8 µm/m-°C (9.89 µin/in-°F) at 0-315°C (32-600°F)
CTE, linear 500°C	18.7 µm/m-°C (10.4 µin/in-°F) at 0-650°C
Specific Heat Capacity	0.5 J/g-°C (0.12 BTU/lb.-°F) from 0-100°C (32-212°F)
Thermal Conductivity	16.2 W/m-K (112 BTU-in/hr-ft²-°F) at 0-100°C, 21.5 W/m°C at 500°C
Melting Point	1400 - 1455 °C (2550 - 2650 °F)
Solidus	1400 °C (2550 °F)
Liquidus	1455 °C (2650 °F)

BRAIDED SLEEVE PARAMETERS

Consistent with the volumetric requirements of the adult size over knee amputee prostheses, the most suitable muscle size was constructed with the braided sleeve PT1.25 which as indicated by the braid parameters lead to an original actuator diameter of 18mm. other braided sleeve diameters and materials were tested in order to get an appropriated sleeve- bladder combination, maximum pulling force and the best performance of the muscle.

Sleeve 32 - PTN1.25PT

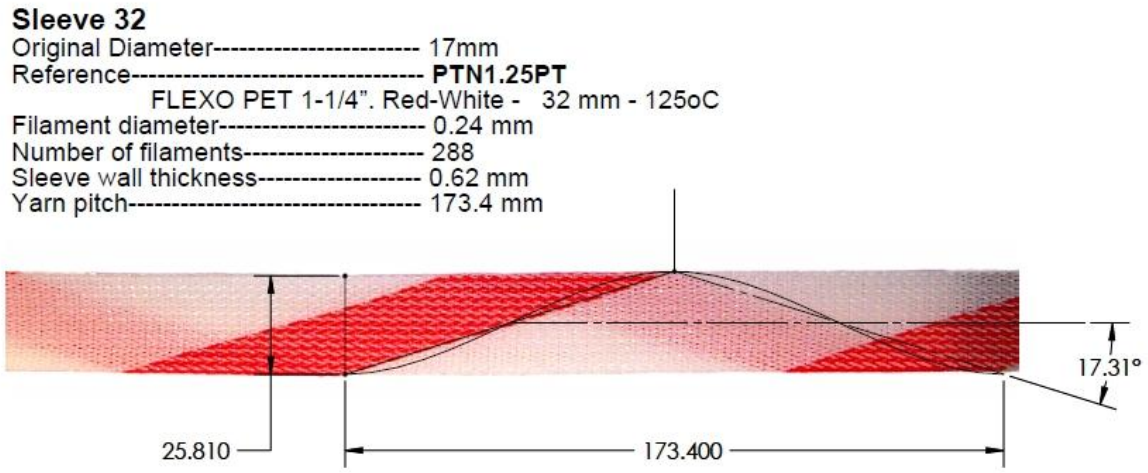

Figure B-18: Braided sleeve 32 mm

Figure B-18 shows the digitized picture of the braided sleeve 32 mm. The information for the five different sleeve models in this analysis was obtained from each example in the biomedical laboratory using an electronic caliper, the help of CAD software and a digital camera. The braided sleeve material for the sleeve 32 is commercially found with the reference PTN1.25PT - FLEXO PET 1-1/4"- Patriot Red, White - 32 mm - 125^{o}C. This flexible braided sleeve is composed by 288 filaments of 0.24mm diameter and spun pitch173.4 mm, distance per filament turn at the sleeve rest position when the filament angle with respect to the longitudinal axis is 17.3 degrees. The braid thickness wall was 0.62 mm.

Sleeve 25 - HWN1.00BK

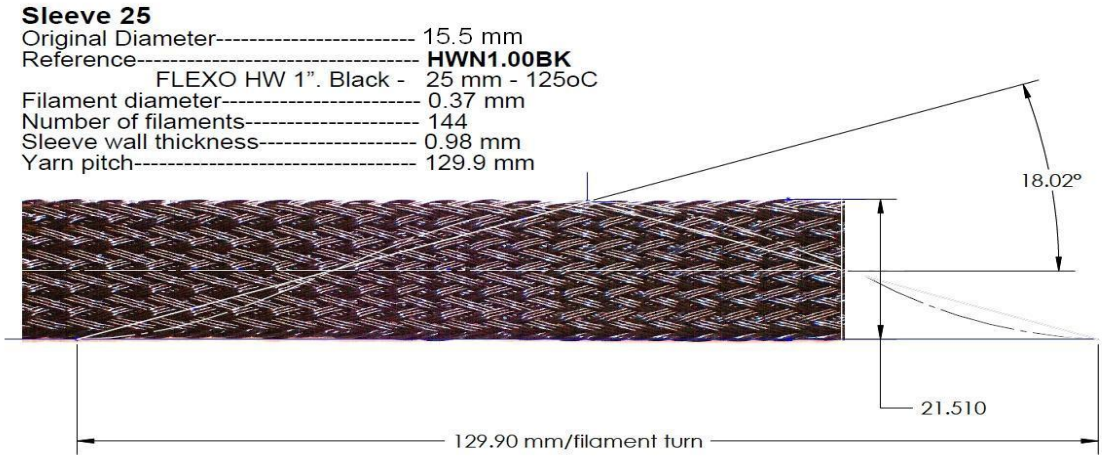

Figure B-19: Braided sleeve 25 mm

Figure B-19 shows the braided sleeve HWN1.00BK, this sleeve has a high abrasion resistance material commercially found as **HWN1.00BK -** FLEXO HW 1"- Black 25 mm - 125^{o}C. This flexible braided fabric is composed by 144 filaments 0.37 mm diameter and yarn pitch 129.9 mm, distance per filament turn, at the sleeve rest position and fiber angle of 18^{o}. The braid thickness wall was 0.98 mm. Yield point at **6249.9** N and **56.7**mm elongation.

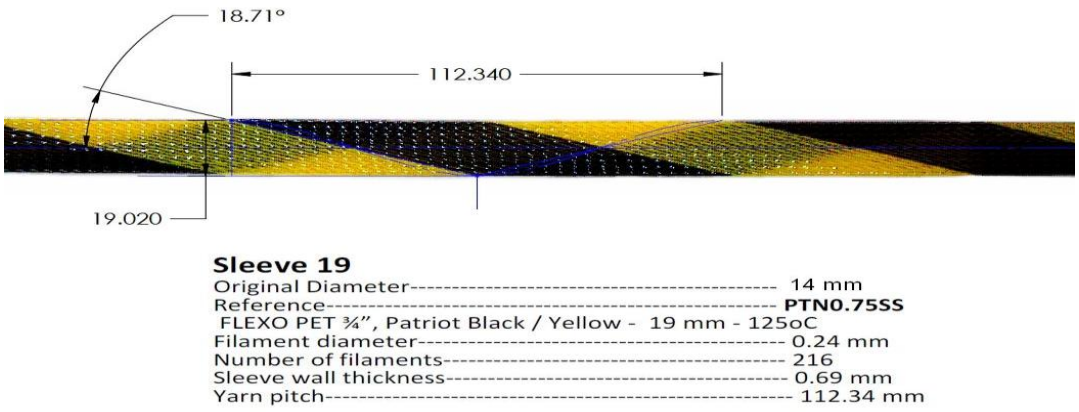

Figure B-20: Braided sleeve 19 mm

Figure B-20 indicates braided sleeve PTN0.75SS. The braided sleeve material is a high abrasion resistance material commercially found as **PTN0.75SS** - FLEXO PET 3/4"- Patriot Black /

Yellow 19 mm - 125°C. This flexible braided sleeve is composed by 216 filaments 0.24 mm diameter and yarn pitch of 112.34 mm, distance per filament turn at the sleeve rest position. The braid thickness wall is 0.69 mm. Yield point at **5141.5** N and **20.2** mm elongation Figure 5-11.

Sleeve 16 - HWN0.63BK

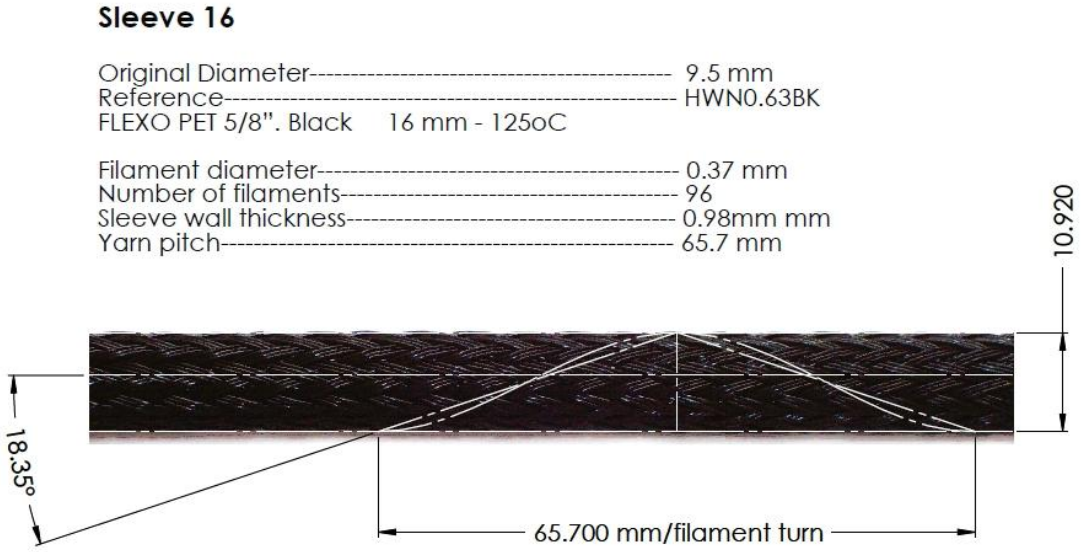

Figure B-21: Braided sleeve 16 mm

Figure B-21 shows the braided sleeve HWN0.63BK. This material is commercially found with the reference HWN0.63BK - FLEXO PET 5/8"- Black 16 mm - 125oC. The flexible braided sleeve is composed by 96 filaments of 0.37 mm diameter and 65.7 mm yarn pitch, distance per filament turn. The sleeve thickness wall was 0.98 mm. The Figure 5-11shows the relationship between the pulling load and displacement during the 16 mm. diameter sleeve test. The testing results reveal a maximum load of 3699Newton with 41 mm. displacement of the example.

Sleeve 13- PTN0.50PT

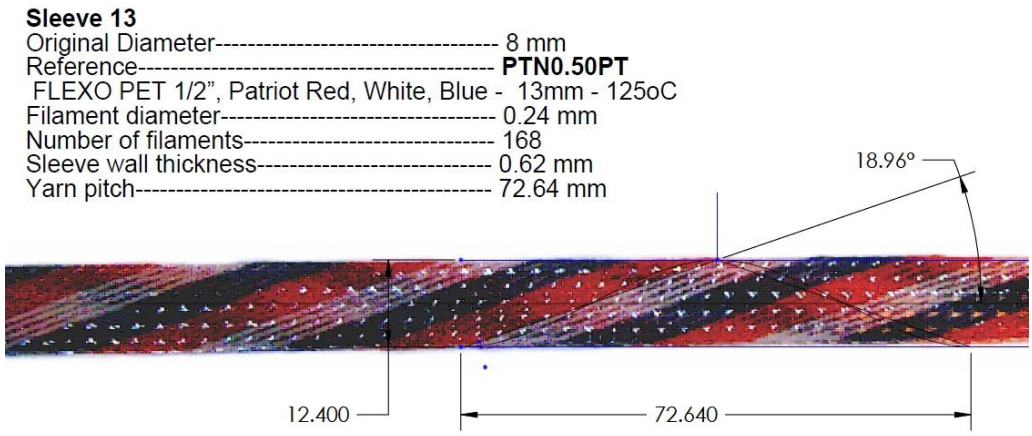

Figure B-22: Braided sleeve 13 mm

Figure B-22 shows the braided sleeve PTN0.50PT. The braided sleeve material is commercially found as PTN0.50PT- FLEXO PET 1/2". Patriot Red, White, Blue - 13 mm - 125^{o}C. This flexible braided sleeve is made with 72filaments of 0.25 mm diameter and yarn pitch 78.66 mm, distance per filament turn at the sleeve rest position. The braid thickness wall was 0.62 mm and filament angle 19^{o}.

Shoe GOO adhesive

Technical data sheet

Manufactured by: Eclectic Products, Inc.
Pineville, LA 71360
Made in the USA
800.767.4667 - Technical Services
eclecticproducts.com
shoegoo.com
shoegooskate.com

Product description

SHOE GOO® has been scientifically formulated to repair, seal and stick to a wide variety of materials with superior strength to any other brand. SHOE GOO® contains a resin system designed for stronger abrasion resistance and better adhesion to flexible materials. Plastic, metal leather, vinyl, rubber, canvas - SHOEGOO® is the most versatile and effective adhesive available. SHOE GOO® is not formulated for exposure to sunlight. Upon fully curing SHOE GOO® it may be painted over to provide UV protection.

Mechanical properties

Chemical resistance	Excellent to water, dilute acids and dilute bases
UV resistance	No; paint over for UV resistance
Hardness	80 Shore A
Dielectric strength	400V/mil (ASTM D-149); this is the maximum voltage that can be applied to a given material without causing it to break down
Tensile strength	3800 lb. /in2 (ASTM D-412)
Elongation	900% (ASTM D-412)
Service temperature	-40 to 150 °F (-40 to 66 °C)
Paint-over time	24 hours

APPENDIX C

BPM EXPERIMENTAL SETUP

Design and construction of a joint setup that imitates knee kinetics and kinematics. Characteristic of the setup

- Resistant Work area
- Easy Adjustable to any muscle length between 50 mm and 900 mm
- Easy to operate
- Minimum deformation under load to eliminate additional stiffness during muscle analysis
- Adaptable
- Imitates knee kinetics and kinematics
- Enough free space to install manipulates and tests the muscle

Solid Works Design

Figure 5-51 shows four initial concepts of the antagonistic joint set up design that imitates the knee kinetics and kinematics. The process design of this mechanism will be not discussed in this section, but later you can see the complete set of detailed construction drawings and the assembly.

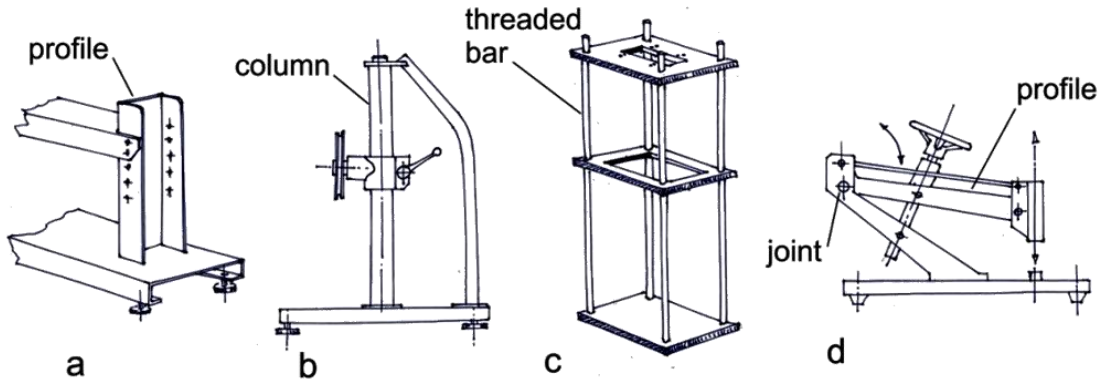

Figure C-1: initial concepts of the antagonistic joint setup design

Figure C-2: Antagonistic joint setup

Part -3

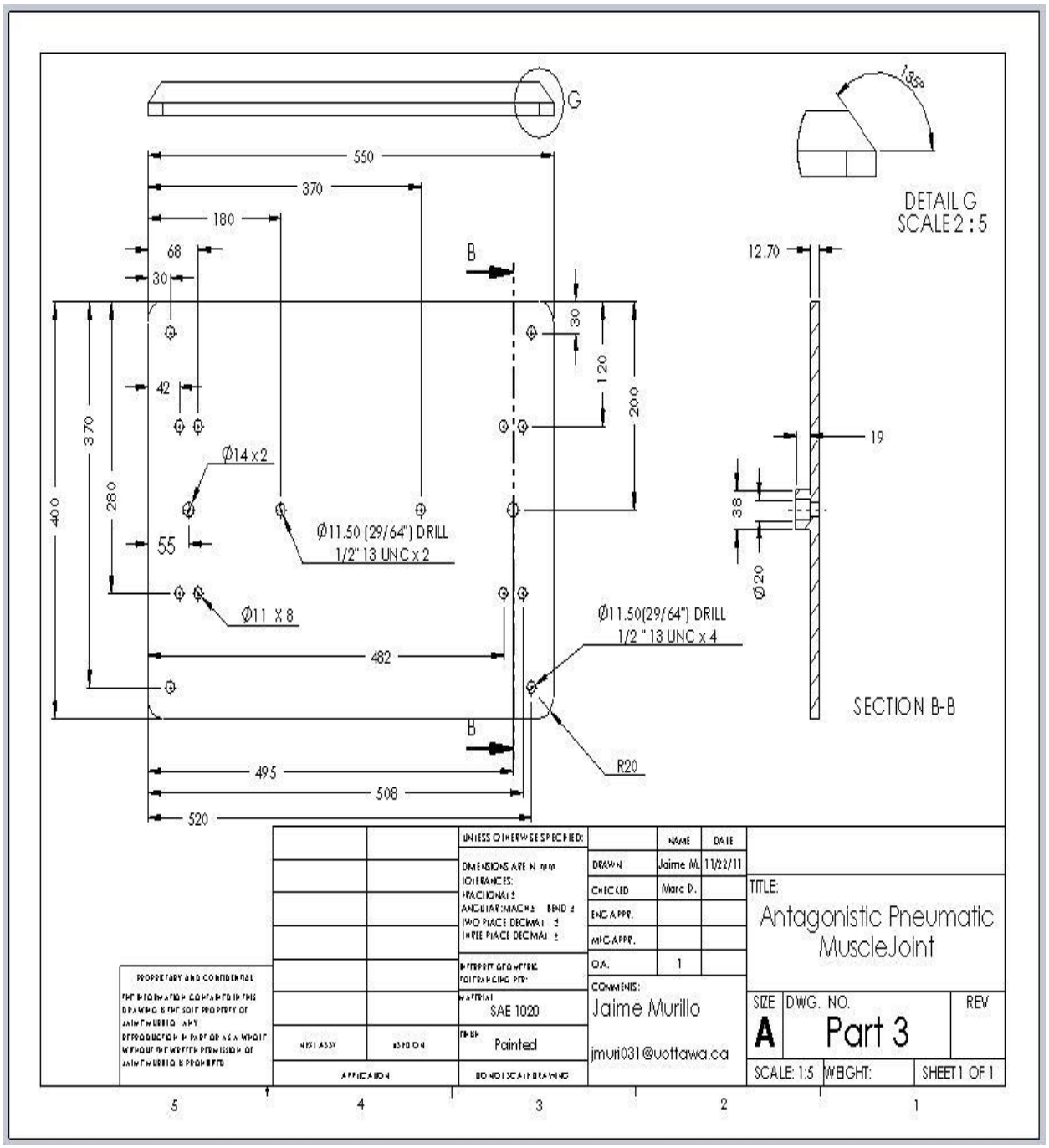

Figure C-3: Part 3 Base beam

Part -4

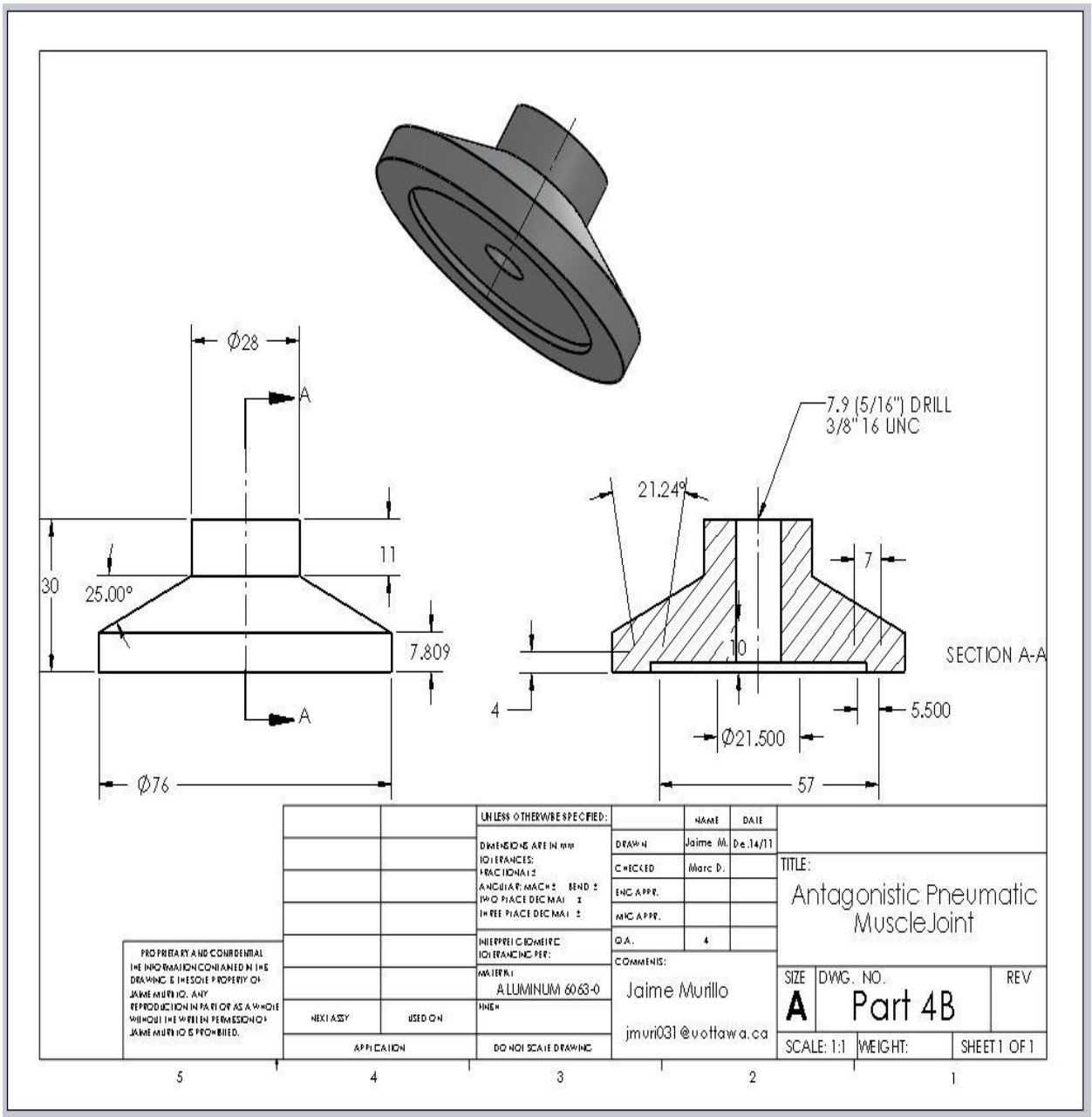

Figure C-4: Part 4 Adjustable feet

Part -5

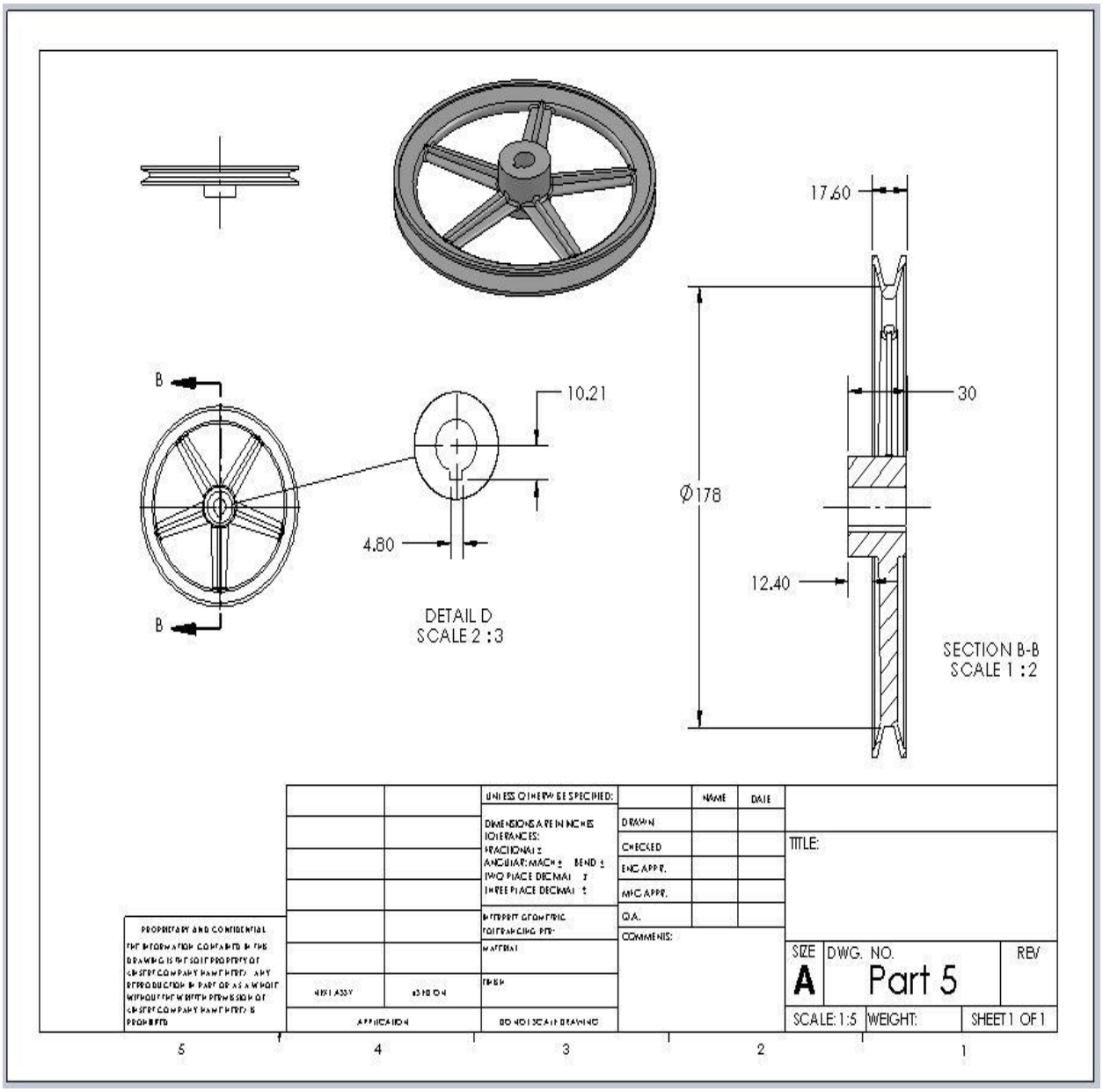

Figure C-5: Part 5 pulley

Part - 6

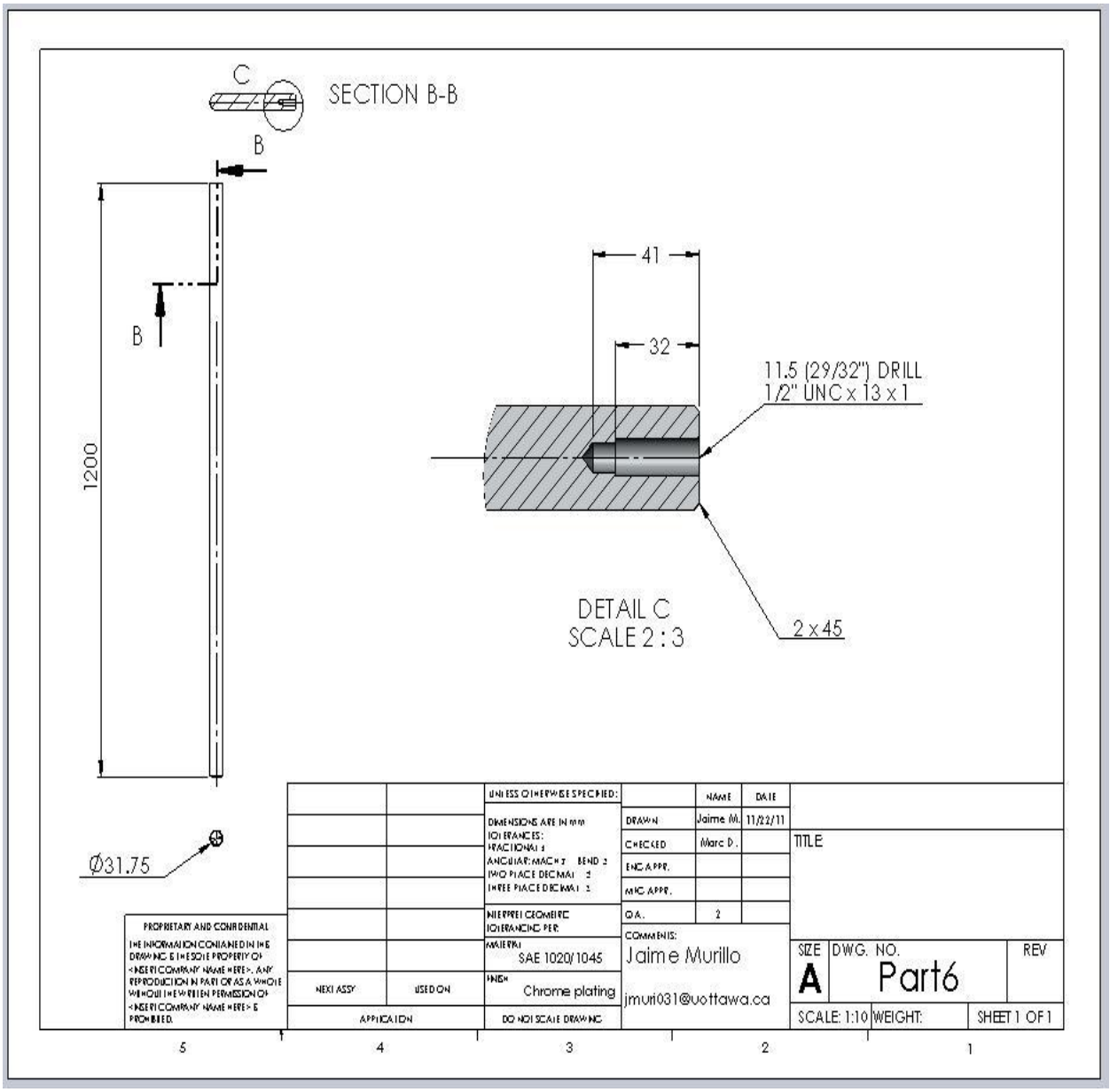

Figure C-6: Part 6 Column

Part - 7

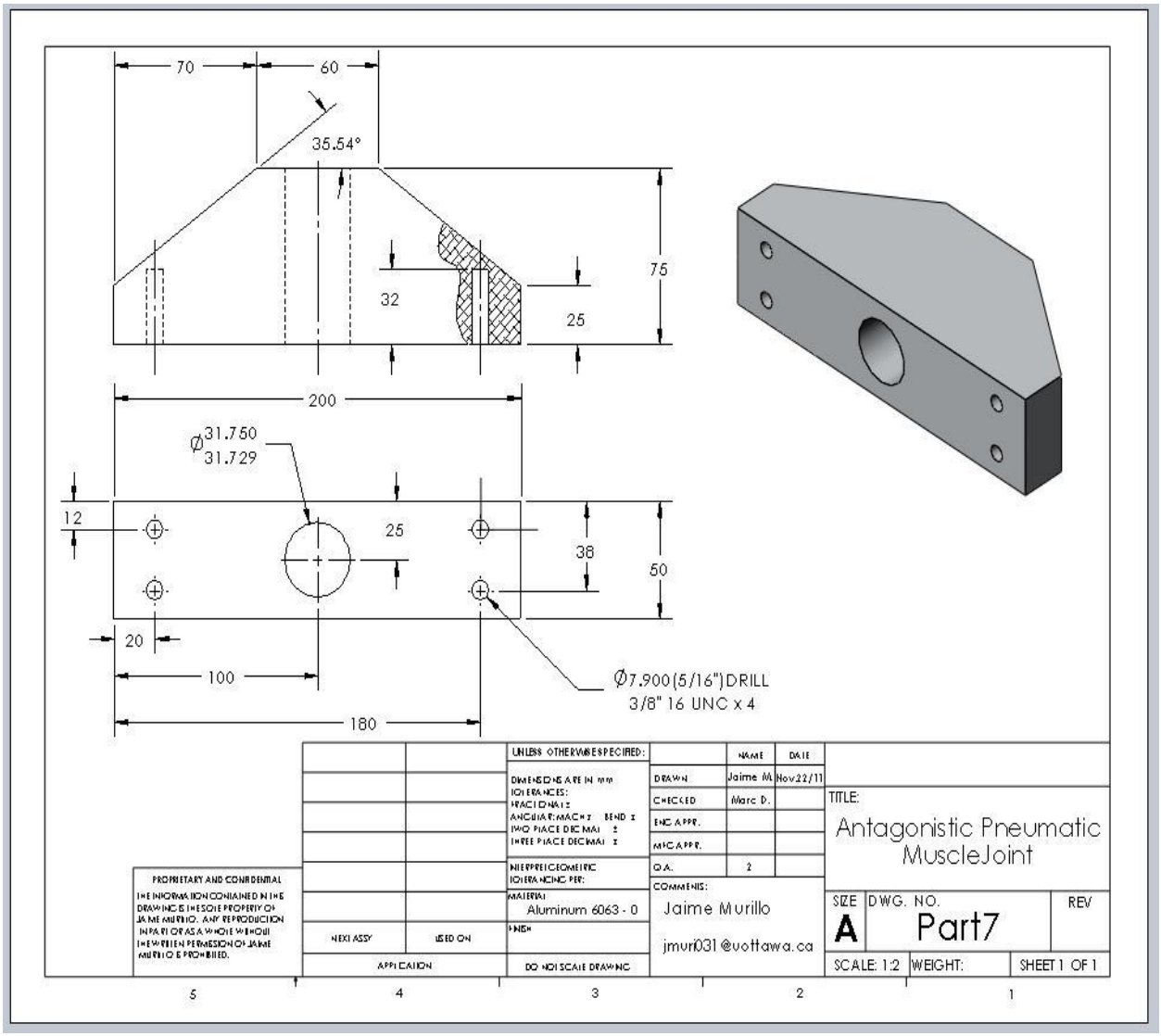

Figure C-7: Part 7 Column support

Part - 8

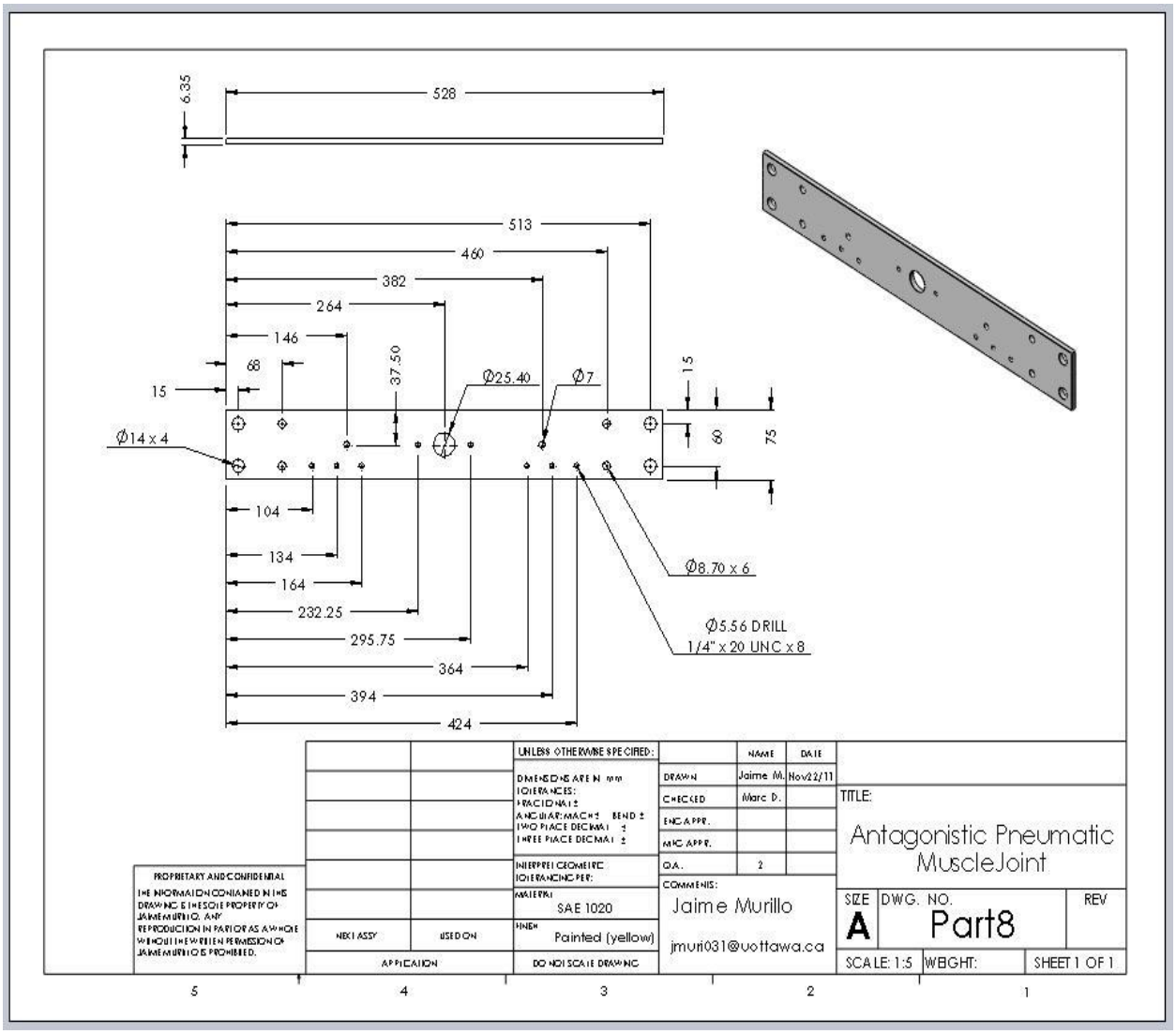

Figure C-8: Part 8 moving beam

Part - 9

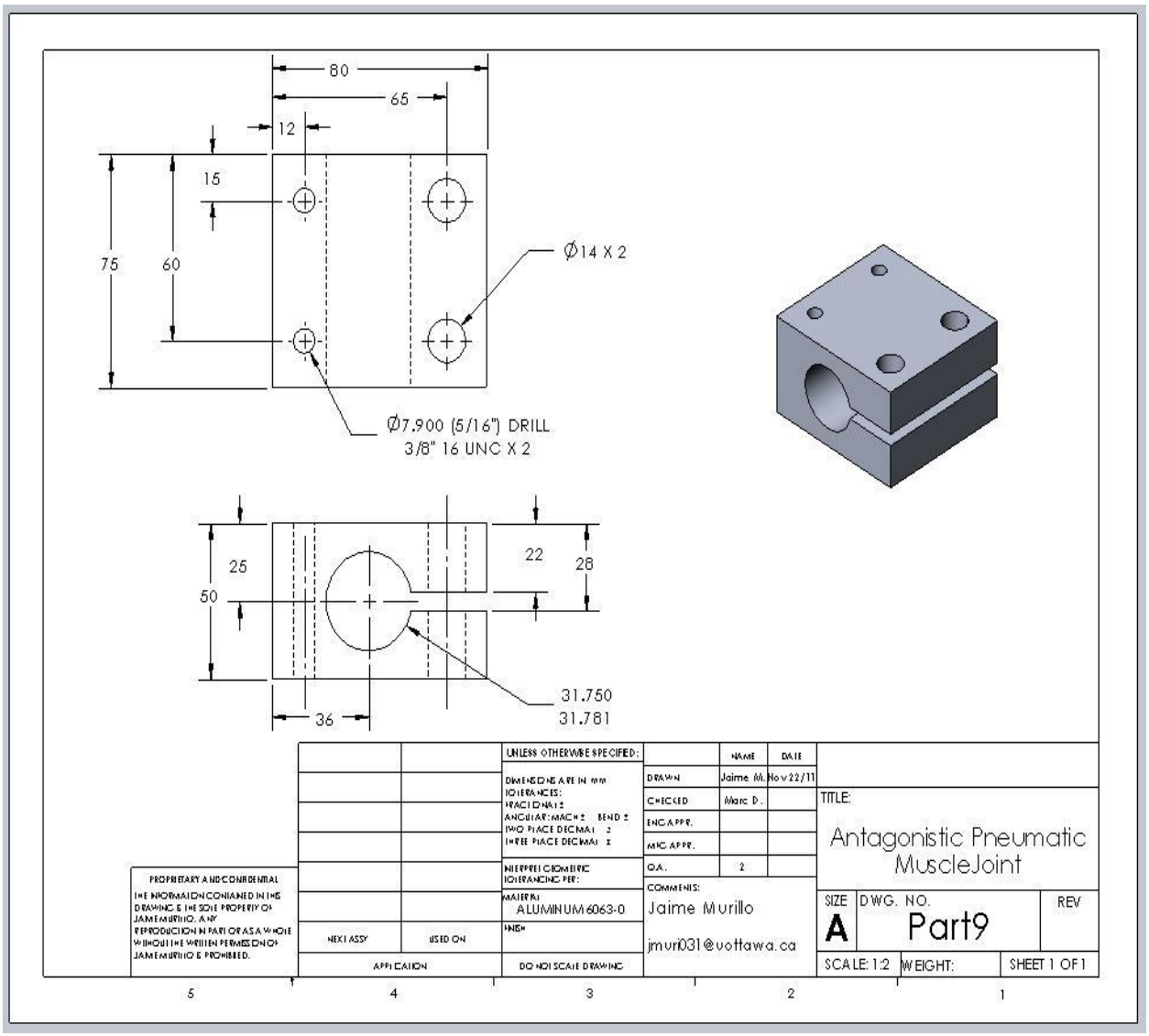

Figure C-9: Part 9 Anchoring piece

Part – 10

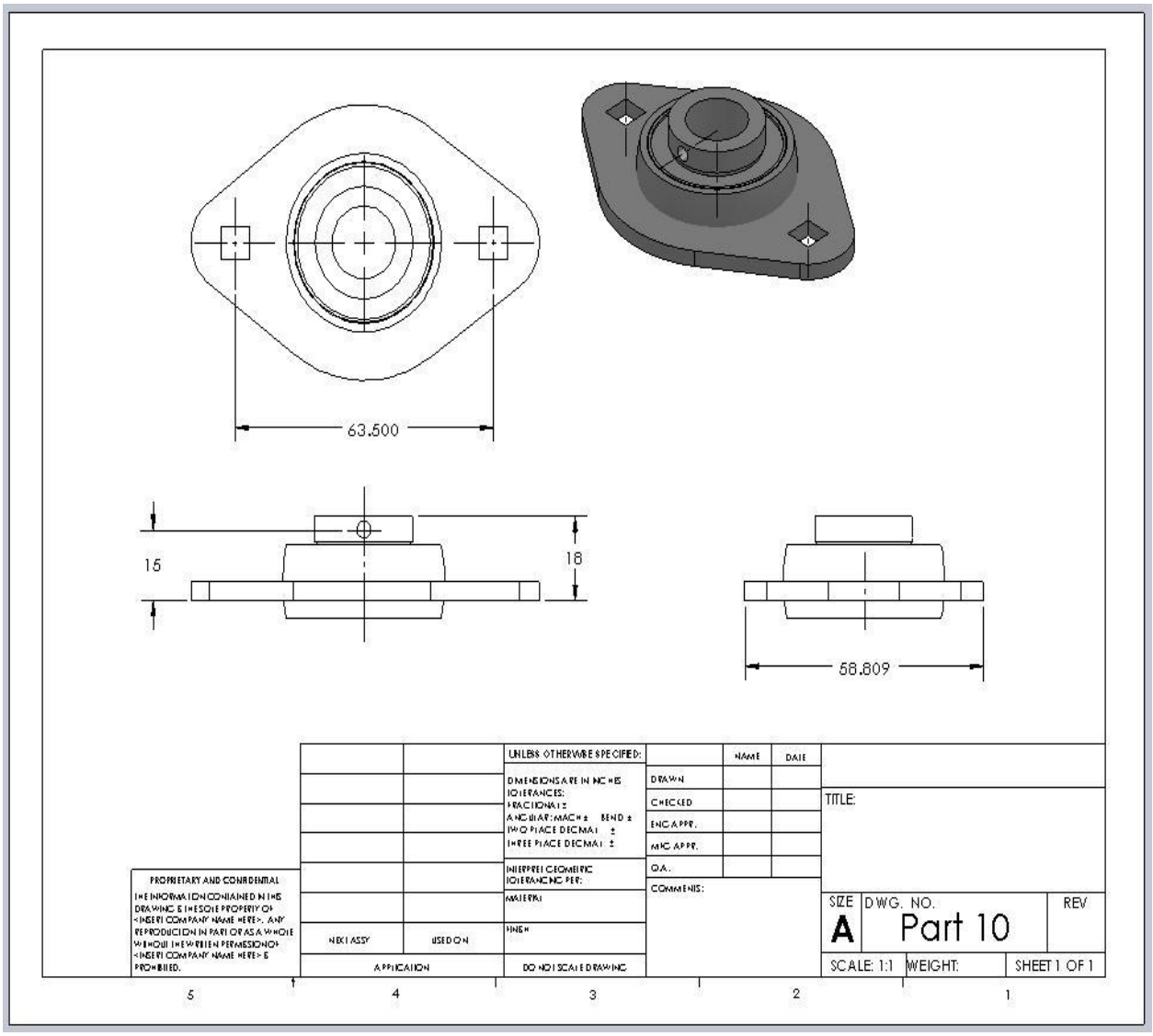

Figure C-10: Part 10 Two-hole flange, 5/8” self-aligning replaceable bearing

Part - 11

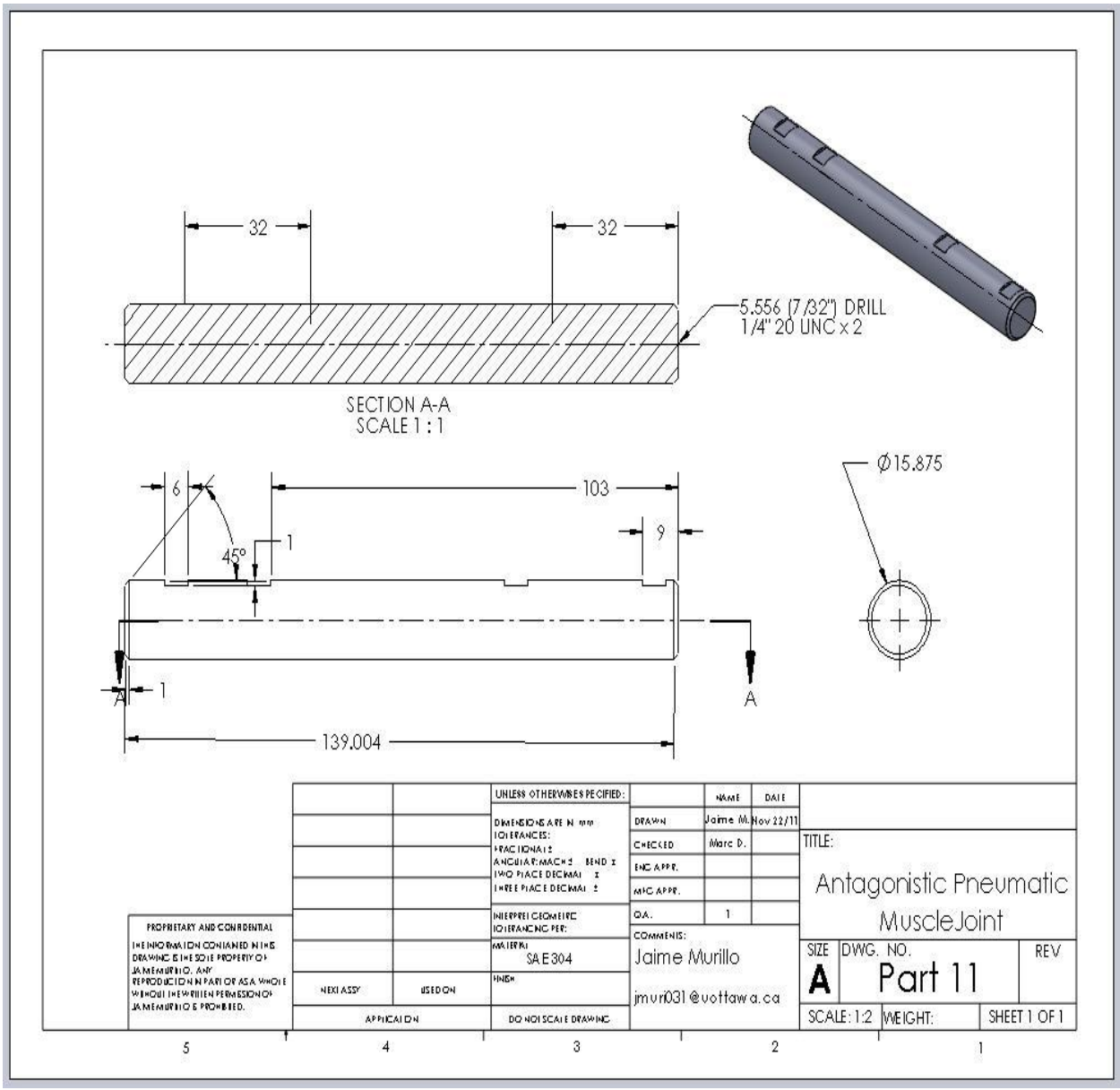

Figure C-11: Part 11 Pulley shaft

Part – 12

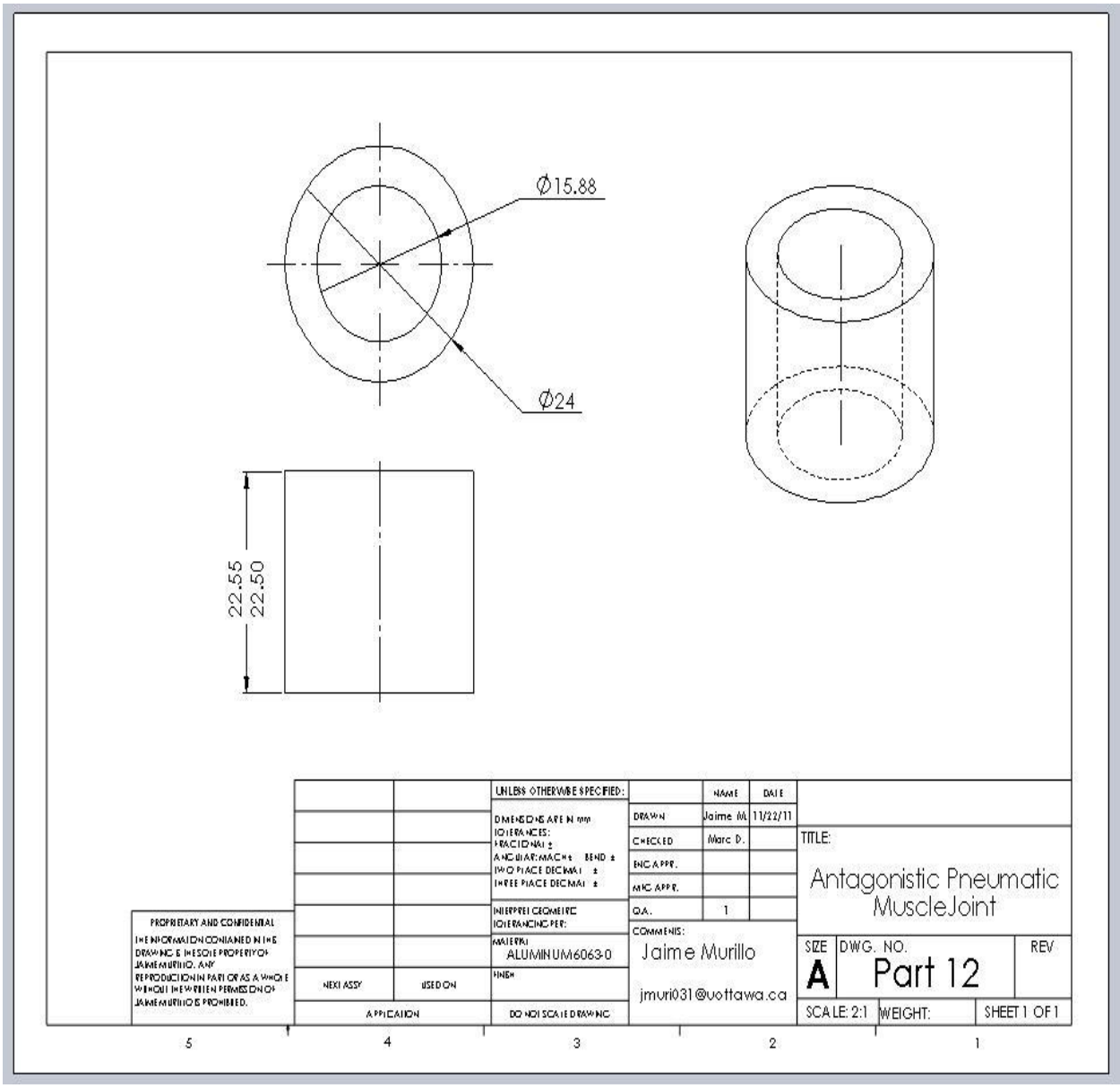

Figure C-12: Part 12 Anterior separator

Part - 14

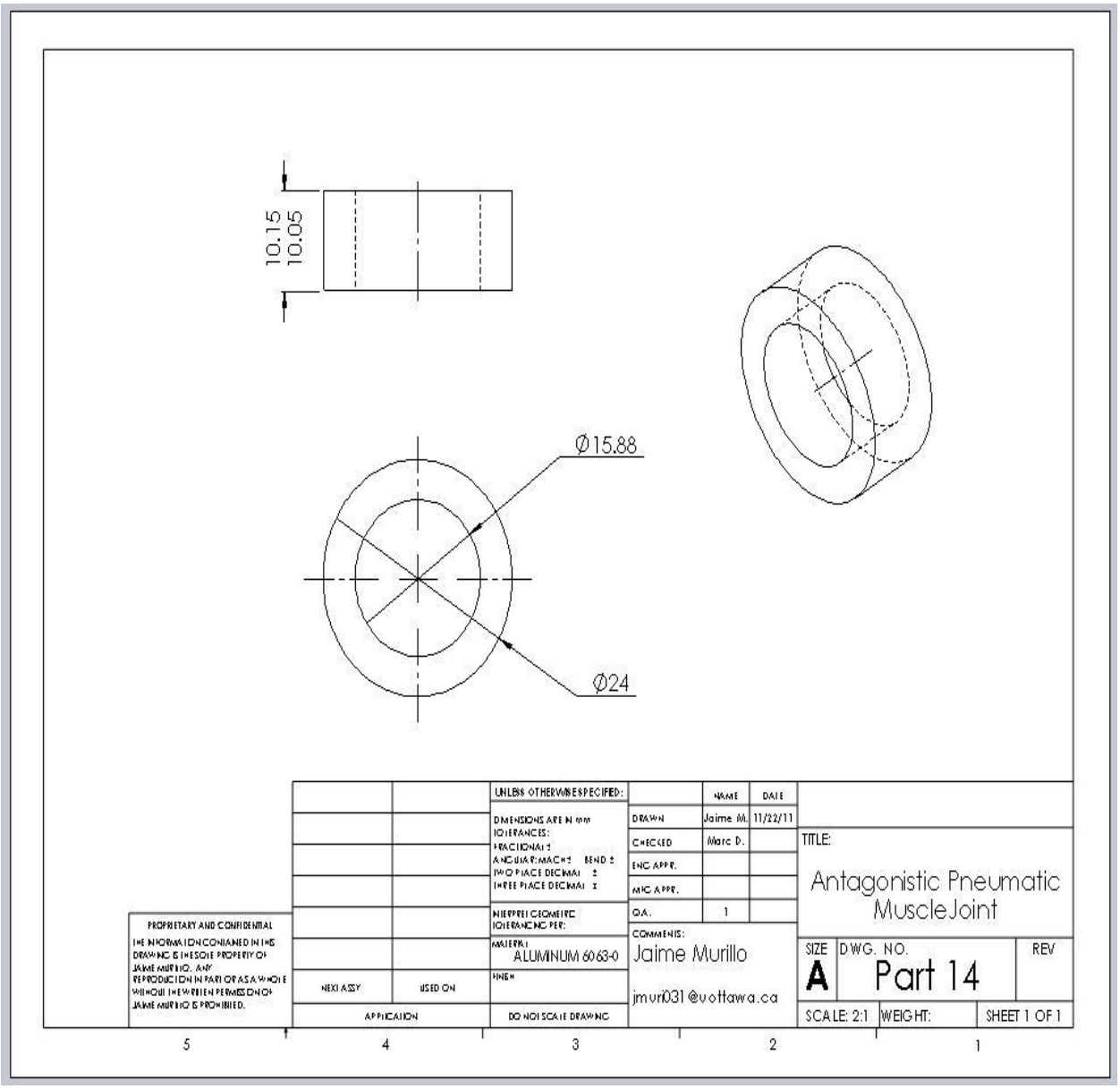

Figure C-13: Part 14 Posterior separator

Part - 16

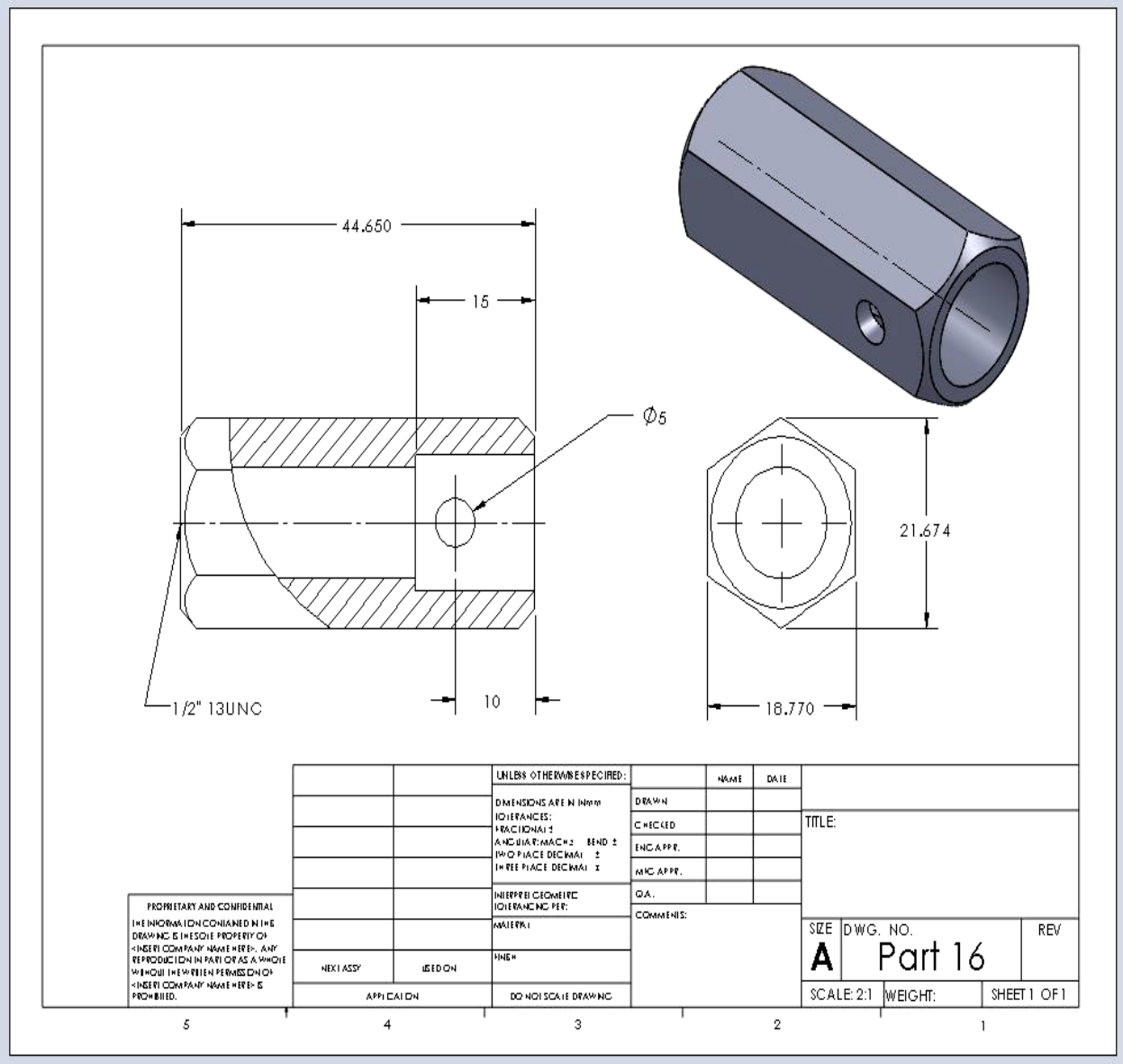

Figure C-14: Part 16Cable muscle connector

Part - 17

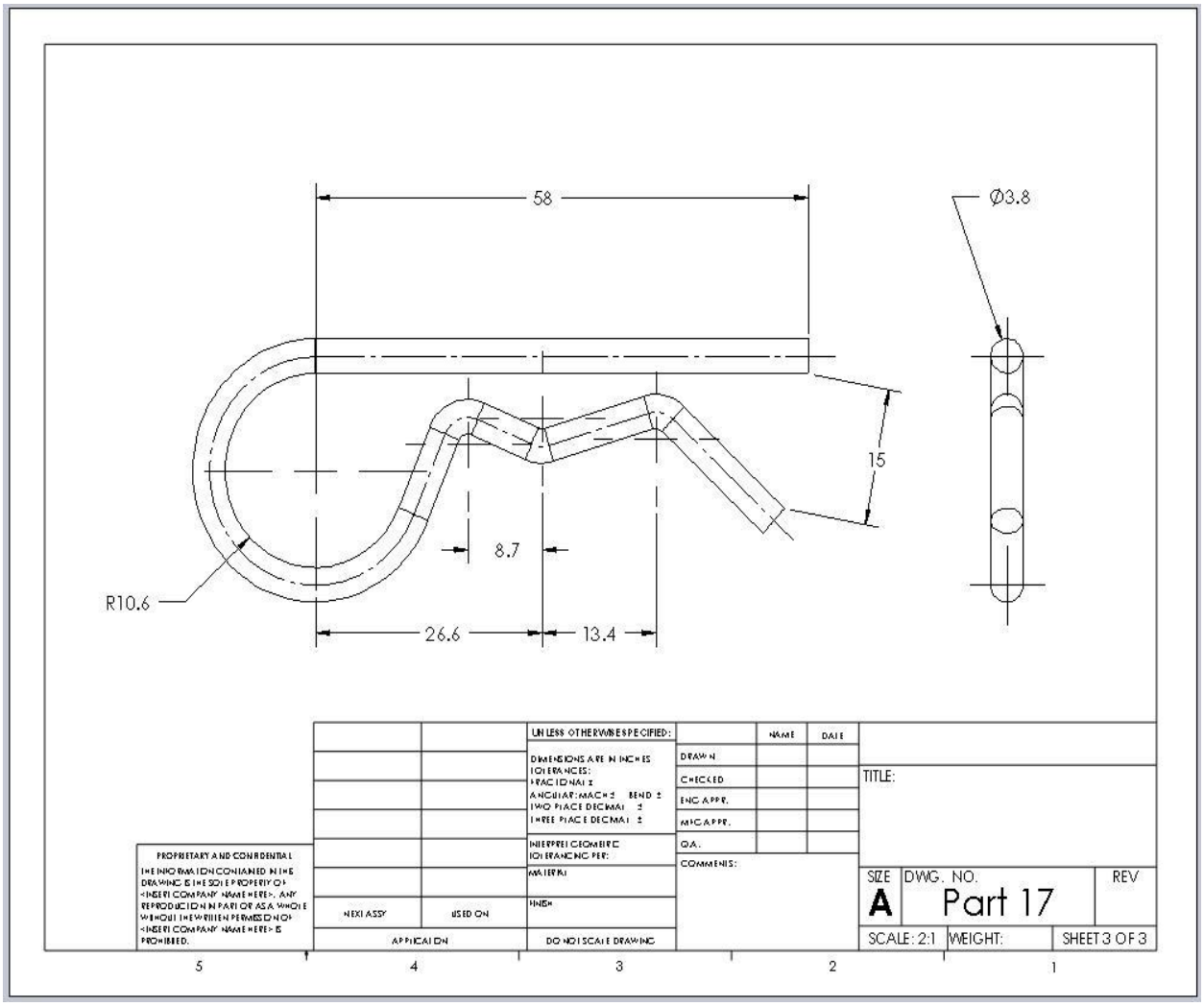

Figure C-15: Part 17 Cable muscle connector pin

Assembly 1-14

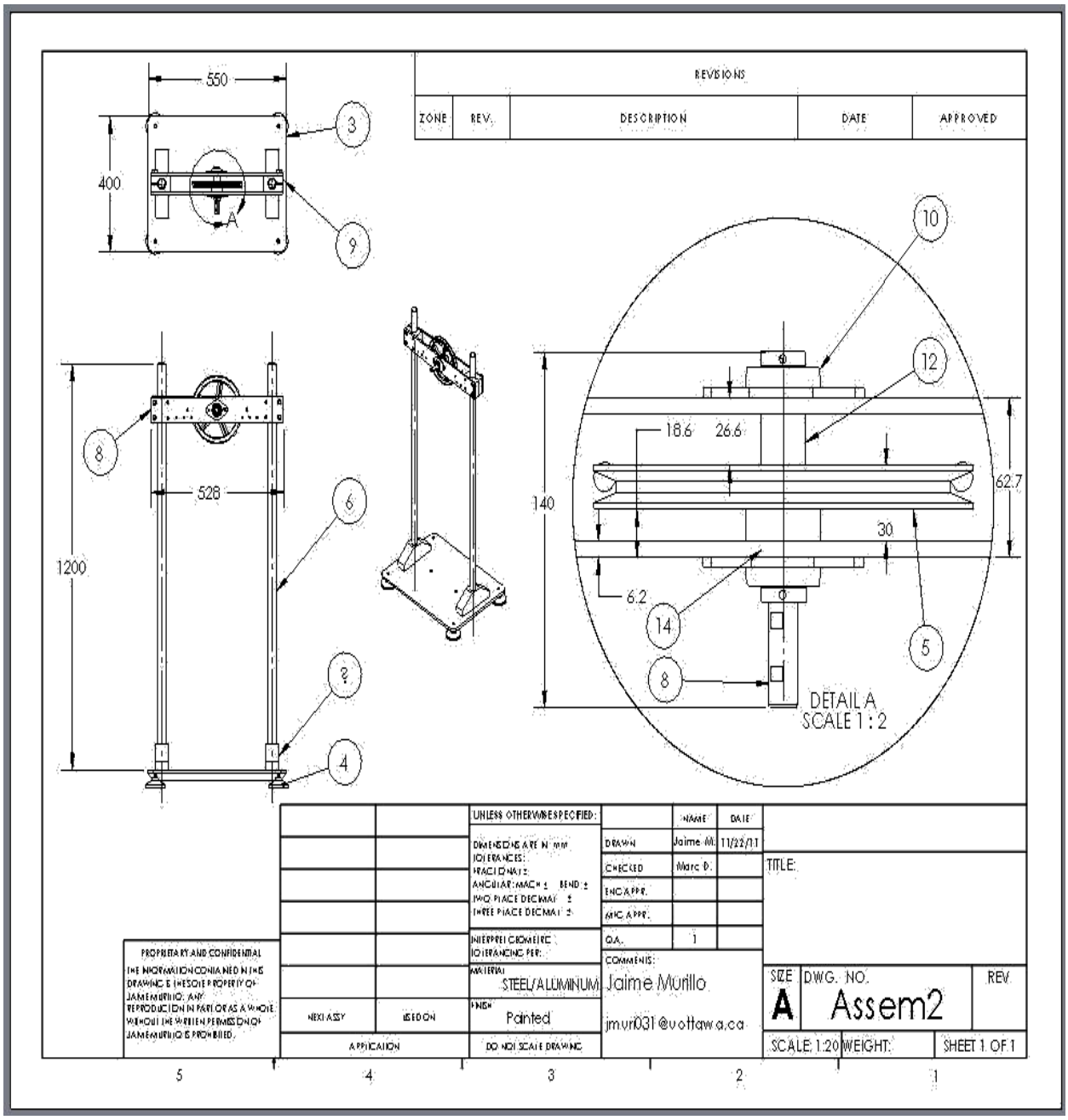

Figure C-16: Antagonistic setup assembly

Finite Element Analysis - Simulation of Assembly

It is assumed that all joints are tighten enough to ensure zero relative displacement between parts and the model can be considered as one solid

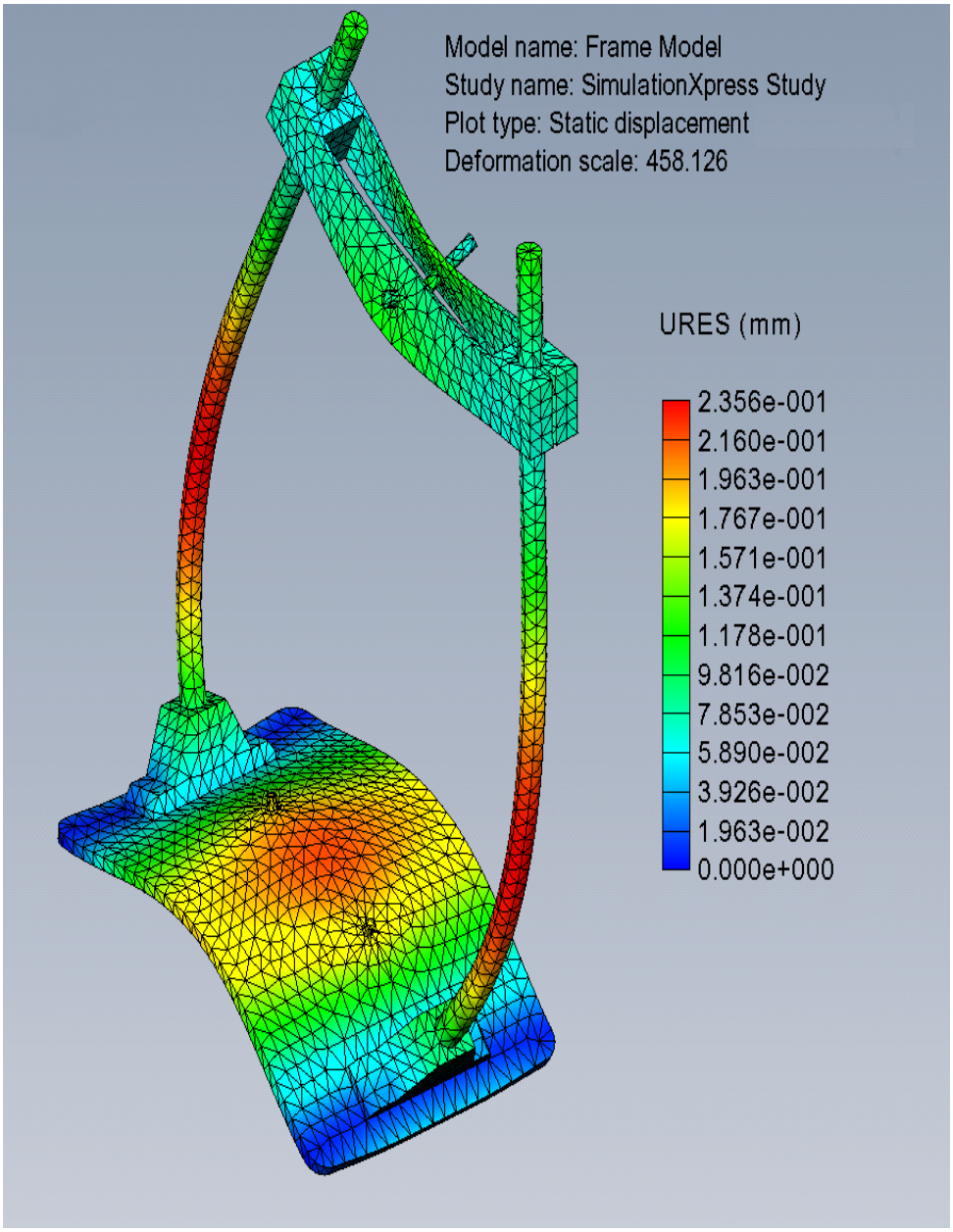

Figure C-17: Finite element model of the experimental setup assembly

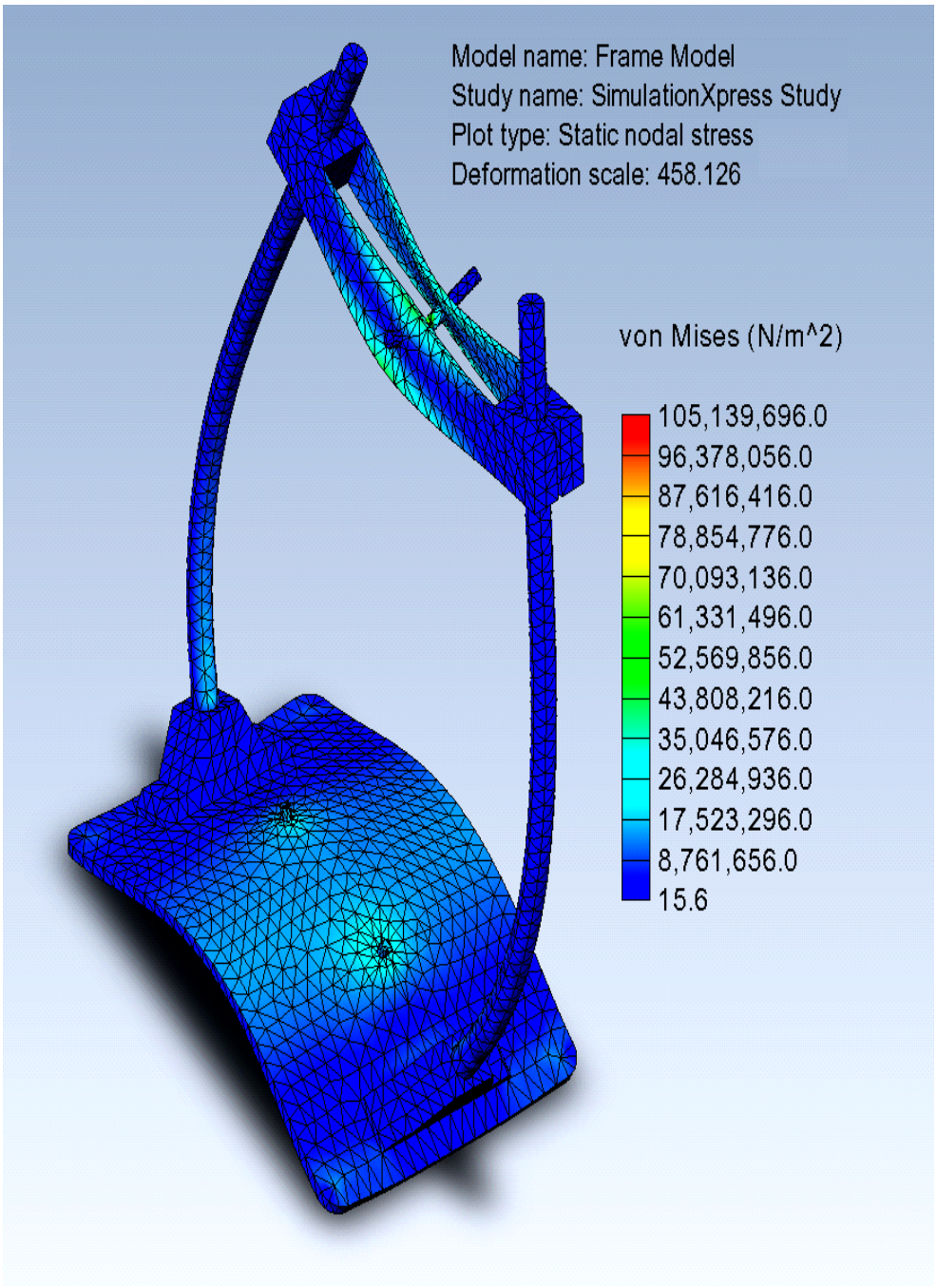

Figure C-18: Finite element model of the experimental setup assembly